Universidade de Aveiro
2011
Departamento de Electrónica, Telecomunicações e Informática

NAVIN KUMAR

SISTEMAS DE COMUNICAÇÂO POR LUZ VISÍVEL NA SEGURANÇA RODOVIÁRIA

VISIBLE LIGHT COMMUNICATION SYSTEMS FOR ROAD SAFETY APPLICATIONS

Universidade de Aveiro
2011
Departamento de Electrónica, Telecomunicações e Informática

NAVIN KUMAR

SISTEMAS DE COMUNICAÇÂO POR LUZ VISÍVEL NA SEGURANÇA RODOVIÁRIA

VISIBLE LIGHT COMMUNICATION SYSTEMS FOR ROAD SAFETY APPLICATIONS

Tese apresentada às Universidades de Minho, Aveiro e Porto para cumprimento dos requisitos necessários à obtenção do grau de Doutor no âmbito do doutoramento conjunto MAP-Tele, realizada sob a orientação científica do Doutor Rui Luis Andrade Aguiar, Professor Associado com Agregação do Departamento de Electrónica, Telecomunicações e Informática da Universidade de Aveiro, e do Doutor Luis Filipe Mesquita Nero Moreira Alves, Professor Auxiliar do Departamento de Electrónica, Telecomunicações e Informática da Universidade de Aveiro.

Apoio financeiro da FCT no âmbito do projecto VIDAS:
PTDC/EEA-TEL/75217/2006.

Apoio financeiro da FCT bolsa de doutoramento:
SFRH/BD/33444/2008

I would like to thank my family and kids who sacrificed their most important and valuable time in my support. My family has shown unconditional love and wisdom that helped me survive these difficult times. I would like to dedicate this thesis to my wife Rinku and sons Anirudh and Aniket.

o júri

presidente

Doutor José Abrunheiro da Silva Cavaleiro
Professor Catedrático do Departamento de Química da Universidade de Aveiro

Doutor Dinis Gomes Magalhães dos Santos
Professor Catedratico do Departamento de Electrónica, Telecomunicações e Informática da Universidade de Aveiro

Doutor Adriano Jorge Cardoso Moreira
Professor Associado da Escola de Engenharia da Universidade do Minho

Doutor Rui Luís Andrade Aguiar
Professor Associado do Departamento de Electrónica, Telecomunicações e Informática da Universidade de Aveiro

Doutor Luís Filipe Mesquita Nero Moreira Alves
Professor Auxiliar do Departamento de Electrónica, Telecomunicações e Informática da Universidade de Aveiro

Doutor Cipriano Rogério Alves Tavares Lomba,
Director da EFACEC

agradecimentos

There are many people that I would like to thank without whom the completion of this thesis would have not been possible.

First and foremost, I would like to express my whole-hearted gratitude to my advisor, Prof. Rui L. A. Aguiar for his invaluable guidance, insight, and encouragement throughout this work. Rui taught me how to think critically about problems and how to present them effectively. I think the best part of working at Institute of Telecommunication with Rui Aguiar was that he prepared me well for professional life.

I would like to thank my co-advisor Prof. Luis Nero Alves for his invaluable time and guidance. He continued working with me very closely, pin-pointing the smallest mistakes ensuring a perfect work throughout the research.

My special appreciation goes to the entire VIDAS team: Nuno Lourenço and Domingos Terra. In fact, without Optical Front-End design which was supported by Nuno and FPGA implementation by Domingos, the transceiver prototype design would have not existed. I also thank for experimental and testing support from Daniel and Paulo Almendra. Daniel has been very-very co-operative and generous.

Furthermore, other individuals whose expert advice was significant to the success are Prof. S. K. Mendriata from Physics department who kept encouraging and continued his support; colleague Azmol Huda has been a great help in the mathematical parts, Prof. Atilio Gameiro and Prof. Carlos Ribeiro. I would also like to thank people from industry Sinalarte, Portugal.

I am extremely thankful to Scientific members of MAP Tele program and specially Prof. Rui Valadas for his invaluable encouragement throughout his stay and even after his discontinuation from this university. I also extend my sincere thank to all my colleagues of the program, especially Vitor Miron, Qi Luo, Miguel Almeida, Saravanan and Eduardo.

My tremendous thanks go to all my lab mates for their technical support and friendship. Miguel Bergano, Margarida Fernandes, Claudia Camacho,Nelson Silva, and Purnachand Nalluri all they made the lab a fun and comfortable environment to work.

My gratefulness is extended to Secretariat staffs Sandra, Susana, Lisbete who have been very kind and helpful throughout my stay at IT and extended all administrative supports. I also warmly thank support staffs, Miguel, Nuno Silva and others as well as security personals Maira, Nuno and Paulo. In fact, IT has an enjoyable working environment and whole staffs researchers are very co-operative and helpful.

Finally, I would like to thank and acknowledge for the grants from FCT.

This work was sponsored, in part, by Foundation of Science project grant PTDC/EEA-TEL/75217/2006 and PhD grant SFRH/BD/33444/2008.

palavras-chave

Comunicação por luz visível, sistemas de transporte inteligentes, díodos emissores de luz, comunicações veículares.

resumo

Esta tese apresenta um estudo exploratório sobre sistemas de comunicação por luz visível e as suas aplicações em sistemas de transporte inteligentes como forma a melhorar a segurança nas estradas. Foram desenvolvidos neste trabalho, modelos conceptuais e analíticos adequados à caracterização deste tipo de sistemas. Foi desenvolvido um protótipo de baixo custo, capaz de suportar a disseminação de informação utilizando semáforos. A sua realização carece de um estudo detalhado, nomeadamente: i) foi necessário obter modelos capazes de descrever os padrões de radiação numa área de serviço pré-definida; ii) foi necessário caracterizar o meio de comunicações; iii) foi necessário estudar o comportamento de vários esquemas de modulação de forma a optar pelo mais robusto; finalmente, iv) obter a implementação do sistema baseado em FPGA e componentes discretos.

O protótipo implementado foi testado em condições reais. Os resultados alcançados mostram os méritos desta solução, chegando mesmo a encorajar a utilização desta tecnologia em outros cenários de aplicação.

key words

visible light communication, intelligent transportation systems, light emitting diodes, vehicle communications.

abstract

This thesis presents a study carried out on the exploration of visible light communication (VLC) for road safety applications in intelligent transportation systems (ITS). We developed conceptual and analytical models for the usage of VLC technologies for human safety. A low cost VLC prototype traffic broadcast system was hardware designed and implemented. In order to realize this prototype a number of exhaustive steps have been designed and implemented.

An optimized illumination distribution was achieved in a defined service area from LED-based traffic lights associated with a VLC emitter. A traffic light system set-up was modeled and designed for optimum performance. The optical wireless channel was characterized and examined. Depending on the characteristics of the channel and specific applications, a robust modulation technique based on direct sequence spread spectrum using sequence inverse keying (DSSS SIK) was analyzed, developed, and implemented. The complete prototype VLC transceiver system was then implemented with field programmable gate arrays (FPGA) and discrete components.

Simulation and experimental validation of system was performed in different scenarios and environments. The obtained results have shown the merits of our approach. A number of findings was experienced which are illustrated at the end. These observations would enhance and encourage potential research in the area and optimize performance of VLC systems for a number of interesting applications in future. A summary of future research challenges is presented at the end.

TABLE OF CONTENTS

LIST OF TABLES

LIST OF FIGURES

LIST OF ACRONYMS

AC	Alternating Current
ADAS	Advanced Driver Assistance Systems
ADC	Analog to Digital Converter
ASCII	American Standard Code for Information Interchange
ASK	Amplitude Shift Keying
AWGN	Additive White Gaussian Noise
BER	Bit Error Rate
BPI	Byte Peripheral Interface
BPSK	Binary Phase Shift Keying
CALM	Communication Access for Land Mobile
CCL	CMOS Configuration Latches
CCLK	Clock
CDMA	Code Division Multiple Access
CFL	Compact Fluorescent Lamp
CMOS	Complementary Metal Oxide Semiconductor
COOPER	Collaborative Open Environment for Project Centered Learning
COMESAFETY	Communication for E-Safety
CPU	Central Processing Unit
CVIS	Co-operative Vehicle Infrastructure Systems
DAC	Digital-to-Analog Converter
DC	Direct Current
DCM	Digital Control Manager
DDR3	Double Data Rate type three Memory
DSB	Double Side Band
DSP	Digital Signal Processing
DSSS	Direct Sequence Spread Spectrum
EDK	Embedded Development Kit

ETSI	European Telecommunications Standards Institute
FIFO	First-In-First-Out
FIR	Finite Impulse Response
FMC	FPGA Mezzanine Connector
FOV	Field of View
FPGA	Field Programmable Gate Array
FSM	Finite State Machine
GBW	Gain Band Width
GEONET	Geographic Addressing and Routing for Vehicular Communication
GPIO	General Purpose Input/Output
HB-LED	High Brightness Light Emitting Diode
HPA	Half Power Angle
HPF	High Pass Filter
HTTP	Hypertext Transfer Protocol
I2V	Infrastructure-to-Vehicle
ICT	Information and Communication Technology
IEEE	Institute of Electrical and Electronic Engineers
IF	Intermediate Frequency
I-LPPM	Inverted L-level Pulse Position Modulation
IM/DD	Intensity Modulation/Direct Detection
IP	Intellectual Property
I-PPM	Inverted Pulse Position Modulation
IPv4	Internet Protocol Version 4
IPv6	Internet Protocol Version 6
IR	Infrared
IRDA	Infrared Data Association
ISE	Integrated Synthesis Environment
ISO	International Standard Organization

ISP	Information Service Provider
IT	Information Technology
ITF	Internet Task Force
ITE VTCSH	Institute of Transportation Engineering Vehicle Traffic Control Signal Heads
ITS	Intelligent Transportation Systems
JTAG	Jack for Tag Port
KBPS	Kilo Bits Per Second
LAN	Local Area Networks
LDT	Luminance Difference Threshold
LED	Light Emitting Diode
LFSR	Linear Feedback Shift Registers
LMB	Local Memory Bus
LNA	Low Noise Amplifier
LOS	Line-of-Sight
LPC	Low Pin Count
LPI	Low Probability of Interference
LPPM	L-level Pulse Position Modulation
MAC	Media Access Control
MANET	Mobile Adhoc Network
MIMO	Multiple-Input-Multiple-Output
ML	Maximum Likelihood
NPN	NPN Transisor
NRZ	Non Return to Zero
OBU	On Board Unit
O/E	Optical-to-Electrical Conversion Efficiency
OFF	Switch OFF
ON	Switch ON
OOK	On Off Keying

OSI	Open System Interconnection
OW	Optical Wireless
OWC	Optical Wireless Communication
PC	Personal Computer
PCI	Peripheral Component Interface
PD	Photo Detector/Diode
PDF	Probability Density Function
PER	Packet Error Rate
PG	Processing Gain
PHY	Physical Layer
PIN	PIN Photo Diode
PLB	Peripheral Local Bus
PN	Pseudo Noise
PPM	Pulse Position Modulation
PRE-DRIVE C2X	Preparation for Driving Car-to-X Communication
PREVENT	Preventive and Active Safety Applications
PSD	Power Spectrum Density
RF	Radio Frequency
RISC	Reduced Instruction Set Computer
RMS	Root Mean Square
RSU	Road Side Unit
RT	Relativity Theory
RVC	Road-to-Vehicle Communication
SAFESPOTS	Cooperative vehicles and road infrastructure for road safety
SCPSK	Sub-Carrier Phase Shift Keying
SEVECOM	SEcure VEhicular Communication
SIK	Sequence Inverse Keying
SINR	Signal-to-Interference-Noise Ratio

SNR	Signal-to-Noise Ratio
SNR OPTICAL	Optical Signal-to-Noise Ratio
SPI	Serial Peripheral Interface
SOC	System-on-Chip
SOPC	System On a Programmable Chip
SRVC	Sparse Road to Vehicle Communication
SSB	Single Side Band
TCP	Transmission Control Protocol
TIA	Transimpedance Amplifier
TV	Television
UART	Universal Asynchronous Receive/Transmit
UDP	User Datagram Protocol
URVC	Ubiquitous Road to Vehicle Communication
UV	Ultra Violet
V2I	Vehicle-to-Infrastructure
V2V	Vehicle-to-Vehicle
VANET	Vehicular Adhoc Network
VC	Vehicular Communication
VIDAS	VIsible light communication for advanced Driver Assistance Systems
VLC	Visible Light Communication
VS	Vehicle Subsystem
VRTT	Vector Radiative Transfer Theory
WHL	Wireless Home Link
WHO	World Health Organization
XNOR	Ex-NOR Gate

CHAPTER 1: INTRODUCTION

Summary

Visible light communication (VLC) is becoming an alternative choice for next-generation wireless technology by offering low cost, unregulated bandwidth and ubiquitous infrastructures support. This technology is envisioned to be used in a wide range of applications both indoor as well as outdoor. This work investigates in detail, designs a VLC prototype and implements in field programmable gate array (FPGA), a traffic broadcast system for road safety applications. This chapter gives detail of motivation, objectives and original contributions. The thesis organization is presented at the end of the chapter.

1.1 Overall Scenario

The demands for solutions for traffic problem such as accidents, jams and environmental impact are increasing. Highway and ordinary roads are becoming more congested every year due to insufficient road development to accommodate the increasing number of vehicles. Heavy economical losses are caused by traffic congestion apart from inconvenience to users. Road crashes are the second leading cause of death globally among young people aged five to 29 and the third leading cause of death among people aged 30 to 44 years. Over 1.2 million people are killed annually because of road accidents [11]. Studies predicted that road accidents would become the sixth largest cause of death in the world in 2020, whereas it was the ninth largest cause of death in 1990. Intelligent Transportation Systems (ITS) [75] have drawn a lot of attention to solve these (and other) traffic problems. ITS, which interrelates humans, roads, and vehicles through state-of-art Information Technology (IT), are new information systems for the purpose of the solution of road transportation problems, aiming to efficient traffic flow and reduction of the environmental load. There are many projects being investigated and realized related to ITS worldwide, such as, PREVent [76], and CALM [77] to reduce road fatality. VIDAS (VIsible light communication for advanced Driver Assistance Systems) is one such project, under the framework of which this thesis was developed.

VIDAS exploits VLC [60, 61]. VLC based on Light Emitting Diodes (LEDs), is an emerging research area. VLC is a novel kind of Optical Wireless Communication (OWC) [62] which uses white and coloured LEDs to simultaneously provide human visible light. Recent progress and advancement in LED technology has challenged the most popular and reasonably inexpensive conventional lamps, the Compact Fluorescent Lamp (CFL) [43]. LEDs have been gradually replacing traffic lights and other conventional lamps because of their merits of huge energy saving, long life, low maintenance cost, better visibility and low temperature generation. Being semiconductor devices, LEDs have inherent characteristics of high rate switching. This combined feature of LEDs (lighting and switching) is unique, and opens the door for very important applications in ITS where the switching characteristics of LEDs are used for data communication without interruption to its normal function of human-visible signaling or lighting. LED-based traffic lights and VLC systems can become an integrated

component of ITS and play a key role in road safety applications by broadcasting traffic information in advance to drivers running vehicles which incorporates a low cost photodiode-based receiver. VLC systems have an impressive advantage of potentially simple implementation on existing infrastructures, requiring only small modifications.

In this thesis, we have investigated and designed a prototype VLC system using LEDs traffic lights as emitter for road safety applications. LEDs illumination characteristics are examined. A model is developed for sets of LEDs for maximum illumination in desired service area. An isolated traffic light, and a traffic light system set-up for multilane road model are developed and the associated optical channel is investigated and analyzed. The Optoelectronics part of both the transmitter and receiver are designed with discrete components while the rest of the systems transceivers are designed and implemented in FPGAs, [56] using two development kits with a Spartan FPGA. Since the data transmission rate is in the few tens of kilo bits per second (kbps), and the channel is expected to be noisy, we have used Direct Sequence Spread Spectrum (DSSS) based Sequence Inverse Keying (SIK) [16] as a modulation scheme. DSSS system is a robust technique able to mitigate the effect of noise. The performance of this VLC system has been evaluated in both a closed pavilion and outside on road lane. It is found that with a 200mm diameter traffic light, integrating 240 high brightness LEDs, it is possible to transmit data around 50m of distance in the absence of sky brightness and around 40m with bright skies.

1.2 Thesis Motivation

The area of ITS is directly related to human and material safety. It uses many technologies to prevent losses and reduce casualties. Advanced Driver Assistant Systems (ADAS) based on VLC is an important concept for road safety applications in ITS. VLC systems, though with high potential to be an integral part of ITS, because of ubiquitous infrastructures support have not been deeply investigated. Therefore, there is a great need to explore this research area and analyze its novel applications in road safety. Furthermore, VLC systems are cost effective, use LEDs and the unregulated visible spectrum. Hence, they are expected to offer broad potential

applications. The research work in this thesis is focused on the outdoor applications of road safety.

1.3 Methodology

The main objective of this research work is to explore the feasibility for efficient and cost effective realization of VLC for road safety applications. Such study involves huge and diverse works, as VLC realization especially in outdoor scenario is challenging. Thus we structure the work in different phases.

In the first place, a feasibility study was carried out and possible challenges were identified. LED-based emitter was characterized. Secondly, an emitter model using arrays of LEDs was designed and developed. In addition, an LED-based traffic light model for emitter or VLC transmitter was designed. Based on available infrastructures, a LED-based traffic light as VLC transmitter was designed and implemented.

In the next phase, the characterization for both the receiver and channel was performed. The VLC channel (optical channel) is different from the free space wireless radio channel. It is dependent on atmospheric variations and many external sources of light such as, natural and artificial which affect the performance of the VLC systems. Therefore, characterization of optical channel and noise is an important segment where attention is needed.

The VLC technology for this application demands a robust modulation technique to minimize the effect of noise interference caused from various sources of light. Finally, the VLC systems were implemented and performance was analyzed.

In the process of investigation and realization, there were multiple software tools and resources used throughout the research work. They are described in the next section.

1.3.1 Software Resources

Realizing a VLC system involves many software tools and resources. Any developed model needs to be examined and verified through simulation and then integrated in hardware. Most of the simulations were performed on Matlab 2009a and R2010a and models were developed

and tested on Matlab/Simulink. The light tools (iLight) and VPI were used for examining the illumination coverage/patterns and LEDs characterization. Matlab was used for model development and simulation study for the expected performance. Simulink model was used to develop complete VLC communication systems assuming various approximations close to the parameters found in characterization. Two different receiver architectures model were developed and examined for their consistency.

Analogue electronics parts of transmitter and receiver were first designed using the EDA tools PSpice and OrCad. They were simulated for the desired response. Using discrete components, the optoelectronic parts were developed in hardware as prototype to validate the simulation results.

An FPGA development kit Spartan SP305/605 was used for the implementation of configurable (signal processing) parts of receiver and transmitter. The results were compared from Simulink model and Xilinx ISE software FPGA implementation.

1.4 Original Contributions

This thesis work comprises several aspects in the realization of visible light communication systems. This work was developed aiming for road safety application area. There are a number of original contributions in this research work. The major contributions are designing a conceptual VLC system and its associated modules, characterization, development and design of the emitter model for LED-based traffic lights. Another key point is the modulation and demodulation technique suitable for VLC broadcast systems.

The conceptual design was important in the beginning to realize the system. This work was reported in the following conference and journal.

[1] Navin Kumar, Nuno Lourenço, Michal Spiez and Rui L. Aguiar, "Visible Light Communication Systems Conception and VIDAS," IETE Technical Review, vol. 25, no. 6, Nov-Dec 2008. (Awarded *Gowri Memorial Award* [India] for the best paper in 2009.)

[2] Navin Kumar, Luis Nero Alves, and Rui L. Aguiar, "Visible Light Communication for Advanced Driver Assistant Systems,"7th International Conference on Telecommunication (ConfTele'09), Feb. 2009.

Another important original contribution in this respect is the submitted paper for IEEE ITS magazine and a book chapter which is one of the supportive conceptual designs of VLC layer architecture.

[3] Navin Kumar, Luis Nero Alves, and Rui L. Aguiar, "VLC Layer Architecture for ITS," Submitted to IEEE Intelligent Transportation Systems Magazine, (Feb 2011).

[4] Navin K., Luis Nero Alves and Rui L. Aguiar,"Traffic Light as Road Side Unit for Road Safety Information Broadcast using Visible Light Communication", Submitted as book chapter to IGI Global for the book Roadside Networks for Vehicular Communications: Architectures, Applications and Test Fields, (Mar 2011).

The development and design of an emitter model was necessary for higher and uniform illumination distribution. There are many design parameters involved in traffic light system set-up. These parameters were optimized through series of simulations. The work and detail investigations were reported in the following papers.

[1] Navin Kumar, Luis Nero Alves, and Rui L. Aguiar, "Design and Analysis of the Basic Parameters for Traffic Information Transmission Using VLC," Proc. of IEEE, (Wireless Communication, Vehicular Technology, Information Theory and Aerospace and Electronic Systems Technology (Wireless VITAE'09), pp. 798 – 802, May 2009.

[2] Navin Kumar, Nuno R. Lourenço, Luis Nero Alves, and Rui L. Aguiar, "LED-based Traffic Light Emitter Model for Road Safety Applications", under review to "Elsevier Journal of Transportation Research: Part C", TRC-D-11-00081, Apr. 2011.

Using an appropriate modulation for communication systems is another key requirement. We have proposed and developed DSSS based SIK modulation technique for this application. It has been tested in Matlab/Simulink and implemented in FPGA for robustness and reliability. The work is reported in the following papers.

[1] Domingos Terra, Navin Kumar, Nuno Lourenço, Luis Nero Alves, and Rui L. Aguiar "Design, Development and Performance Analysis of DSSS-based Transceiver for VLC", IEEE Proc. International Conference on Computer as a Tool, (EUROCON'2011), Lisbon, pp. 1-4, Jun. 2011.

[2] Navin Kumar, Luis Nero Alves, and Rui L. Aguiar, "Performance Study of Direct Sequence Spread Spectrum Based Visible Light Communication Systems for Traffic Information Transmission" (in the process of submission)

The whole systems with some of the partial performance evaluation were reported in the following conference:

[3] Navin Kumar, Domingos Terra; Nuno Lourenço; Luis Nero Alves, and Rui L. Aguiar," Visible Light Communication for Intelligent Transportation in Road Safety Application", IEEE Proc. 7th International Wireless Communication and Mobile Computing Conference (IWCMC'2011), Vehicular Communications Symposium, Istanbul, pp. 1514-1518, Aug. 2011.

Apart from the above, there are few minor contributions such as characterizing outdoor optical channel, measurement and characterization of noise, characterization of receiver, implementation in FPGA and development of optoelectronics devices.

1.5 Thesis Organization

The work reported in this thesis is divided in seven chapters. The content of the following chapters is briefly described.

Chapter 2 presents brief description of ITS and vehicular communications. In this chapter ongoing development of ITS architecture and existing communication facilities are discussed. It is also described, why VLC is important in ITS and how can it be integrated into ongoing development of ITS. Some of the important application scenarios are also illustrated. This chapter also differentiates VLC from radio communication systems. Conceptual design and VLC architecture for traffic broadcast systems are presented. Finally, some of the recent

advancement, developments and important challenging issues in realization of VLC systems are outlined.

In chapter 3, two main issues are discussed: LED based traffic light emitter model, and channel and noise characterization. Road illumination using LEDs and traffic specifications for visibility perspective are also discussed. An emitter model is developed for an array of high brightness LEDs for uniform illumination distribution and coverage of service area (area of data transmission). In this chapter, we have also discussed and characterized channel variation and noise caused by natural as well as artificial light sources. Important simulation and experimental results are presented.

Chapter 4 describes the modulation technique in detail. Various candidates for modulation methods are discussed and their performances are analyzed. Based on the performance and the results especially in noisy environment, a direct sequence spread spectrum based sequence inverse keying modulation is recommended. This modulation is found to be suitable for low data rate in outdoor applications such as traffic information broadcasting. Model for VLC systems are developed in Matlab/Simulink to verify the analytical and simulation results. The VLC system models are developed for two receiver architectures in Matlab/Simulink and their performances are evaluated.

VLC systems design and implementation is presented in chapter 5. In this chapter, first optoelectronic hardware design of VLC transmitter and receiver are presented. The later part of chapter deals with implementation of prototype in FPGA. Brief discussion on main building blocks is discussed. Finally, result from Simulink model and FPGA implementation of VLC system is compared.

In chapter 6, the experimental validation is discussed. Experiments are performed in different environments and conditions and important results are presented.

Chapter 7 reports the concluding part of the thesis. Some guidelines for future study and investigation are also discussed.

CHAPTER 2: VISIBLE LIGHT COMMUNICATION SYSTEMS FOR ITS

Summary

There is great concern over growing road accidents and associated fatalities. In order to reduce the accidents, congestion and offer smooth flow of traffic, several measures such as providing intelligency to transport, providing communication infrastructure along the road, vehicular communication and likewise are being undertaken. Traffic safety information broadcast from traffic lights using VLC systems is a new cost effective technology which assists drivers to take necessary safety measures. VLC Systems exploit the inherent characteristics of LEDs of high data rate switching without interruption to the primary use of signaling or lighting. Leveraging from the benefits of using existing infrastructures, VLC systems are going to play very important role in ever increasing road safety applications in ITS. This chapter presents an overview of ITS and vehicular communication systems. It also presents how the VLC systems can emerge an important access network in ongoing ITS architecture. Some of the important characteristics and benefits over most popular radio systems are also highlighted. Finally, a brief description of VLC systems architecture is presented focusing on information broadcast systems.

2.1 Introduction

The application of information and communication technology (ICT) to surface transport is called “Intelligent Transportation Systems”. ITS provides the ability to gather, organize, analyze, use, and share information about transportation systems. In the modern world, this ability is crucial to the effective and economical construction and operation of transportation systems and to their efficient use. ITS is being incorporated by manufacturers in “intelligent equipment” that can be installed as part of the transportation infrastructures to gather and disseminate traveler information, control traffic signals and variable message signs, electronically collect tolls, and help manage the system. In fact, information and communications technologies are extensively used in ITS for road safety, both at the roadside and in the vehicle itself.

Increase in fatality on road is becoming severe even with the introduction of many intelligent and communication devices on board vehicle and alongside road. Road crashes are the leading cause of death globally especially among young people. The report from the World Health Organization (WHO) [11] predicts further increase in death in future even with the use of many safety devices.

To minimize road accidents and fatalities, various modes of vehicular communications, such as vehicle-to-infrastructure (V2I), vehicle-to-vehicle (V2V) and infrastructure-to-vehicle (I2V) are being investigated. Emergence of IEEE 802.11p standard [12] for short to medium range inter-vehicle communication and the allocation of a dedicated frequency band for ITS communication in Europe have paved the way for future implementations of communication-based ITS safety applications. The standard 802.11p for vehicular environment [34] or WiMax currently contribute to road safety. The Car2Car Communication Consortium [78] is dedicated to the objective of further increasing road traffic safety and efficiency by means of cooperative ITS with Inter-Vehicle Communications supported by Vehicle-2-Roadside Communications and vice versa. ITS [75] are new transport systems for the purpose of the minimizing road transportation problems, aiming for efficient traffic flow

and reduction of the environmental load. A lot of research activities in ITS are seen recently to solve various traffic problems.

Many ITS related projects such as SAFESPOT [79], PREVent [76], and CALM [77] are being investigated to reduce road fatality. VIDAS (VIsible light communication for advanced Driver Assistant Systems) is another challenging project which promises to be used on existing infrastructures resulting in low cost communication systems. VLC is normally based on LEDs which have many advantages such as highly energy efficient, long life, harmless to human and friendly to environment (green technology).

LED-based VLC [62] systems can be deployed in vehicular environment on existing infrastructures such as LEDs traffic signal lights. The VLC systems broadcast road traffic safety information minimizing the possible accidents and increasing smooth flow of traffic on road. Furthermore, LED-based road lights can offer ubiquitous road to vehicle communication (URVC) [44] throughout travel.

This chapter introduces how a VLC system can be efficiently deployed in ITS and play key role in ever increasing road safety applications. This chapter also presents benefits of using VLC systems as access networks and how the system can be integrated in ongoing ITS architecture. System architecture for information broadcast is discussed highlighting important differences and merits over most popular radio frequency solutions.

2.2 Brief Overview of ITS

With the growth of population in major urban areas and accelerated increase in number of cars, traffic is becoming generically chaotic. The problem of congestions not only affects the day-to-day life of citizens but also has a great impact on business and economic activities. These issues therefore generate less income, affecting the sustainable growth of cities throughout the world.

Considering current problems of traffic management, control and planning, especially fearing the consequences of their medium and long term effects, both practitioners and the scientific communities have strived to tackle congestion in large urban

networks. Research has been carried out basically towards the design and specification of future transport solutions featuring autonomy, putting the user in the centre of all concerns and largely oriented to services. Such efforts were eventually to culminate in the emergence of the concept of ITS. Now the user is a central aspect of transportation systems, forcing architectures to become adaptable and accessible by different means so as to meet different requirements and a wide range of purposes.

Two of the main features of today's intelligent transportation are as follows:

Automated computation is an important requirement of ITS. Future transport systems must make decisions automatically, analyzing input information and acting accordingly, triggering coordinated actions to improve system performance. Demand for flexibility and freedom of choice is another important aspect on the user's side. The current lack of flexibility in transportation systems limits their potential to users, especially in what concerns personalized services, which is a major target for criticism by many users. ITS then should be open to flexibility, different options and driver choices, as well as personalized services. As transportation systems are greatly dependent on the network topology and other characteristics, intelligent infrastructures become fundamental. New communication technologies, including mobile, wireless and ad-hoc networks are improving infrastructures a great deal, enabling it to become an active and interactive part of the system.

A distributed architecture accounting for asynchronous, control algorithms, coordination and management autonomous elements is undoubtedly one of the major currently researched areas of ITS. There are several requirements that must be satisfied, from user-centered to service-based functionalities, turning intelligent transportation into a complex, heterogeneous and intricate artificial society. Current research already considers that ITS architecture must explore distributed algorithms using exogenous information from various sources, making greater use of parallelism and asynchronous capacities of pro-active entities.

ITS encompasses a broad range of wireless and wired communications-based information, control and electronics technologies. When integrated into the transportation

systems infrastructures, and in vehicles themselves, these technologies help monitor and manage traffic flow, reduce congestion, provide alternate routes to travelers, enhance productivity, and save lives, time and money. Based on wireless short-range technology, vehicles are able to exchange information with road side units (RSUs) spontaneously. However, with advancement of long range wireless systems, vehicles are able to communicate among themselves. The following sections give a brief detail of vehicular communication and the offered services.

2.2.1 Vehicular Communications

Both academia and car manufacturers are progressively paying more and more attention to Vehicular Communications (VC), that allow vehicles to connect to each other and with the roadside infrastructure to form a Vehicular Ad-hoc Network (VANET). VANETs [35, 36] are special types of mobile ad-hoc networks (MANETs) [80], where wireless-equipped vehicles spontaneously form a network while traveling along the road. The nodes of a VANET are commonly divided in two categories: On-Board Units (OBU), that are radio devices installed on vehicles, and RSU, that constitute the network infrastructure. RSUs are placed along the roadside. VC will enable the development of systems to support several services, for instance road safety, traffic information diffusion, automatic tolling and entertainment [37]. VC is regarded as being a major innovative feature for in-car and V2I technology. Thus vehicular communication combined with ITS is becoming extremely important. They offer numerous of services in vehicular environment.

2.2.2 Important Services in Vehicular Environment

One of the important factors of success of a technology is its different kinds of applications and offered quality of services. With the expansion of applications scenarios from safe navigation and collision avoidance to content distribution, emergency operations recovery (natural disasters, terrorist attacks, etc.) and urban pervasive sensing, a brand new set of services will emerge in the Vehicular Network, such as priority oriented broadcast of vehicle alarms, vehicle to vehicle routing, and so on. The new vehicular applications will also place

new service requests to the Internet infrastructure, such as geo addressing as opposed to (or in addition of) traditional IP addressing, directory service support, service discovery, mobile resource monitoring, and mobility management [81].

There are many high priority road safety applications and services of VLC systems in vehicular environment. All of them assist drivers making safe decisions in traffic and complying with traffic regulations. The traffic signal violation warning and curve speed warning applications allow infrastructure to transmit to vehicles, traffic light states and road curvature respectively.

Vehicular applications span different network scenarios as discussed before and require a range of network services. Furthermore, the information dissemination in these scenarios can occur over multiple hops or be limited to single hop. These network services, either stand-alone or combined, provide all the services required for vehicular applications. Main network services for the support of various applications are given in Table 2-1 [12].

I2V or Roadside-to-Vehicle Communication (RVC) Systems assume that all communications take place between roadside infrastructures (including RSUs) and vehicles. Depending on the application, two different types of infrastructure can be distinguished, sparse RVC (SRVC) and ubiquitous RVC (URVC) systems. SRVC systems are capable of providing communication services at hot spots. A busy intersection scheduling traffic light, a gas station advertising its existence (and prices), and parking availability at an airport, are examples of applications requiring an SRVC system. An SRVC system can be deployed gradually, thus not requiring substantial investments before any available benefits.

An URVC system is the holy grail of vehicular communication: providing all roads with high-speed communication which would enable applications unavailable with any of the other systems. Unfortunately, an URVC system may require considerable investments for providing full (even significant) coverage of existing roadways (especially in large and developing countries like the India, China, etc.).

Table 2-1: Vehicular Network Services

Network Services	Description and important applications/services
I2V one-hop Broadcasting	Required by traffic signal violation warning and curve speed warning applications. Combined with the V2I one-hop anycasting, it can provide service for the left turn assistant, and stop sign movement assistant applications where bi-directional information exchange between the vehicles and infrastructure nodes is required.
V2I one-hop Anycasting	On receipt of information, infrastructure node processes through backbone network. This network service, along with I2V one-hop broadcasting service, can be combined with the multihop inter-vehicle forwarding. The combination maximizes the utilization of the backbone infrastructure network and vehicles as relays and the chance to reach every node.
Multihop Inter-vehicle Forwarding	In this case each vehicle acts as a relay and forwards data packets following a set of rules to prevent unnecessary broadcast flooding, e.g., there is a time-to-live limit on each packet, and a packet is forwarded only once by each vehicle. This network service maximizes the possibility that information is disseminated quickly and reliably among a large number of vehicles. Therefore, it is suitable for providing service to event-triggered, urgent message delivering applications, such as cooperative forward collision warning, pre-crash sensing, and emergency electronic brake lights.
Limited Neighbor Broadcasting	This service also operates in the V2V scenario, but over single hop. Each vehicle broadcasts information from all of its transmitters to its neighboring vehicles. But, the information dissemination is limited to one hop, and the neighboring vehicles do not forward information that they receive. Thus, this network service only provides vehicles with information in close vicinity; by limiting the extent of broadcasting. It prevents network performance degradation due to high volume flooding. Thus, it provides service to the applications that need periodic, local information. For example, the lane change warning application requires this network service because vehicles constantly need to know about the positions of the nearby vehicles when making lane changes, but information from other distant vehicles is irrelevant.
Vehicle-to/from-Infrastructure Unicasting	The vehicle-to/from-infrastructure unicasting network service takes place in the V2I and I2V network scenarios, with each scenario providing uplink and downlink for vehicular Internet access applications respectively. This service works over single hops and multiple hops to/from a gateway infrastructure node. By using routing protocols, vehicles first find routes to a gateway infrastructure node and then start transmission to that gateway, which may use other vehicles as relays. This service requires routing protocols to discover routes, and other services find paths to vehicles and infrastructure nodes via single hop transmissions and multihop broadcasting.

However, for these services and applications; vehicular networks require interaction in virtually all levels. In fact ITS, rely on distributed and advanced communication infrastructures. Interoperability and integration become crucial in this scenario. This novel scenario has been motivating and challenging practitioners and scientific community. In the following section, we highlight ongoing development of ITS architectural scenario to accomplish this.

2.3 ITS Architecture and Communication Facilities

ITS will have a great and positive effect on future mobility of people and goods. ITS use a number of technologies and many more are likely to be used as we progress. The integration of information and communication technology with road infrastructures and vehicles leads to cooperative systems that help to improve road safety, traffic efficiency, transportation times, fuel consumption, and driving pleasure. Connecting cooperative systems to backend services, ITS enable the integration of up-to-date road traffic information into business processes of central IT systems. The ITS network reference model has to be tied to the specific interconnections between the transportation systems or subsystem, e.g., connection between Information Service Provider (ISP) subsystem and a vehicle subsystem (VS). A brief description of ITS architecture and ongoing development is presented in the following section.

2.3.1 ITS Architecture

European Telecommunications Standards Institute (ETSI) has contributed significantly towards development of ISO TC 204 ITS architecture [77]. It is considered a major breakthrough in the area of ITS. ITS development is strongly driven by large-scale research and development projects on cooperative systems (CVIS, SAFESPOT, COOPERS) complemented by more focused projects (GEONET, SEVECOM) [80, 81]. To consolidate these efforts towards a European solution, the COMeSafety project [83] defines a common European ITS communication architecture as a basis for future development and standardization. This architecture framework is currently being refined and complemented by

the European research and development project PRE-DRIVE C2X [84] working towards future field operational tests for cooperative systems.

In summary, the COMeSafety architecture framework specifies reference protocol architecture of ITS systems. The ITS represents a generic component for vehicles and roadside communication infrastructures. The reference protocol architecture basically obeys the ISO/OSI reference model, vertically extended by a management and security layer (Fig. 2.1).

The ITS standards [75, 38] promise to offer various access technologies. This family of standards specifies a common architecture, network protocols and communication interface definitions for wired and wireless communications using various access technologies including cellular 2G, 3G, satellite, infrared, 5GHz micro-wave, 60GHz millimeter-wave, and mobile wireless broadband. These and other access technologies that can be incorporated are designed to provide broadcast, unicast and multicast communications between mobile stations, between mobile and fixed stations and between fixed stations in the ITS sector. Networking and Transport layer offers Internet connectivity and routing and consists of many basic

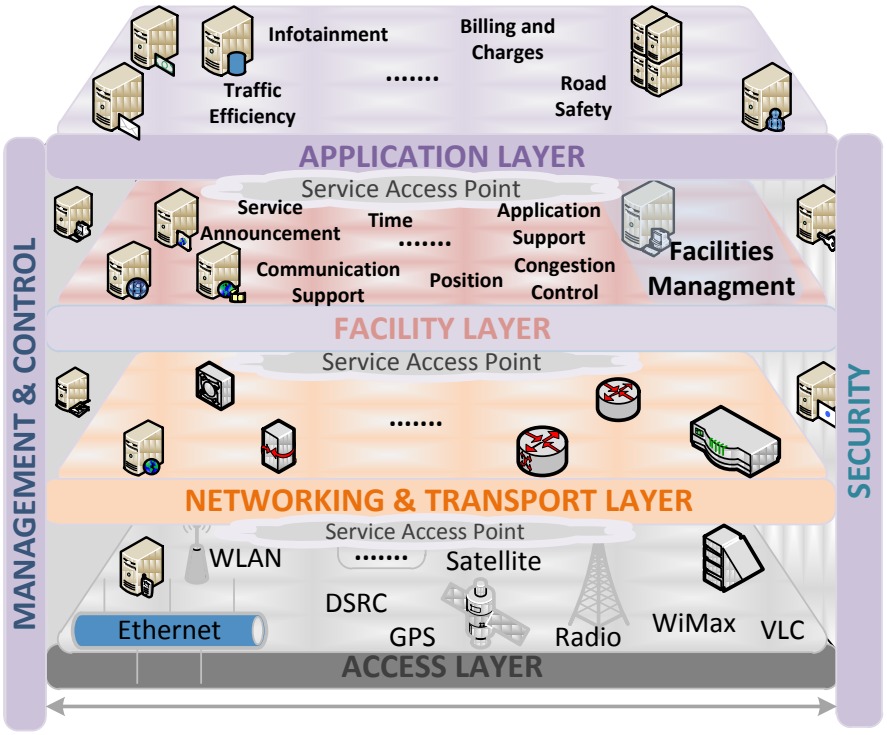

Fig. 2.1: Reference Model for ITS

transport protocols and Internet protocol specifically IPv6. For communication support, application support, service announcement and so on, facility layer is included into the model while safety related, efficient traffic relay and value added dedicated applications are handled using application layer. A security layer monitors and offer authentication for extended services and applications. A management and control layer becomes necessary for the reference model for proper control and operation of various components.

The National ITS [75, 84] architecture can be viewed as a framework that ties together the transportation and telecommunication world. This framework enables the creation and effective delivery of the broad spectrum of ITS services.

There are also many challenges in interconnecting the dissimilar components of any end-to-end ITS solution, encompassing various transportation and communication issues. It has been critical, therefore, to promote an architectural concept that mitigates the complexity of interconnecting many transportation systems with multiple types of communication links. A brief description is given below.

2.3.2 ITS Communication Architecture

A generic communication architecture for ITS is given in Fig. 2.2. The ITS communication architecture encompasses communication systems designed for ITS and made of four physically separated subsystem components:

- the vehicle subsystem component (Vehicle Station),
- the mobile subsystem component (Personal Station),
- the roadside subsystem component (Roadside Station),
- the central subsystem component (Central Station);

ITS communication architecture contains the ITS subsystem components and usually a vehicle gateway connecting the ITS Station to legacy systems. The vehicle requires a vehicle gateway connected to the vehicle station and to the vehicle manufacturer's proprietary vehicle network. These components are inter-linked by a communication network. The communication between the vehicle subsystem component and the mobile subsystem

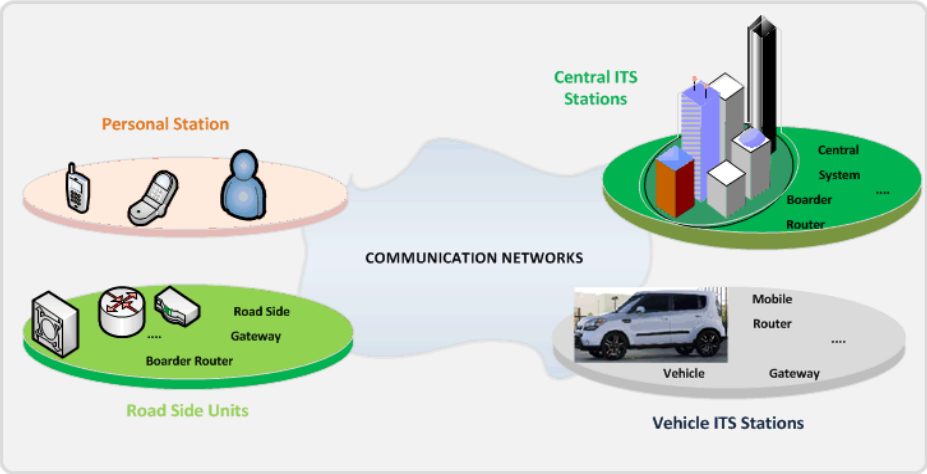

Fig. 2.2: ITS Communication Architecture

component are performed over a short range wireless or wired communication media. Similarly, vehicle communication systems interact with RSUs which consist of many communication infrastructures and access networks. Access point routers, variable message sign and gateways are responsible for offering information data connectivity between mobile units (vehicles) and Internet. However, these radio systems are not cost effective. It is very difficult to use wireless based access point all along the road at small intervals.

Radio and VLC System Comparision

The Radio Law does restrict the free usage of the radio wave wireless communication. On the other hand, the VLC does not require any license at present. Also, due to the limited licensed bandwidth, the radio spectrum is becoming increasingly congested. In summary, the radio wireless communications have the following several problems although they are widely in use in cell phones and wireless local area networks (LANs).

- the electric transmission power cannot be increased because of harm effects to the human health which has been acknowledged by WHO recently [13];
- due to radio wave restrictions, frequency bands are licensing congested.

These radio wave problems above are effectively mitigated by VLC.

A LED-based VLC system would consume less energy than the radio system, allowing the expansion of communication networks without added energy requirements and potentially

reducing carbon emissions over the long term. This technology leads a Green growth as it uses eco-friendly IT green technology which is an added benefit to ITS. In comparison to the radio wireless communication, VLC systems have the following main advantages:

- there are no licensing requirements or tariffs for its utilization;
- there are no RF radiation hazards, visible light is very safe for humans. Visible light has been around since the dawn of human kind.
- it has a large bandwidth, which enables very high data rates;
- it has low power consumption –most of the power is spent on the traffic signaling;
- lights are set everywhere. Then, wireless transmission can be easily established through the VLC device attached to the lightings/infrastructures.

2.4 VLC in ITS

VLC systems can play a key role in ITS from broadcasting important traffic information to V2V and vehicle2infrastructure communication facilities. Authors in [63] carried out basic study on traffic information system using LED traffic lights. They analyzed basic performance and defined a service area for requisite data rate using basic intensity modulation. Road-to-Vehicle communication system using LED traffic light was discussed in [64, 39]. The authors in this study proposed a parallel optical wireless communication system based on LED traffic light as transmitter and high speed camera as receiver. They discussed modulating LED individually and receiving by its corresponding camera. A communication protocol for the inter-vehicle communication system was proposed in [40]. The proposed system configures a dynamic code division multiple access (CDMA) network by changing the spreading code using code hopping technique on every packet. A new fast responding VLC receiving system in ITS based on photo diode (PD), the imaging optics and tracking mechanism was proposed by authors T. Hara et al.[65].

VLC is not only suitable for a broadcast system as road-to-vehicle or I2V communication systems but it can be equally effective in V2V and V2I communication systems. In case of V2V scenario, a vehicle in the front of traffic lights receives the traffic

safety information and passes it using the brake lights to the vehicle running behind. They can even form vehicle ad-hoc network and share information among themselves. An example of a scenario is illustrated in Fig. 2.3. Similarly, the running car can request information from RSUs using LED-based front head light thereby forming a full duplex communication systems.

RSUs such as, LED-based traffic lights are well suited for broadcast communication in I2V mode [41] of vehicular communication systems. Traffic safety related information can be continuously broadcasted without extra power usage enhancing smooth traffic flow as well as reducing accident fatality. The light emitted from a traffic light (consisting of an array of LEDs) is modulated at a frequency undetectable to human eyes. The modulated light is then detected by a photo detector (PD) based receiver on the vehicle, providing useful safety information to the driver in advance. More advanced perspectives may employ inter-vehicle communication means, as a way to convey information between vehicles stopped near traffic control posts.

Hence, LED-based traffic light offers a very suitable option to be included as RSU and integrated with ITS architecture [42]. One of the suitable scenarios of interaction and communication from RSU to vehicle communication is presented in Fig.2.4

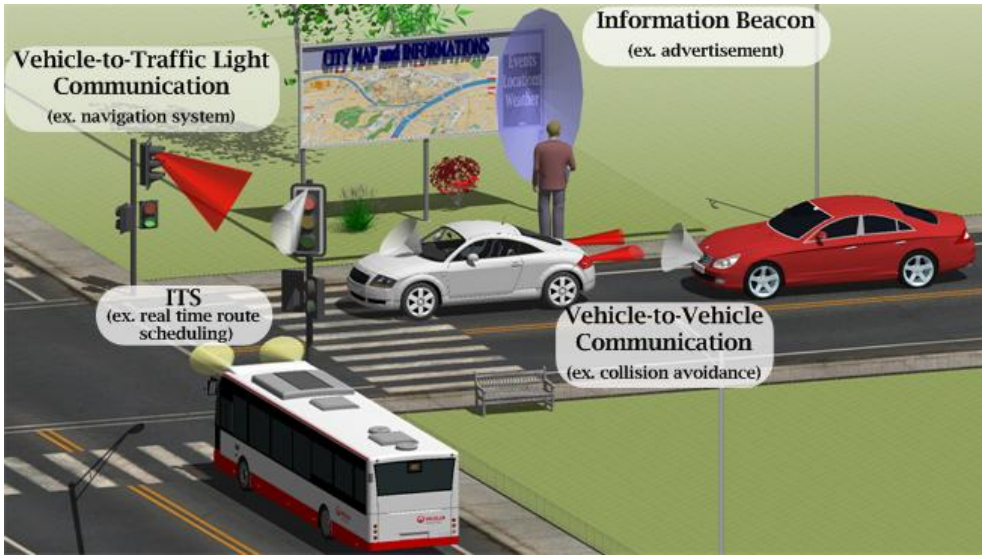

Fig. 2.3: Application Scenario Outdoor

2.4.1 LEDs Traffic Light based VLC in ITS

LED Traffic lights working as emitters for VLC systems can be used for broadcasting safety information in ITS for the reason that traffic light already exists, and replacement of LED-based traffic lights in many cities worldwide is currently underway. Even vehicles are now equipped with LEDs brake and head lights. They are environment friendly and have better visibility. Therefore, VLC can be considered as a supplementary communication systems not only for broadcast but also uplink communication connectivity and V2V communication facility. However, we have focused mainly in a broadcast system using LED-based VLC system for road safety applications.

Along with many access technologies, LED-based VLC can be used. An additional traffic control and monitor unit is included which can provide additional support information in conjunction with other RSUs. In this systems therefore, integrating LED-based traffic light unit for broadcasting safety related information offer a cost effective method of implementation. Since, replacement of conventional traffic light with LED-based traffic light is getting momentum, it is highly desirable to use the dual function of LED; in this case signaling and traffic broadcast unit. The integration of traffic light VLC systems will also minimize the use of IR and short range based costly communication infrastructures. Furthermore, in the long run it will support the ubiquitous road communication throughout the travel using LEDs road illumination systems [44]. It is possible to use ubiquitous communication infrastructures, such as, wireless access point routers, variable message sign and gateways for offering information data connectivity between mobile units (vehicles) and Internet. But this solution is

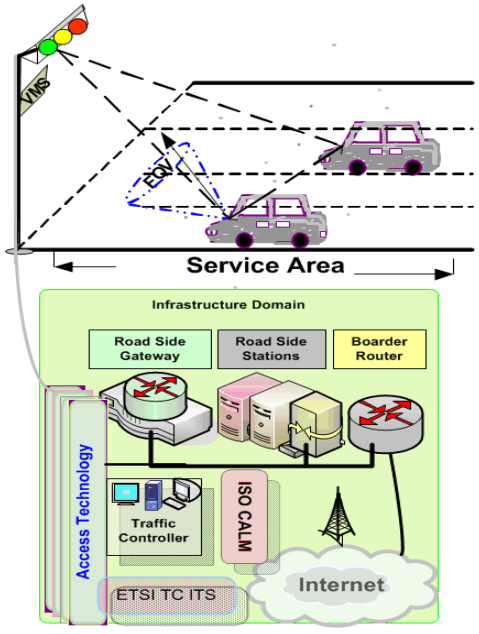

Fig.2.4: A scenario of Traffic Light Integration with ITS Architecture

not cost effective. It is very difficult to use wireless based access point all along the road at small intervals.

For VLC to be used, no major changes in the infrastructure are needed from the emitter side. On the other hand, receivers are very low cost, and so no embryonic light receivers are required as automatic light sensors are common components in cars. The following sections present VLC system architecture and discuss the function of the major blocks.

2.4.2 VLC System Architecture

VLC is a fast-growing technology able to provide data communication using low-cost and omni-present LEDs and photodiodes. It uses the visible spectrum (as shown in Fig. 2.5) in the range of approximately 390nm-750nm between IR and UV. Therefore, much of the properties and technological details from IR are useful and relevant for the investigation of VLC. However, it remains one of the least researched areas. In this section, we introduce a basic VLC transceiver system. The block diagram representation along with brief description of transmitter and receiver are presented.

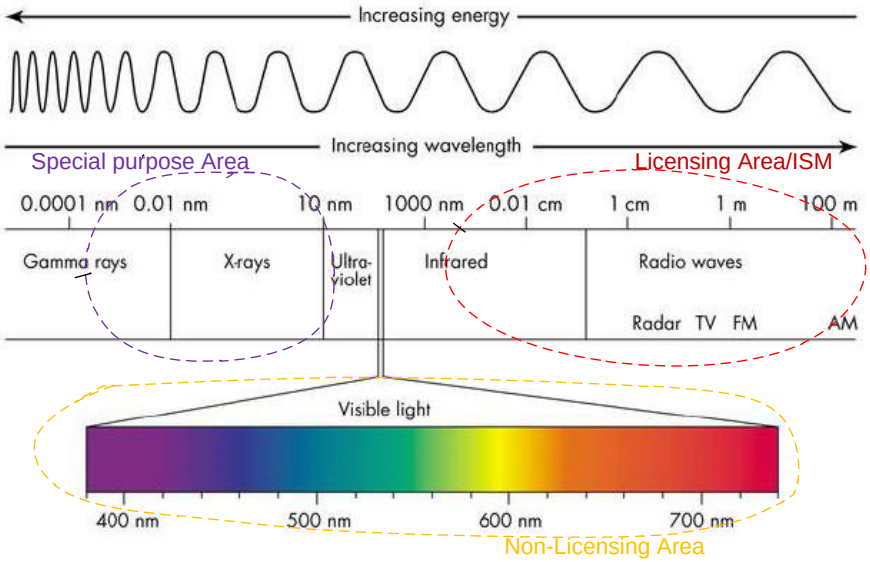

Fig. 2.5: Frequency Spectrum

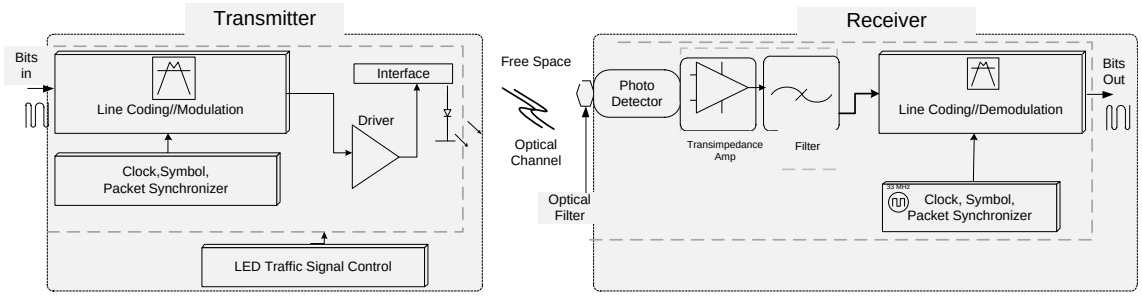

Fig. 2.6: Transceiver Block Diagram Representation

The block diagram representation of VLC systems architecture [60, 61] is shown in Fig. 2.6. Devices such as laptop, mobile phones can be used for transmitting and receiving information signal. The transmitter part consists of a light source, modulator and a pulse shaper to switch the LEDs at the rate of data transmission. The light source emits data using light wave as the medium while illuminating. Data is sent between two or more terminals.

2.4.2.1 VLC Transmitter

A VLC Transmitter (also called emitter) is an electro-optical transducer device that transmits information using visible light waves over the transmission medium. VLC systems have become a more viable technology for the future of wireless data transmission, in large part due to the developments in the area of solid-state lighting.

The digital data signal is passed to a data encoder that modulates the signal with the purpose to switch the LEDs at the expected rate of data transmission. The modulation method used must offer high robustness to background light and at the same time, light should be as bright as possible. Intensity modulation/direct detection (IM/DD) often used in IR can also be used in VLC. Other option is pulse position modulation (PPM), which specifies the modulation of information on the light carrier [17, 19]. This way information is formatted before applying to the carrier. Spread Spectrum is another technique that can be considered. (Chapter four discusses various modulation schemes). It increases resistance to interference and jamming, and also allows the establishment of secure communications.

In a practical aspect, the modulator also receives information from the traffic control unit so that it can hold information while the light colour changes. This ensures: (i) there is no

transmission in the brief period of change in traffic signal; and (ii) transmission is synchronized. The resulting signal is then used to control the switching of the LED through the output driver. The output driver combined with the control signal should ensure sufficient optical power, in order to achieve the expected range of communication. Sometimes the electrical characteristics of the different colour LED's, like the maximum forward current or the forward voltage, might imply the usage of an output driver with distinct channels and a slightly different switching.

The encoder can be integrated, or the range of input signals specified. To build this block, a microprocessor is a relatively cost effective solution but upgrading it is not an easy process. Using an FPGA would be more expensive, but has better data processing capabilities, and it also makes upgrading easier. In the front-end electronics, integrating the LED matrix is essential to specify power consumption, optical range, and maximum operating frequency.

VLC data rate is limited by the switching speed of the emitter LEDs. On the other hand, long distance communication is limited by the transmitted power and background light sources.

2.4.2.2 VLC Receiver

The VLC receiver is an optic-electronic transducer that receives information, previously modulated in the visible light spectrum, and converts it into electrical signal capable of being processed by a demodulator-decoder. The correct design of this device is crucial to ensure good performance of the overall VLC system. Among other concerning factors are the presence of low-level signals and high noise interference.

The visible light pulses, originated at the system's emitter, are collected in a photo-detector; an optical IR cut-off filter is a viable solution for eliminating unwanted spectral content. Reversely biased photodiode operates in the photoconductive mode, generating a current proportional to the collected light. This current has small values thus requiring pre-amplification to convert it into a voltage. This preamplifier should have low distortion and a large gain-bandwidth product. Transimpedance amplifiers represent the best compromise between bandwidth and noise for this kind of applications [18]. The resulting voltage is then

applied to a low-pass filter to remove any high-frequency noise. The signal is then further amplified in the final voltage amplifier stage. Also, DC signal filtering is applied at the input of the amplifying and filtering stages, which helps reduce the DC noise component of the captured signal as well as low-frequency components. The final voltage signal should correspond to the received light pulses which are then decoded in the final decoder block, thus extracting the digital data. This final block performs the inverse function of the emitter's encoder block, but it can also be implemented with a microprocessor or, even better, an FPGA. The demodulation scheme will depend on the modulation scheme used in emitter side. A practical down-conversion technique that can be considered is direct detection. Clock recovery is necessary to synchronize the receiver with the transmitter. In addition, the system will also need the protocol management unit and data/clock recovery block for the synchronization of received packets.

The detector is characterized by the parameter field of view (FOV), responsivity, and area. For a larger service area, a receiver with a wider FOV is preferable. However, a wider FOV leads to performance degradation because of possibilities of receiving unwanted light signals. Among the received signals there are also many undesired noise components, which are processed simultaneously.

2.4.2.3 VLC Channel

One of the stringent requirements of VLC is direct line-of-sight (LoS). Though, in some instances of indoor applications diffused channel configurations are also used. A scenario of LoS and diffused links is illustrated in Fig. 2.7. The emitted light from LED carries data information in wireless medium. Thus, the intensity of light of the emitter becomes an important parameter on which range of transmission depends. There are many external light noise sources such as Sun light, road/street lights. These are the major issues to be considered in link design. They deteriorate/deceive the intensity of emitter light and may cause false triggering of the photo diode. Optical filters should be used to minimize this effect.

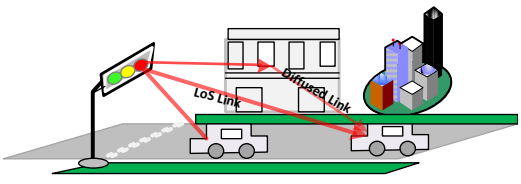

Fig. 2.7: LoS Link and Diffused Link Scenario

Overall, design of VLC systems for outdoor applications is complex and difficult. It involves different areas of knowledge such as optical, electronics, communication and networking. In the following section, we discuss recent directives and figure out important issues and challenges on the implementation of VLC systems.

2.5 Recent Directions and Challenges

VLC systems leveraging benefits from LED advancements have been recognized as one of the important technologies. This can be considered as ubiquitous for the reason that light can be made available at all places. Many devices such as PC, TVs, Cell phones and advertising boards use visible light. LED components are recently exploited by these devices. IrDA and small LED lamps attached to home appliances have been often utilized everywhere. VLC can be seamlessly employed in conjunction with these devices and terminals. Thus, it will be possible to have a human interface communication system which is secure, high-speed response, low power consumption and harmless to humans. VLC is very suitable to the ubiquitous environment in terms of human interface to assure comfortable human life. Towards this end, IEEE personal area network working group is discussing standardization issues of VLC technology.

Standardization: Important steps have already been taken by IEEE 802.15 VLC working group towards standardization [86]. The standard would be recognized as IEEE 802.15.7. The working group standardizes PHY and MAC for VLC personal area networks. They have been discussing for last two years and by the end of this year, they are expected to bring forward the draft version. Therefore, the technology is expected to be more popular in coming years.

VLC systems have multiple benefits, however a number of complex challenging issues need to be addressed. The first and the foremost, while the requirement of LoS link can be thought of as a drawback of the system, it becomes advantageous in the indoor from one room to another room or cell based links without interference from each other. There is no fear of interception from eves dropping. Some of the challenges are outlined as follows:

- Long Range Limitation: Because of LoS path requirement, the technology is suitable for short range communication.
- Ambient and other sources of intense noise: Especially in outdoor applications, overcoming and minimizing the effect of natural and artificial lights is a major challenging task.
- Increasing data rate: The limited bandwidth of LEDs is another major challenge for high-speed communication.
- Provision of Uplink: Using illumination sources is naturally suited to broadcast applications. Providing uplink communication will be problematic.
- Complex modulation: The most simple and useful modulation technique based on direct detection intensity modulation is too weak to overcome many challenges. A complex modulation technique would be needed to support effective and desirable data communication.
- Parallel communication (Optical multiple-input-multiple-output (MIMO)): It is an interesting scenario of VLC. Though, theoretically it can be realizable, the implementation would be a real challenge.
- Complex receiver based on equalizer: As an extension of IR, some studies proposed the use of equalizers at the receiver at the cost of increased complexity.
- Regulatory challenges: VLC is subject to regulation (in most cases) by non-communication standard such as eye-safety standard, automotive standard. Therefore, coordination across regulatory bodies and frameworks become challenging.

Some of the challenges aiming for outdoor applications in ITS for road safety are addressed in this work. For example, source model are discussed at length and suitable model is developed. A detail description of LED source emitter and LED-based traffic light model is presented in the next chapter to show how effectively LED-based emitter can be designed for VLC systems.

2.6 Concluding Remarks

In this chapter, importance of ITS, its architecture and vehicular communication systems were discussed. Important applications in outdoor scenarios and research progress were presented. VLC layered architecture based on Open System Interconnect (OSI) model is proposed. It was also discussed, how VLC can be incorporated in ongoing development of ITS architecture. Characteristics and differences from radio systems were highlighted. VLC architectures suitable for broadcast information were briefly explained. Major components of the systems were discussed in brief. Challenges in implementation of VLC systems were also highlighted.

CHAPTER 3: VLC EMITTER SOURCE MODEL AND CHANNEL CHARACTERIZATION

Summary

Visible light communication especially in outdoor environment is challenging. The light wave medium in free space for data transmission demands LoS path between emitter and receiver as well as sufficient radiation intensity from the emitter so that light is detected by tiny photo diode detector based receiver on the moving vehicles. The array of LEDs is used as emitter source offering necessary intensity for data transmission at the same time better visibility and preserving safety issues. In this chapter emitter source model and a LED-based traffic light system model is developed and designed for experiment. Important experimental results are presented.

This chapter also discusses channel characteristics. Optical channel depends on atmospheric conditions and varies over time. In addition, outdoor environment is subject to various kinds of noise sources from artificial and natural lights which will affect the performance of the system. Important sources of noise have also been discussed. SNR performance for various noise conditions is presented.

3.1 Introduction

VLC systems use LED-based emitter for information transmission. In ITS, LED-based traffic light emitter is also used for signaling at the same time. Furthermore, it is understood that a number of LEDs are needed to offer visibility at longer distance and data transmission, to cover a larger road area along the road length. Wide coverage of light illumination is expected to offer larger service area that is, the area in which data information is received reliably. Therefore, similar to the light illumination characteristic in the indoor environment, uniform and directive illumination becomes important. For example, light illumination pattern is different for illuminating road from that of traffic lights. Designing LEDs light for illuminating entire road may be easier than LED-based traffic lights; however, later one is cost effective. But combination of both of these resources will able to offer uninterrupted and ubiquitous communication throughout driving.

However, in the absence of LEDs road illumination lights, traffic lights VLC system's topology become dynamic and consequently characterized by the variability of the transmission channel. Emitter-receiver distance and ambient noise can change, making the signal-to-noise ratio (SNR) vary significantly in the outdoor optical communication channel. Shorter distances between emitter and receiver allow the use of higher transmission rates; on the other hand, an increase in the ambient noise intensity can be counterbalanced by the decrease on transmission rate.

It is known that in VLC communication, the connectivity is more important than the transmission rate, putting under an obligation that these systems must be provided with transmission rate adaptation mechanisms. This property allows the system to respond to the network topology and channel dynamic nature, also offering the perspective of use in multiple applications and granting compatibility guaranties with other existing systems.

Under this background, we discuss two main issues in this chapter. First, the design and development of an LED emitter and traffic system model for the desired illumination characteristics; and the second, characterization of optical channel and noise. Before a source

model is developed, road illumination pattern using LEDs lighting is discussed to understand ubiquitous connectivity along the road.

3.2 LEDs Road Illumination

LEDs have changed the concept of lighting not only in an expectation of the ultimate efficiency but also in tremendous opportunities for versatile and "smart" lighting applications. LED-based lighting technology, solid-state lighting [44-47] allows for unprecedented versatility in control over the radiation spectrum, which can be tailored for specific needs from general to medical and agricultural lighting, lighting for space flights, lighting for elderly, lighting for people with special colour needs, lighting for animals, lighting for museums and for illuminating art objects, and lights for theatrical productions [45]. Low-voltage driver, fast switching, and compatibility with networked computer controls enable intelligent lighting systems with software-controlled stability, operating function, adaptation, and energy savings. Such systems are expected to emerge and become disruptive and a revolutionary technology in the near future. We investigate and study road and traffic illumination pattern aiming for higher light illumination coverage.

LEDs usage is not limited to traffic lights and parking areas. It is expected that in large light sources such as road illuminations, LEDs will be utilized in near future. This will enable high quality communication. The road illumination using LEDs may remove many of the communication systems, for example, infrared (IR) beacons will not be necessary. Since, illumination will also be used for communication; large powers can be used efficiently while this was not possible with radio and IR communication. Therefore, it is expected to be able to communicate using wide band.

The illumination distribution is the function of height of emitter, radiation pattern/angle of emitter, FOV, half power angle of the receiver, tilt between emitter and receiver and distance between emitter and receiver. A possible scenario of LED road illumination is shown in Fig. 3.1. A study was conducted in 2003 by authors in [44] and through numerical analysis they showed that communication is possible using LED road illumination. LED radiation

pattern was approximated as Lambertian model. They considered two lanes one sided road and proposed a LED lamp post every 30m interval. They analyzed the SNR distribution along road for different receiver's attachment angle and FOV and observed that a data rate of around 100kbps is possible using this illumination technique.

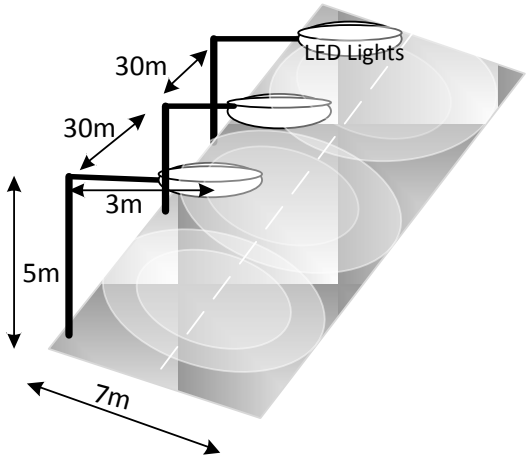

Fig. 3.1: LEDs Road Illumination Scenario

Road illumination and communication using white LEDs can be realized as proposed and discussed above. However, traffic lights use colour lens to produce red, green and yellow signs. Therefore, traffic signaling requires colour LEDs. In the recent past, various cities in the world [47, 48], [87] have replaced conventional traffic lights with LED-based traffic lights. More and more cities are gradually following the same footstep because of various distinct features of LEDs. Some of them are: low maintenance cost, better visibility, long life and low energy consumption. Apart from offering data communication without interruption in normal signaling function, they are also expected to offer better and comfortable human visibility following the traffic signal standards [14]. In the following section, we discuss human visibility perspective in brief and examine the standards set for traffic signal visibility.

3.3 Human Visibility Perspective

The visibility of traffic signal is very important for safe driving. It depends on many factors, the most important of which are colour, luminous intensity and luminous intensity distribution.

There are two situations:

- Difficulties in detectability of traffic signal, and
- Ability to discriminate between signal signs.

Luminance Difference Threshold (LDT) is a factor that decides the visibility of a general object [15]. For humans to perceive an object and recognize it, its object luminance needs to

be different from its background luminance, and the difference of luminance has to be larger than the minimum luminance difference (LDT) that the human eye can perceive. This LDT is influenced by such factors as observer's visual ability and mental condition, property of an object, luminance condition in eyesight, and so on. That is, the driver's visibility condition can be highly influenced by weather and time. Authors in [49] have described in detail these criterions. These aspects are examined in brief considering luminous intensity and distribution for some of the standards.

3.3.1 Luminous Intensity, Uniformity and Distribution

The two primary factors that determine the luminous intensity requirements of a signal light are:

- the luminance of the background (L_B), and
- the distance (d) from which the signal light is to be seen.

There is a linear relationship [15] between the background luminance (L_B) and required luminance of a signal light (L_s) of a fixed size.

$$\frac{L_S}{L_B} = C_1 \tag{3.1}$$

where C_1 is a constant. Also, the optimal luminance intensity of a traffic signal light is independent of size:

$$L_s\varphi = C_2 \tag{3.2}$$

where C_2 is a constant and φ is the solid angle subtended by the signal light. Since, φ is equal to the area (A) of the signal divided by the square of the distance (d) to the signal and the luminance intensity is the luminance times the area:

$$\varphi = \frac{A}{d^2} \; ; \quad and \quad I = L_s A \tag{3.3}$$

then,

$$\frac{I}{d^2} = C_2 \tag{3.4}$$

Therefore, the luminance intensity necessary for a signal light to be seen at a prescribed distance is:

$$I_d = C\ d^2 L_B \quad (cd) \tag{3.5}$$

where, *C* is a constant, *cd* is Candela, the unit of luminous intensity.

The optimum intensity depends on sky luminance and distance of the driver from the signal. A sky luminance of 10,000 cd/m^2, was established as a standard condition [50]. It is recommended that a red signal light of 200cd, viewed under standard conditions, will be detected quickly and with certainty. The relevant equation for calculation is given as:

$$I_d = 2E-6\ d^2\ L_B \quad (cd) \tag{3.6}$$

where, the value 2E-6 is taken for the constant *C*, *d* is the distance, and L_B is the luminance of the background.

For most signals, the visual range must be at least 100m to allow safe stopping conditions for cars moving at 60kmph and with the brightest sky of about 10^4cd/m^2. Under these conditions, the optimum intensity of the red light signal is 200cd, according to equation (3.6).

In [51], authors reported that the value of 200cd for a red signal light (200mm size), viewed under standard conditions, was needed at an offset angle from the drive's line of sight of 3º. They also found that as the angle increased from 3º, the luminous intensity requirements also increased, with the following relationship:

$$I_\theta = I\left(\frac{\theta}{3}\right)^{1.33} \tag{3.7}$$

Therefore, the well known Fisher Equation [15] for the necessary luminous intensity requirements (considering incandescent lights) is given as:

$$I_{d,\theta} = 2E-6\left(\frac{\theta}{3}\right)^{1.33} d^2\ L_B\ (cd) \tag{3.8}$$

where, $I_{d,\theta}$ is the required luminous intensity (cd), θ is the angle from the driver's line of sight (deg), and L_B is the background luminance (cd/m^2).

However, for the green and yellow signal lights the luminous intensity need to be higher than that of a red signal light. This is due to the Helmoholtz-Kohlrausch effect [52]. The Helmholtz-Kohlrausch effect comes into play when a chromatic stimulus appears to have a greater brightness than a white reference stimulus of the same luminance. The ratio of the luminance of the chromatic stimulus, with equal brightness is written as *B/L*. The effect varies by wavelength and saturation, with highly saturated reds and blues having a higher *B/L* value than yellow or greens. However, final recommendation for the intensity ratio for red, yellow and green (R:Y:G) is suggested to be (1:2.5:1.3) [53].

3.3.2 Luminous Intensity Requirements for LED-based Traffic Lights

The Fisher equation was re-evaluated by the Institute of Transportation Engineers "Vehicle Traffic Control Signal Heads" (ITE VTCSH) for United States LED traffic lights photometric requirements. A series of measurements were taken and evaluated to provide standard specifications [53]. ITE VTCSH then formulated the equation for minimum maintained intensity requirements for LED-based traffic lights, which is given as:

$$I(\theta_{horiz}, \theta_{vert}, size, colour) = f(I_{horiz})\, f(I_{vert})\, I(-2.5,0) \tag{3.9}$$

where, for all values of θ_{horiz}:

$$f(I_{horiz}) = 0.05 + \left(0.95 exp^{\left[-\frac{1}{2}\left(\frac{\theta_{horiz}}{11}\right)^2\right]}\right) \tag{3.10}$$

$\theta_{vert} >$ - 2.5º;

$$f(I_{vert}) = 0.05 + \left(0.9434 exp^{\left[-\frac{\theta_{vert}+2.5}{5.3}\right]}\right) \tag{3.11}$$

$\theta_{vert} \leq$ - 2.5º;

$$f(I_{vert}) = 0.26 + \left(\frac{\theta_{vert}}{143}\right) + 0.76\left[exp^{-0.02(\theta_{vert}+2.5)^2}\right]^{(-0.07(\theta_{vert}))} \tag{3.12}$$

and, I(-2.5,0) = **Colour**	**Traffic Light(200mm)**	**T.L(300mm)**
Red	165cd	365cd
Yellow	410cd	910cd
Green	215cd	475cd

Fig. 3.2. provides minimum maintained red signal luminous intensity requirement on traffic light axis at 50m and 34.65m and at different horizontal angles (across the road width) resulting from installation of traffic light at a height of 5m, while Fig. 3.3. illustrates for all three colour signals at 50m distance. Table 3-1 [88] illustrates the minimum and maximum peak intensity requirements from standard traffic lights, while Table 3-2 gives the detail specifications at various distances and angular offsets. Table 3-2 provides data for luminous intensity requirements off 2.5º from axis that is, at θ_{vert} = -2.5º and θ_{Horiz} = 0º, [I(-2.5,0)] for the three main standards. It can be seen that European standard has minimum requirements as compared to American and Japanese standards. (complete specifications are not available from Japanese standard).

Table 3-1: Comparison of Traffic signal luminous Intensity from three Standards

Luminous Intensity (cd): (in the reference axis)	**ITE: VTCSH Part 2: LED Vehicle Traffic Signal Modules: June 1998**				**Draft- European Standard: Traffic Control Equipment – Signal Heads: January 1998**				**Japanese Standard: April 1986**			
	Min		Max		Min		Max		Min		Max	
	200 mm	300 mm	200 mm	300 mm	200 mm	300 mm	200 mm	300 mm	200 mm	300 mm	200 mm	
Red (λ= 620-630nm)	133	399	800	800	100	339	400	800	240		Not specified	
Yellow (λ = 580-690nm)	617	1571	3700	3700	100	339	400	800	240		Not specified	
Green (λ = 530-660nm)	267	678	1600	1600	100	339	400	800	240		Not specified	

These specifications provide significant inputs for comparison and design of LED-based traffic lights which are gradually becoming popular. However, as discussed before, they can be designed aiming for multiple functions of signaling, data transmission and illumination.

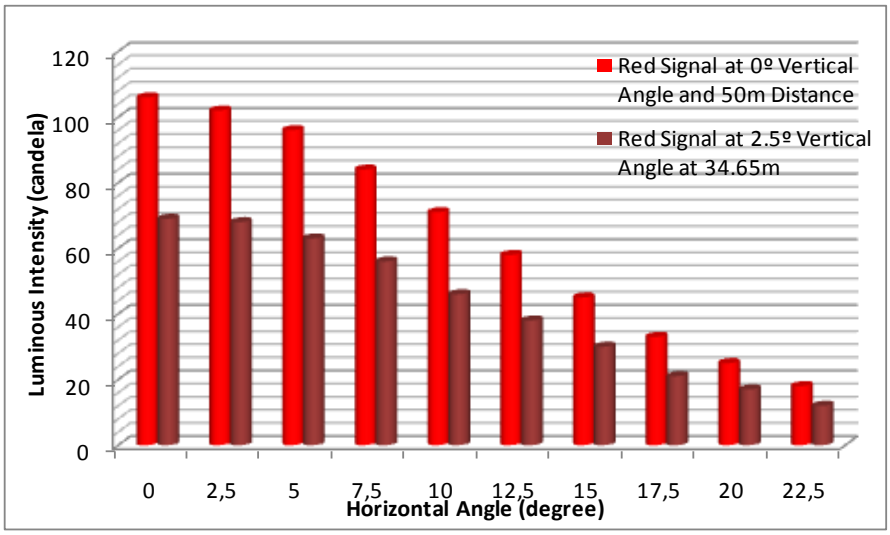

Fig. 3.2.: Red Signal Luminous Intensity Requirement at 50 m and 34.65m

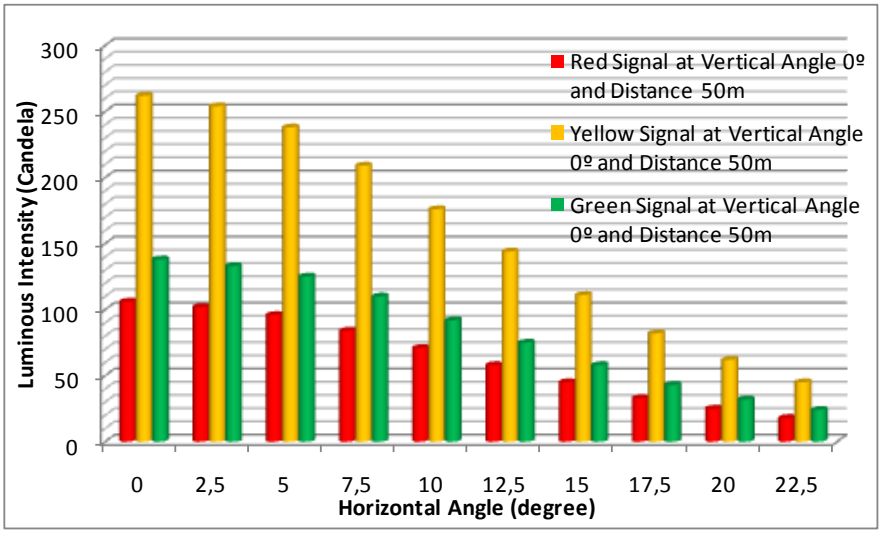

Fig. 3.3.: Red, Yellow and Green Signal Luminous Intensity at 50m Distances

Table 3-2: Minimum maintained Luminous Intensity

Vertical Angle (deg)	Horizontal Angle (deg)	Luminous Intensity (candela)					
		200mm (8 in)			300mm (12 in)		
		Red	Yellow	Green	Red	Yellow	Green
0.0 (d=50m) h_t=5m w_t=14m	0.0	106	262	138	234	582	304
	2.5	102	254	133	226	564	295
	5.0	96	238	125	212	528	276
	7.5	84	209	110	186	464	242
	10.0	71	176	92	157	391	204
	12.5	58	144	75	128	319	166
	15.0	45	111	58	99	246	128
	17.5	33	82	43	73	182	95
	20.0	25	62	32	55	137	71
	22.5	18	45	24	40	100	52
2.5 (d=34.65m)	0.0	69	172	90	153	382	200
	2.5	68	168	88	150	373	195
	5.0	63	156	82	139	346	181
	7.5	56	139	73	124	309	162
	10.0	46	115	60	102	255	133
	12.5	38	94	49	84	209	109
	15.0	30	74	39	66	164	86
	17.5	21	53	28	47	118	62
	20.0	17	41	22	37	91	48
	22.5	12	29	15	26	64	33
5.0 (d=26.43m)	0.0	46	115	60	102	255	133
	2.5	45	111	58	99	246	128
	5.0	41	103	54	91	228	119
	7.5	36	90	47	80	200	105
	10.0	31	78	41	69	173	90
	12.5	25	62	32	55	137	71
7.5 (d=21.3m)	0.0	31	78	41	69	173	90
	2.5	31	78	41	69	173	90
	5.0	28	70	37	62	155	81
	7.5	25	62	32	55	137	71
	10.0	21	53	28	47	118	62
	12.5	18	45	24	40	100	52
10.0 (d=17.7m)	0.0	23	57	30	51	127	67
	2.5	23	57	30	51	127	67
	5.0	21	53	28	47	118	62
	7.5	18	45	24	40	100	52
12.5 (d=15.2m)	0.0	18	45	24	40	100	52
	2.5	17	41	22	37	91	48
	5.0	17	41	22	37	91	48
	7.5	13	33	17	29	73	38

3.4 LED For Traffic Light Signal

LED-based traffic lights offer many distinctive features such as better visibility, low maintenance cost, long life and energy saving. There have been two main standard sizes of traffic lights; 200mm diameter and 300mm diameter. LED-based traffic lights system may consist of a large number of LEDs, that is, hundreds of spatially distributed HB-LEDs. The distance of visibility as well as signal transmission will increase with the illumination. Intensity definition only applies to point sources. The radiation emanating from a source whose dimensions are negligible in comparison with the distance from which it is detected may be considered coming from a point. Therefore first, it is imperative to review a single source LED model.

3.4.1 LED Point Source

Ideally, a LED source is a Lambertian emitter, i.e., irradiance distribution or illuminance is a cosine function of the viewing angle. In practice, this dependence turns out to be a power law that primarily depends on the encapsulant and semiconductor region shapes. A practical approximation of the irradiance distribution following the illustration in (Fig. 3.4) is given as:

$$E(d,\theta) = E_0(d)\cos^m(\theta) \tag{3.13}$$

where θ is the viewing angle and $E_0(d)$ is the irradiance (W/m^2), also given in luminous flux (lm) on the axis at a distance d from the LED. The value of m depends on the relative position of the LED emitting region from the curvature center of the spherical encapsulant. If the chip position coincides with the curvature center, the number m≈1, and the source is nearly a perfect Lambertian (e.g., some Lumileds and Lamina LEDs). Typical LEDs often have values of m> 30, and the drop of intensity with the viewing angle is pronounced. The number m is given by the half power angle, $\theta_{1/2}$, an angle provided by

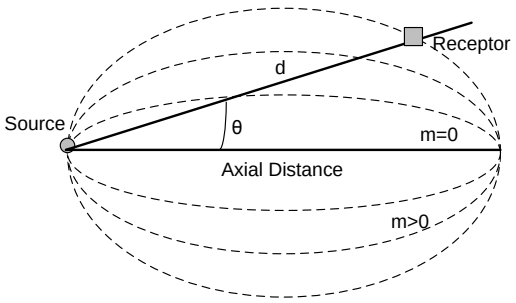

Fig. 3.4: Lambertian Emitter Source

the manufacturer, defined as the view angle when irradiance is half of the value at 0°. The relation between $\theta_{1/2}$ and m can be expressed as:

$$m = -\frac{ln2}{ln\left(cos(\theta_{1/2})\right)} \tag{3.14}$$

Typically, LEDs with half power angle (hpa) of 15º to 45º are used. The LED emitter is modeled using a generalized Lambertian radiation pattern {$R_E(\theta, m)$} [19, 20].

Assuming that P_t is the transmitted power, the radiation intensity is given by:

$$R_E(\theta, m) = \frac{m+1}{2\pi} P_t \cos^m(\theta); \;\; \theta \in \left[\frac{-\pi}{2} \;\; \frac{\pi}{2}\right] \tag{3.15}$$

Fig. 3.5(a) shows the polar plot for different mode number of the radiation lobe while Fig. 3.5(b) illustrates the same for the normalized values. It is seen that as 'm' increases the directivity of the radiation pattern increases.

3.4.2 LED-Based Traffic Light Emitter Model

To model the traffic light as emitter, we normally have to use many low cost high intensity LEDs. However, there are different kinds of LEDs with different characteristics in terms of intensity, half power angle, size and cost.

Normally, conventional and HB-LEDs come with three diameters; 3mm, 5mm and

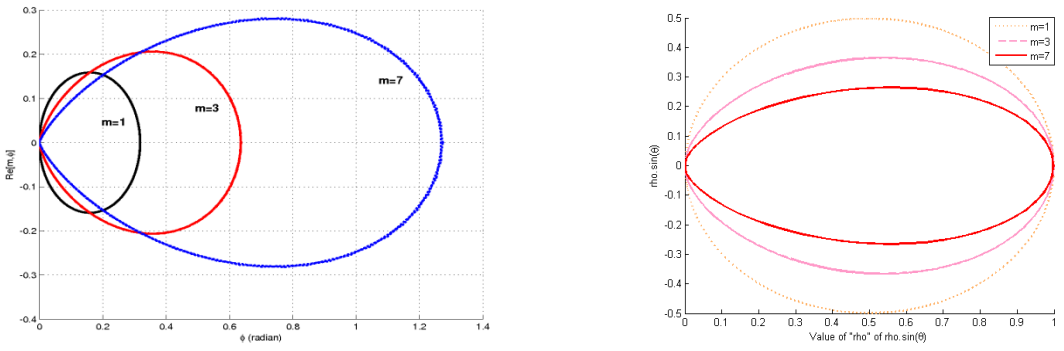

(a) (b)

Fig. 3.5: Radiation Pattern: (a) Function of *m, and φ*; (b) For Different values of *m* of LEDs

8mm. We consider 5mm LEDs due to their wide availability. The area of one LED is approximately 19.63mm^2. The conventional LEDs have very small values of lumen (brightness) in the order of less than unity, generally given in milli Candela (mcd). Therefore, we would need a large number of such LEDs to get few tens of lumen in total. Also, the area of the available traffic lights is not sufficient to accommodate over thousands of LEDs, even without considering manufacturing constraints. Hence, there are two alternatives: to use HB-LEDs able to provide few lumens of intensity but highly directive, and power LEDs which have few tens of lumen and wide viewing angles. A comparative analysis is presented to justify the choice made on the frame work of this project.

Table 3-3 presents an example of LEDs with technical specifications. We will consider these HB-LEDs and Power LEDs for further study. Table 3-4 lists comparative study for HB and Power LEDs with one case study. From the selected LEDs, for the same brightness level there will be 370 HB-LEDs while 69 power LEDs. A simple schematic diagram is shown in Fig. 3.6. Power dissipation and current drawn are approximately the same in both the cases.

Table 3-3: Specifications of LEDs

Type of LED (part List)	Manufacturer	Colour & (λ- nm)	V_f Typ (v)	V_f Max (v)	I_f (mA)	Vr (v)	hpa (°)	Luminous Flux
Clear 5mm Standard (L-7113C)	Kingbright	Red (625)	2.0	2.5	30	5	30	200(mcd)
		Green (565)	2.2	2.5	25	5	30	150(mcd)
		Yellow (590)	2.1	2.5	30	5	30	80(mcd)
5mm White	TruOpto	Red (625)	2.2	2.6	75	5	15	30000(mcd)
		Green (525)	3.6	4.2	75	5	15	30000(mcd)
		Yellow (585)	2.2	2.6	75	5	15	30000(mcd)
Power HB (max. consumption 2W)	Golden Dragon (Osram)	Red (625)	2.2	2.6	350		120	Approx. 80000-200000 (mcd)
		Green (528)	3.2	4.2	350		120	Approx. 80000-200000 (mcd)

Table 3-4: Comparison of HB-LED and POWER LED

<table>
<tr><th colspan="5">Golden Dragon (Power LED)</th><th colspan="5">TruOpto 5mm HB-LED</th></tr>
<tr><td rowspan="5"></td><td colspan="4">Power Consumption (max) 2W,
Maximum forward current up to 500mA</td><td colspan="5">Power Dissipation 500mW,
Pulse forward current 100mA</td></tr>
<tr><td colspan="4">High Reliability, long life – 50,000 hrs</td><td colspan="5">High reliability, long life, Energy efficient</td></tr>
<tr><td colspan="4">Total Lumen approx. 2450 each @ 35lm</td><td colspan="5">Total Lumen : 2450 each @5lm</td></tr>
<tr><td colspan="4">Optical efficiency (lm/w) [60 to 86]</td><td colspan="5"></td></tr>
<tr><td colspan="4">Lens Needed (costly)</td><td colspan="5">Does not require lens</td></tr>
<tr><td rowspan="4">Cost</td><td colspan="4">Qty</td><td colspan="5">Qty</td></tr>
<tr><td colspan="2">(1-24)</td><td colspan="2">(25-100)</td><td colspan="2">(1-99)</td><td colspan="3">(100-500)</td></tr>
<tr><td colspan="2">@1.60 USD</td><td colspan="2">@1.40 USD</td><td colspan="2">@0.25 USD</td><td colspan="3">@0.22 USD</td></tr>
<tr><td colspan="4">Lens >500USD</td><td colspan="5">Transparent glass/Fiber @ aprrox. 1USD</td></tr>
<tr><td rowspan="5">Case Study:-

370 HB LEDs wired in 12 Co-centric rings in 200mm diameter traffic light</td><td colspan="4">69 LED wired in 5 rings plus one in the centre would be needed to illuminate the same brightness. (Fig. 3.7 is referred)</td><td colspan="5">370 LEDs wired in 12 co-centric rings plus one in the centre.</td></tr>
<tr><td colspan="4">Cost Analysis (USD per Module)
Not included VAT, Transportation and Case</td><td colspan="5">Cost Analysis (USD per Module)
Not included VAT, Transportation and Case</td></tr>
<tr><td>LED</td><td>Lens</td><td>Manufac-turing</td><td>Total</td><td>LED</td><td>Lens</td><td>Manufa-cturing</td><td colspan="2">Total</td></tr>
<tr><td>70*1.40 = 98.00</td><td>500.00</td><td>5.00</td><td>603.00</td><td>371*0.22 = 81.62</td><td>1</td><td>10.00</td><td colspan="2">92.00</td></tr>
<tr><td colspan="4">Example: With +24V source, 7x10 array, 4.7 Ohm 1W resistor in all 10 arms
-All resistors dissipate 8225 mW,
-Together diodes dissipate 77000 mW
-Total power dissipated by the array is 85225 mW,
-The array draws current of 3500 mA from the source</td><td colspan="5">With +24V source, 10x37 Array, 22 Ohm ½ W
-All resistors dissipate 8140 mW
-Together diodes dissipate 81400 mW
-Total power dissipated by the array is 89540 mW
-The array draws current of 3700 mA from the source.</td></tr>
<tr><td>Reliability Issue</td><td colspan="4">Failure of one LED causes one arm failure (10LEDs), loss of 350 lm, Effect is not only noticeable but reduced service area</td><td colspan="5">Failure of one LED causes one arm failure (10LEDs), loss of 64 lm, not so noticeable, may not affect</td></tr>
</table>

Source- www.rapidonline.com

The main difference is found to be in both the cost and reliability. From the table we see that there is reasonable difference in the cost. Power LEDs normally have wide view angles and therefore, lens becomes necessary to obtain adequate radiation pattern. The lens is very costly as compared to LEDs. On the other hand, HB-LEDs come with narrow view angles

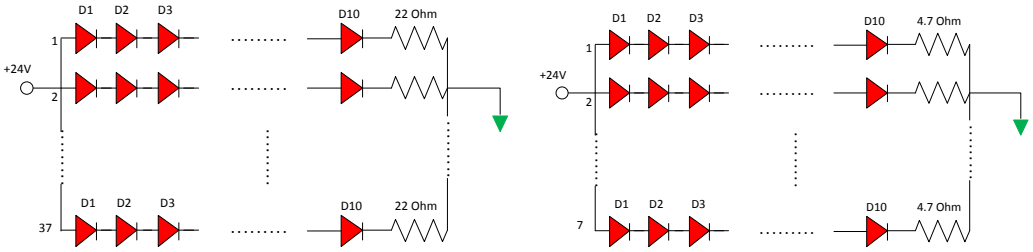

(a) (b)

Fig. 3.6: Schematic of Series/parallel Connection: (a) 370 HB-LEDs; (b) 69 Power LEDs.

which can be used without lens. Therefore, using power LEDs for traffic light would be more expensive than HB-LED. Another major difference is found to be in the reliability. For example as shown in Fig. 3.6, each arm of schematic wires 10 LEDs. If one of the power LED fails, the traffic light would lose nearly 350 lm affecting the coverage area. However, if one of the HB-LED fails, the traffic light would lose nearly 64 lm which may not affect so significantly. Hence, the usage of HB-LEDs improves the robustness of traffic light, implying less performance degradation under damaged condition.

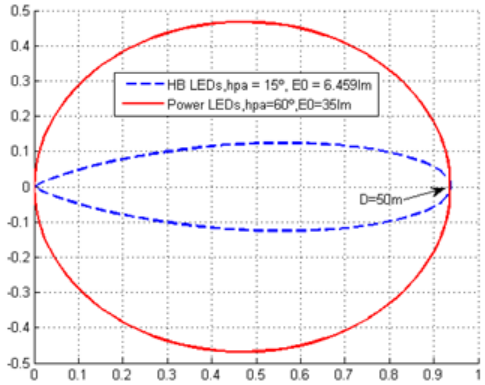

Fig. 3.7: Irradiation Distribution

Moreover, illumination distribution of HB-LEDs can be improved for traffic light signaling based on viewing angle. Therefore, the service area for data communication can be improved. The service area is the coverage area along the road in which data is expected to be received reliably. In the following sections, a model for LED-based traffic lights for optimized illumination distribution is discussed and presented.

3.4.3 LEDs Traffic Light VLC Emitter Model

LED-based traffic light systems may consist of a large number of spatially distributed HB-LEDs. The distance of signal transmission will increase with the intensity. Though modern high-power LEDs produce up to 120 lm per device, several individual LEDs must be mounted

on panels to obtain practical powers. Therefore, on the working distance, both the optical modeling and experimental characterization of a light source must be performed in different ways. Far field point [54, 55] source approach is the simplest model, because of discrete nature of the source this assumption may not always hold. We consider discrete point source with the consideration of HB-LEDs and therefore, the angular intensity from each has been taken into account. A model is developed based on these considerations.

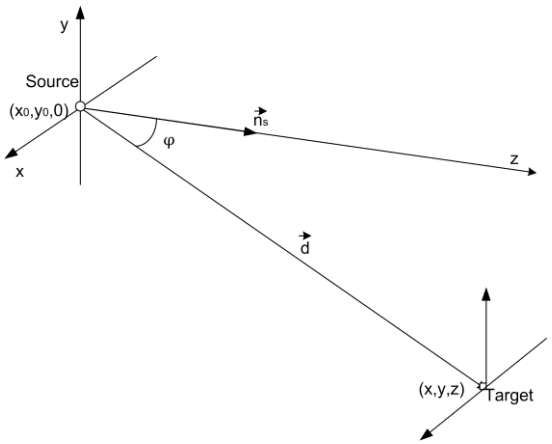

Fig. 3.8: Illustration of LED and Illumination

3.4.3.1 Arrays of LEDs with Discrete Sources

Considering one LED placed at (x_0, y_0, 0) over a plane (as shown in Fig. 3.8), in Cartesian coordinates (x, y, z), the target placed at (x, y, z), and $\overrightarrow{n_s}$ represents the heading of the source. From geometry:

$$cos(\varphi) = \frac{\langle \overrightarrow{n_s}\, \vec{d} \rangle}{\|\overrightarrow{n_s}\|\, \|\vec{d}\|} \tag{3.16}$$

where, $\overrightarrow{n_s}.\vec{d}$ is the dot product of the vectors $\overrightarrow{n_s}$ and $\overrightarrow{d}$. Assuming that $\overrightarrow{n_s}$ is normalized, that is, $\|\overrightarrow{n_s}\| = 1, and,$

$$\|\vec{d}\| = \sqrt{(x - x_0)^2 + (y - y_0)^2 + z^2} \tag{3.17}$$

For the geometrical set-up in Fig. 3.8, we have assumed $\overrightarrow{n_s}$ = (0, 0, 1) and $\vec{d}$ = (x - x_0, y – y_0, z). Thus, the irradiance is therefore, given as: [66, 67]:

$$E(x, y, z) = \frac{m+1}{2\pi} \frac{\cos^m(\varphi)}{\|\vec{d}\|^2} E(0) \tag{3.18}$$

That is:

$$E(x,y,z) = \frac{m+1}{2\pi} E(0) \frac{z^m}{\|\vec{d}\|^2 \|\vec{d}\|^m} \quad (3.19)$$

where *E(0)* is the irradiance of the LED on the axis. Equation (3.19) can then be written as:

$$E(x,y,z) = E(0) \frac{m+1}{2\pi} \frac{z^m}{[(x-x_0)^2+(y-y_0)^2+z^2]^{\left(\frac{m+2}{2}\right)}} \quad (3.20)$$

3.4.3.2 LED Array Patterns for VLC Emitter

There are many possible arrangements in which LEDs can be uniformly arranged for the signaling and lighting. For example; square arrays, triangular arrays and ring arrays are shown in Fig. 3.9(a), (b) and (c). However, such arrangements set a lower and also higher limit on the number of LEDs to be used. For example; a square pattern would need at least 4 LEDs and certain maximum number for a given size of traffic light. Moreover, square arrays are normally used for lighting and for uniform illumination over larger coverage areas. However, in the application of traffic lights, circular arrays are normally preferred and used. Although, many arrangements are studied and analyzed, circular ring (Fig. 3.9(d, e) pattern is found to perform better. A summary of outcome of the study [66] is illustrated in Table 3-5. We therefore, focus on developing a model suitable for traffic lights consisting of circular arrays of LEDs.

3.4.3.3 Circular Ring Array Pattern

A circular ring pattern with LEDs placed on the circumference is shown in Fig. 3.9(c, d, e). Extending the illustration as shown in Fig. 3.10 and assuming that, $\|\vec{d}\| \gg r_m$, where r_m is the radius of outer ring, the position of each LED is (x_i, y_i, 0) and the target is considered to be an ideal receiver, that is; full FOV and infinitesimal detection area; $\overrightarrow{d_\iota}$ is given as:

$$\overrightarrow{d_\iota} = (x - x_i, y - y_i, z) \quad (3.21)$$

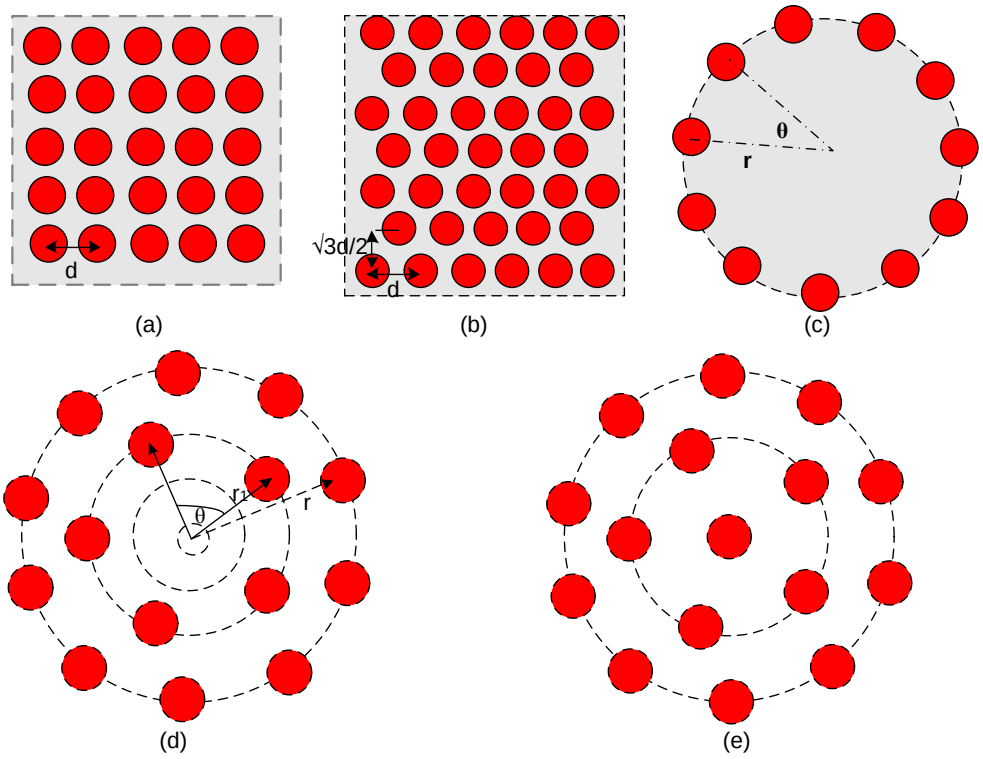

Fig. 3.9: Array Arrangements: (a) Square; (b) Triangular; (c) Circular Ring; (d) Co-centric Ring Array; (e) Co-centric ring with an LED in the centre

and LED coordinates become:

$$x_i = r_k \cos\left(\frac{2\pi i}{N_k}\right) + x_0$$
$$y_i = r_k \sin\left(\frac{2\pi i}{N_k}\right) + y_0 \qquad (3.22)$$

where; i for index of LEDs on the ring, since each ring will have some number of LEDs, k is the index for LEDs in a ring, as there will be multiple number of co-centric rings, r_k are the radii of the rings, and N_k are the number of LEDs on the ring k.

When k = 0; r_0 = 0 and N_0 = 1, indicating the center LED placed at (x_0, y_0, 0).

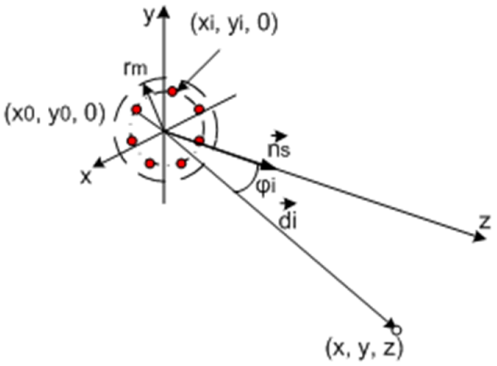

Fig. 3.10: LEDs Circular Ring

Therefore, for a single ring the irradiance is given as:

$$E(x,y,z) = E(0)\frac{m+1}{2\pi}\sum_{i=0}^{N_k-1}\frac{z^m}{[(x-x_i)^2+(y-y_i)^2+z^2]^{\left(\frac{m+2}{2}\right)}} \quad (3.23)$$

If there are multiple co-centric rings, the irradiance will become [67]:

$$E(x,y,z) = E(0)\frac{m+1}{2\pi}\sum_{k=0}^{M-1}\sum_{i=0}^{N_k-1}\frac{z^m}{[(x-x_i)^2+(y-y_i)^2+z^2]^{\left(\frac{m+2}{2}\right)}} \quad (3.24)$$

where M is the total number of the rings in the array. (Note: In equation 3.24, index k is embedded in LED's coordinates x_i and y_i, according to equation 3.22).

Table 3-5: Arrangement for LED Arrays

Array Traffic Light Diameter		Maximum		Road Widthwise Coverage (at 10m)[1]	LED Occupancy (%)	Visibility
		No. of LEDs	Luminous Intensity			
Triangular	200mm	274	4421 cd	2.94m	40.72	Light output is perceived as a high intensity source in the center with some dark area in the dome periphery
	300mm	554	9801 cd	6.38m	41.63	
Square	200mm	361	5957 cd	4.32m	50.77	Light output is more uniform with reduced dark areas. However creates a stripe pattern effect
	300mm	841	13877 cd	7.42m	52.56	
Co-centric Rings	200mm	580	9570 cd	6.32m	81.56	Produces the most uniform light perception with the LEDs covering the entire dome
	300mm	1310	21615 cd	8.58m	81.88	

NOTE: Standard 5mm diameter LEDs with assembly tolerance radius of 1.25mm and luminous output of 16,5 cd

1) Maintaining a minimum of 40uW/m^2

3.4.3.4 Optimum Placement

Though co-centric configuration has an edge over other arrays, we are not sure of getting desired illumination distribution especially when certain conditions such as number of LEDs and the size of the traffic light are given. A suitable placement to optimize illumination distribution under these conditions becomes essential. Therefore, we simulated the placement under various conditions, for example, knowing only size of the traffic lights and the size of the LEDs. Under these conditions, we have maximum number of LEDs with hundred percent of occupancy on the perimeters of each ring. However, we need to ensure and preserve the human eyes safety issues because of light power output, as it increases with the number of LEDs. Then, in the second method we tried to optimize placement as well as illumination distribution with available size of traffic lights and available number of LEDs. Both of these methods no doubt, increase the service area but lot of power is wasted towards the edges of the road. In order to focus and concentrate the illuminated power along the road and cover the same area lengthwise, we adopted different techniques. This is one of the intelligent placements to achieve desired illumination distribution in the given service area.

In this method, we choose 100% occupancy in the inner half of the total number of rings while maintaining the equal number of LEDs in the rest of the outer rings with that from middle ring. The algorithm works as follows:

1) Setting the main parameters traffic light diameter, LED directivity, LED diameter and assembly tolerance, number of available LEDs (or calculated by program).
2) Calculate and set LED distribution parameters for the co-centric rings array after verification (type of distribution, number of rings, radius).
3) Calculate occupancy percentage as a function of available LEDs and type of distribution selected and place them;
    i) If selection is linear progression distribution, the LEDs distribution are uniform on all the rings;
    ii) If dense centre cluster distribution is selected, the inner first half of rings keep higher occupancy percentage, while the second half of rings maintain a constant number of LEDs per ring, equal to the number of LEDs in the middle ring.

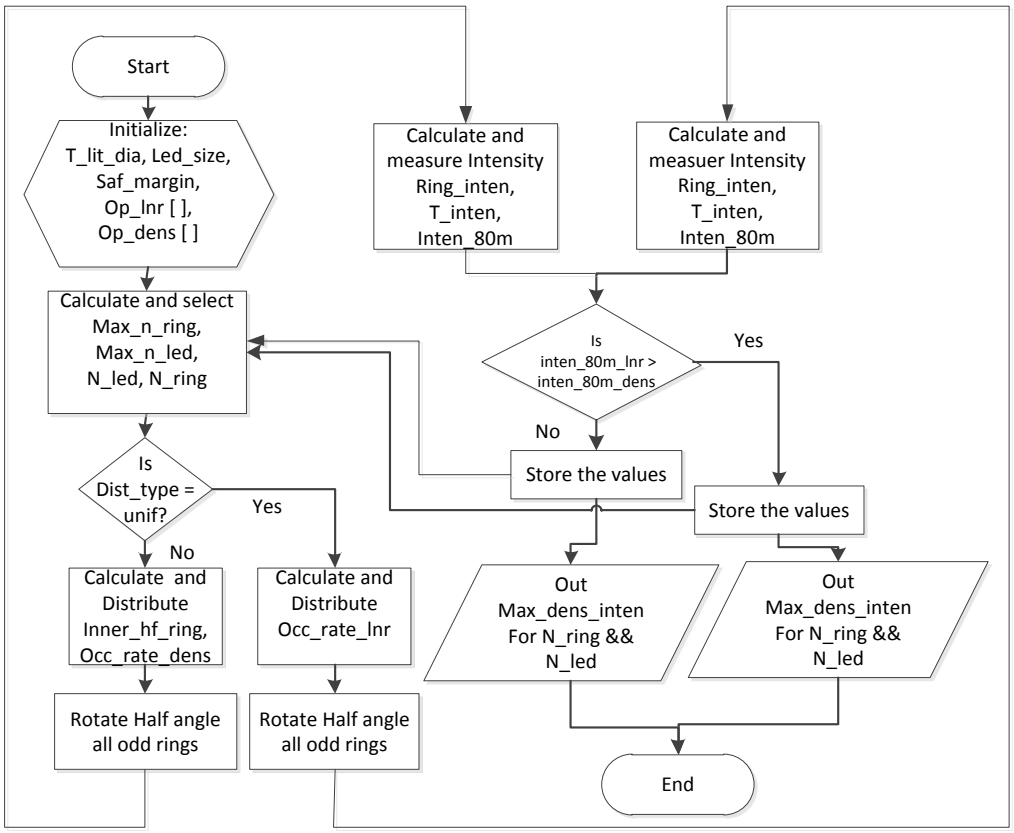

Fig. 3.11: Flow chart Illustrating Optimization Algorithm

iii) Rotate by half the angle between two consecutive LEDs for every odd numbered rings.

4) Calculate and plot illumination charts for different settings (along road length or width at different distances).

5) Repeat steps 2 to 4, find the maximum illumination intensity and display the settings.

This can be illustrated in flow chart as shown in Fig. 3.11.

As for the placement of LEDs, the odd numbered rings are rotated by half the angle between two consecutive LEDs in order to provide a more uniform distribution, thus removing the stripe effect caused by LEDs with similar placing angles. Extensive study was submitted as internal report in the Institute of Telecommunications. The algorithm is flexible enough in order to provide illumination from each of the ring and total illumination at different distances.

This arrangement not only reduces the number of LEDs in total thereby reducing total radiated power but also minimizes unnecessary illumination towards the edges of the road. The effect of such placement also reduces the sharp fall in illumination immediately after short distance of around 10 meters.

3.4.3.5 Optimized Placement

Considering a 200mm diameter traffic light, 5mm diameter HB-LEDs and a safety margin of 2 x 1.5mm (necessary for installation and wiring). Keeping the same occupancy percentage of LEDs along the perimeters of the co-centric rings a total of 370 LEDs can be distributed efficiently in 12 rings to provide maximum illumination distribution along axial distance. The placement is shown in the Fig. 3.12(a). However, with this arrangement the radiation distribution also increases as we move away from the axial points. But to keep the illumination distribution maximum on axial direction while reducing it towards the edges of the road, a different strategy can be followed.

In this method, we keep 100% occupancy in the inner rings (half of the number of rings) while reducing the occupancy rate in rest outer rings by maintaining the same number of

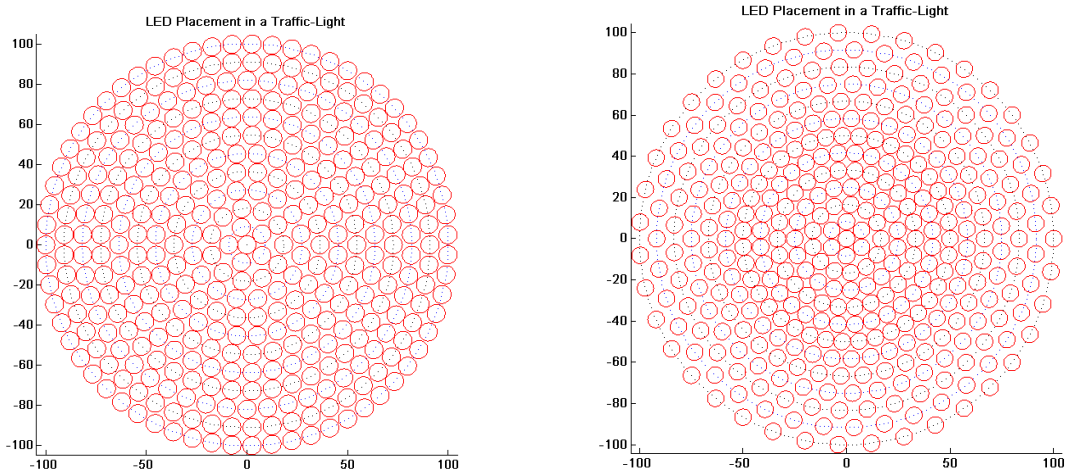

(a) (b)

Fig. 3.12: (a) Placement of 370 LEDs in 12 Co-centric rings with Approximately Equal Percentage of Occupancy along Perimeter; (b) Placement of 370 LEDs in 12 Co-centric rings with 100% Occupancy in the Inner half number of rings and reducing the Occupancy in Outer rings while keeping Same number of LEDs in the Outer rings as in the Middle ring.

LEDs as in the middle ring. For example, if there are 13 (12 rings + 1 LED in centre) co-centric rings; first 6 inner rings (from 1– 6) have 100% occupancy while rings from 7-13 will have the same number of LEDs as on ring 6. It is shown in Fig. 3.12(b). Different strategies were verified but these two are most suitable and the later gives better illumination distribution for road traffic lights application.

3.4.4 Illumination Distribution from LEDs Traffic Lights VLC Emitter

The illumination distribution over distance from both of these arrangements is shown in Fig. 3.13. It is seen that with same number of LEDs and rings the later arrangement results in slightly better illuminance. It can also be seen that the sharp fall in the irradiance near to traffic point is reduced.

In the next section, we discuss the complete traffic system set-up using the developed traffic light model.

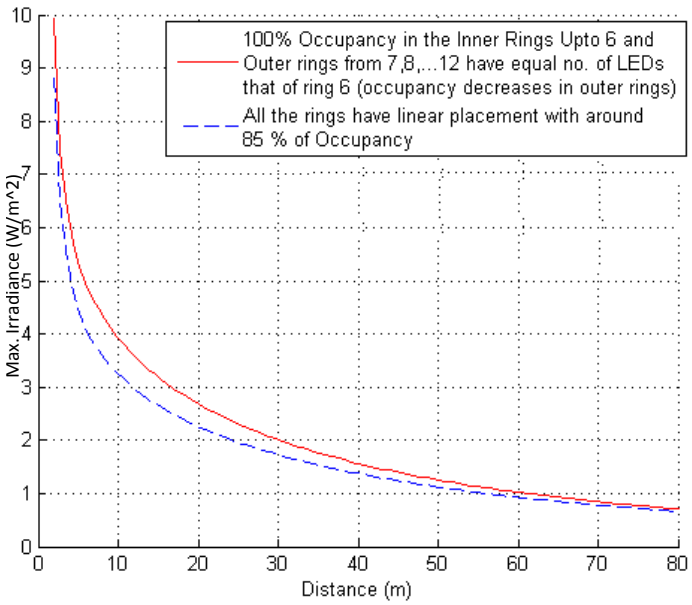

Fig. 3.13: Illumination distribution, both the Arrangements of Co-centric Rings

3.5 Multilane Generic Traffic Light Set-up

A Generic Multilane Traffic Light system set-up is shown in the Fig. 3.14. Table 3-6 summarizes the parameters involved. Each LED on the array has co-ordinate (x_i, y_i + h, 0), while the receiver position specified as (x, y, z). The traffic light is considered to be at the height of *h* from the receiver plane. As shown in the Fig. 3.14, assuming receiver orientation of θ with respect to the normal and σ_i *is* the angle of incidence while φ_i being the angle of

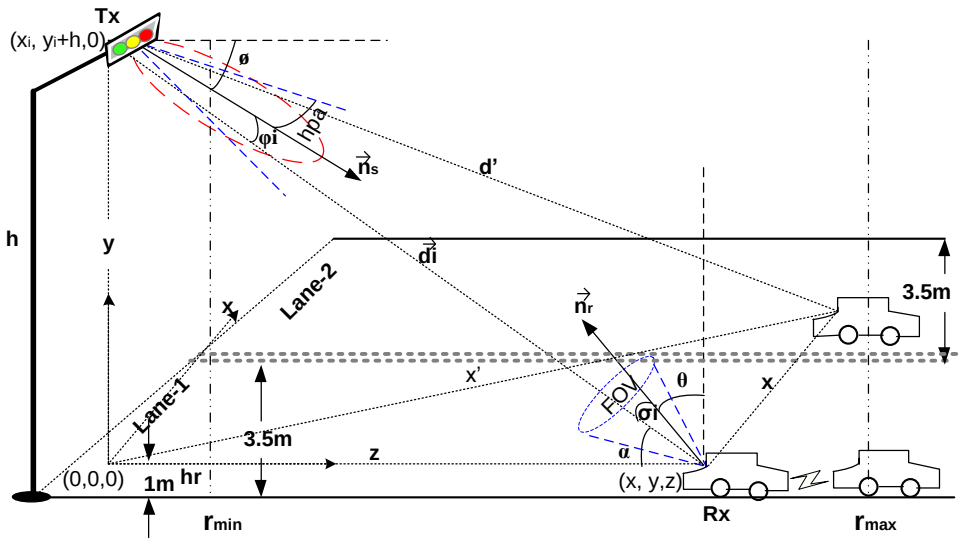

Fig. 3.14: Multilane Traffic System Set-up

Table 3-6: Traffic Light Design Parameters

Parameters	Meaning/definition and value
h	Height of Traffic Light (represents y-axis)
z	Distance from traffic light base to the vehicle in lane-1
Lane Width	3.5 m
x	Distance from traffic light base to the vehicle in lane-2
d_i	Direct distance from emitter to the detector
$ø_{1/2}$ (hpa)	Half power semi-angle of emitter
φ_i	Angle of irradiation
θ	Orientation of Receiver
σ_i	Angle of incidence
Width of the vehicle	(1.8m)
FOV	Field of view

Heights and distances are defined in meters.
Angles, orientations and FOV are defined in degrees.

irradiance. For a multilane traffic system each lane width is considered to be 3.5m. The optical power detected by a photo detector with active area A_d at a distance d from the single LED emitting source is given by:

$$E_r(x,y,z) = A_d E(0)\ \frac{m+1}{2}\ \frac{\cos^m(\varphi)}{d^2}\ cos(\sigma)\ rect\left(\frac{\sigma}{FOV}\right) \tag{3.25}$$

where, φ and α represent the angles between the direct path from the emitter to the source; $\overrightarrow{n_s}$ is the heading vector of the source and $\overrightarrow{n_r}$ is the heading vector of the receiver. The *rect* function defines bound on FOV as σ_i <*FOV*>*90º*. Its value is 0 for 0º and 1 for 90º. FOV represents the field of view of the receiver. When the emitter source is a circular array of LEDs, the detected optical power is given by a double summation. For this case, *d*, φ and σ depend on the position of each LED on the array. The direct distance d_i between each LED in the emitter source and receiving detector is given as:

$$\vec{d}_i = (x - x_i, y - y_i - h, z) \tag{3.26}$$

and,

$$\left\|\vec{d}_i\right\| = \sqrt{[(x-x_i)^2 + (y-y_i-h)^2 + z^2]} \tag{3.27}$$

Hence, the cosine terms can be found using internal product definition, giving:

$$cos(\varphi_i) = \frac{z}{[(x-x_i)^2+(y-y_i-h)^2+z^2]^{1/2}} \tag{3.28}$$

while,

$$cos(\sigma_i) = \frac{(y-y_i-h)cos\theta + z\ sin\theta}{[(x-x_i)^2+(y-y_i-h)^2+z^2]^{1/2}} \tag{3.29}$$

Therefore, the total irradiation from a traffic light consisting of an array of LEDs which is detected by receiver in LoS link is given as [61]:

$$E_T(x,y,z) = A_d E(0)\frac{m+1}{2\pi}\sum_{k=0}^{M-1}\sum_{i=0}^{N_k-1}\frac{\cos^m(\varphi_i)cos(\sigma_i)}{[(x-x_i)^2+(y-y_i-h)^2+z^2]^{\left(\frac{m+3}{2}\right)}}\ rect\left(\frac{\sigma_i}{FOV}\right) \tag{3.30}$$

LED lights thus form a part of traffic signaling device and VLC Emitter. We examine the emitter illumination performance in the following sections.

3.6 VLC Emitter Illumination Performance

In these sub-sections, experiments with the emitter design are discussed and measurement results are presented.

3.6.1 Experimental Set-up for the Measurement of Illumination Distribution

Experimental measurements were carried out in a closed pavilion with an area of 60 x 40m. Measurements were undertaken with our own assembled LED traffic lights. The used LED

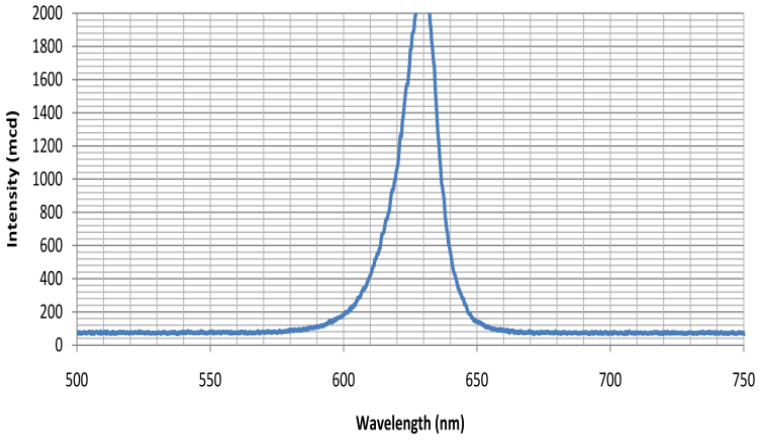

Fig. 3.15: LED Spectrum Used in Traffic Light

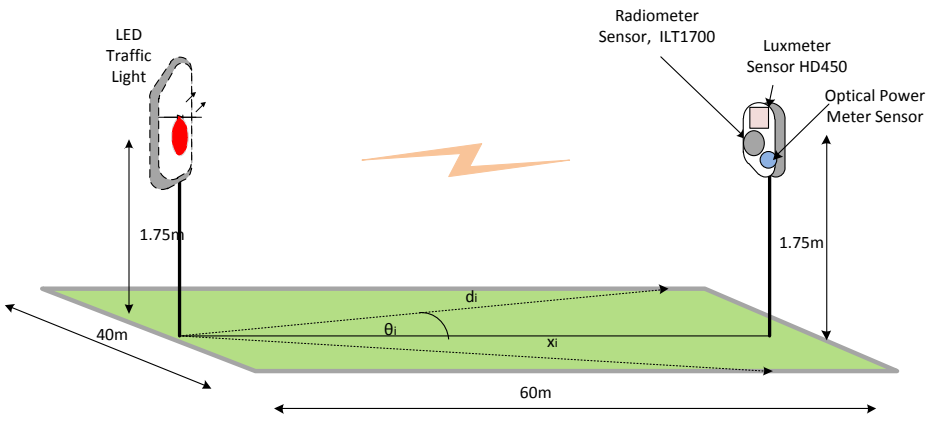

Fig. 3.16: Measurement Scenario for Irradiance Distribution in a Pavilion of size 60x40m

spectral response is shown in Fig. 3.15 which shows a peak response at 630nm wavelength. Fig. 3.16 illustrates the measurement set-up in the pavilion.

Three different sensors have been used for measurement of irradiance, flux and power. The sensors are: a) A Radiometer SED033 equipped with sensor ILT 1700, from International Light Technology, calibrated to measure irradiance; b) A Sensor with Data logging luxmeter HD450 from Extech Instruments, tuned to measure illuminance (lux) parameter; and c) FDS1010 sensor with an optical power meter designed and developed by our Institute, calibrated to measure power in watts. Traffic light and sensors were aligned in the same horizontal axis at a height of 2.05m without any inclination. Detail specifications of these sensors and instruments are shown in Table. I of appendix -I. LED specifications with set-up

Table 3-7: LED, Traffic Light and Measurement Systems

Items Name	Parameters	Description and Value
LED (AVAGO)		HLMP-EG1A-Z10DD
	Colour	Red (λ=626nm)
	Typical Viewing Angle	15º (2 $\theta_{1/2}$)
	Luminous Intensity (mcd) at 20mA	Min 12000 – Max. 21000
	Typical & Max. forward voltage	2.1 V and 2.4V
Traffic Light (200mm diameter)	No. of LEDs	240
	Optimized Arrangement	Higher occupancy rate in the half inner rings and reduced occupancy in the half outer rings
	Power Supply	+24V DC regulated
Measurement System	Height of Emitter	2.05m
	Height of Receiver	2.05m

parameters are listed in Table 3-7. The maximum axial distance was 60m and measurements were recorded at 2.5m (d_i and x_i) intervals along the axis. Also, an angular sweep (θ_i) was performed with 2.5º intervals up to 75º on both sides of axial distance as shown in Fig**.** 3.16. However, closer to the traffic light up to 5m, measurements were recorded at one meter intervals. The detail layout and illuminated traffic light is illustrated in Fig. I of appendix-I.

The assembled LED traffic lights have 200mm diameter with a total of 240 LEDs which are wired in series/parallel configuration. Each arm is driven by a power transistor. It has been found that different manufactures use different types of LEDs with different intensities. (for example, British Road Business Technology Co. Ltd. (INROLL – www.bbled.com), China based 200mm traffic light uses 90 LEDs). The one which we obtained (from Sinalarte Portugal) uses 120 LEDs. In both cases the criteria of visibility are maintained. However, there is no uniformity in the design. Our design purpose was not only to get illumination and fulfill the standard criteria of visibility but also to obtain sufficient intensity at longer distance for data communication. At the same time, it is also ensured that one of the advantages of LED lights, harmless to the human eyes is maintained. Moreover, due to communication purposes, the illumination power is reduced. For example, assuming that 0's and 1's are equiprobable, this means that half of the time the LEDs are switched off. Thus, traffic lights addressing communication and signaling at the same time must rely on larger numbers of LEDs (more or less two times the number of LEDs required only with illumination standards, assuming same type of LEDs).

In the experiment of illumination measurement in the pavilion all other light sources were switched off. Background light was measured to be very small in the order of 0.1×10^{-8} W/cm^2 or less.

3.6.1.1 Measurement for power distribution

Power distribution over a wide coverage area was measured. To better understand the power distribution, the values are plotted using Matlab as presented in Fig. 3.17 and Fig. 3.18. Fig. 3.17 shows the power density values from 5m distance.

For better understanding the intensity level over the distance is shown in colour. Because of high directivity of the used LEDs, illumination is concentrated within 10m of road width which is approximately equal to 3 road lanes. This is shown roughly in Fig. 3.18.

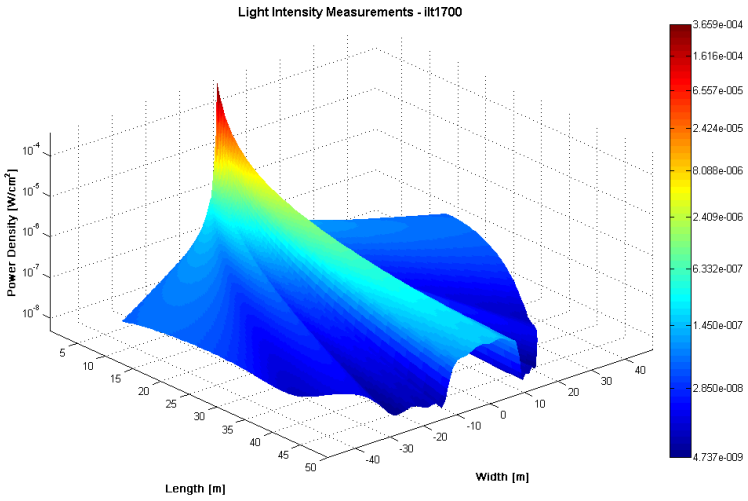

Fig. 3.17: Power Density Measurement from 5m of Distance from Traffic Light

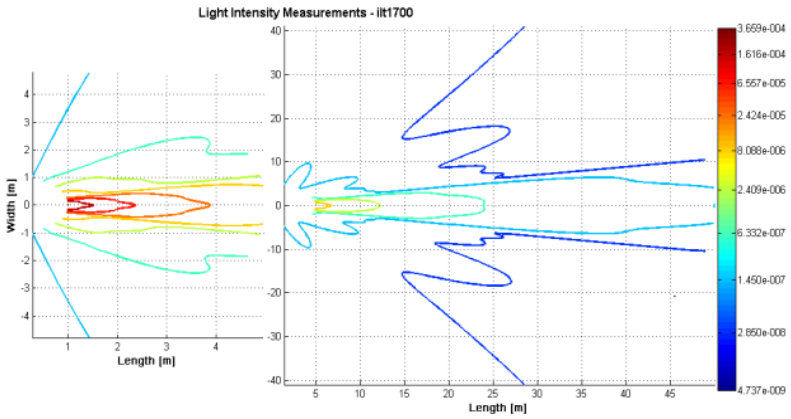

Fig. 3.18: Light Power Distribution (W/cm^2)

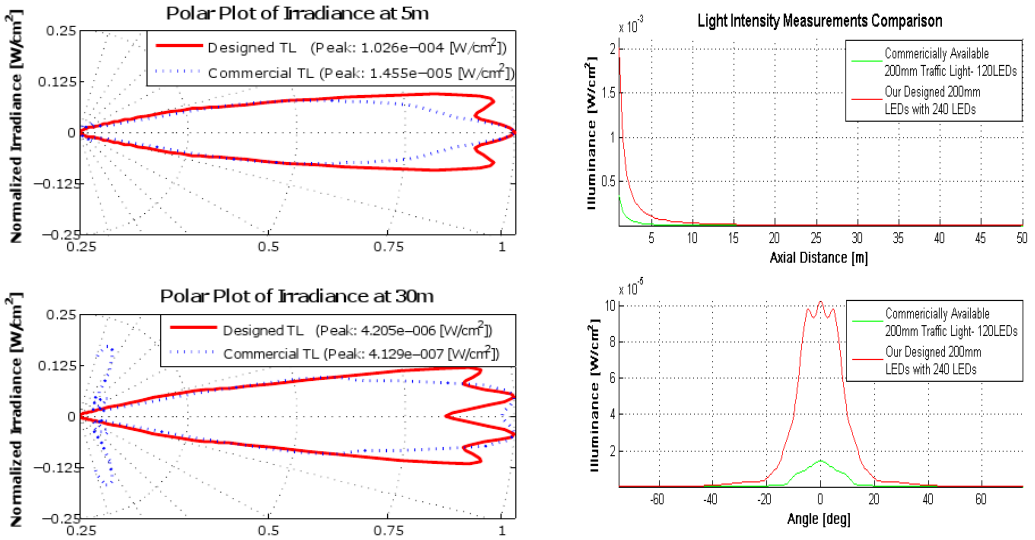

Fig. 3.19: Irradiance and Illuminance from Commercially available/ Local designed 200mm LED Traffic lights

Polar plot and irradiance for both is shown in Fig. 3.19. It can be seen that as the detector moves away from the traffic light emitter, the designed traffic light covers more area as compared to available commercial traffic light. The plot is normalized; however, the peak irradiance is shown for both. The number of LEDs used in both of the traffic lights is different with one double in numbers to other (commercially available with 120 LEDs). However, the intensity recorded to be higher than the double. These measurements were taken when LEDs were ON and not modulated.

Fig. 3.20 shows the measured values irradiance at axis, 2.5º angle and 5º angle from axis. This measurement gives the expected area of coverage along road. It is observed that values are very close in this area. A sample of the measured values from all the detectors is given in Table. II of appendix-I.

The light waves emitted from LED-based traffic light emitter through free space channel undergo variations due to atmospheric conditions. Channel characteristics and behaviors are important factors in designing a communication link. Therefore, it becomes necessary to examine the behavior of the channel for these systems.

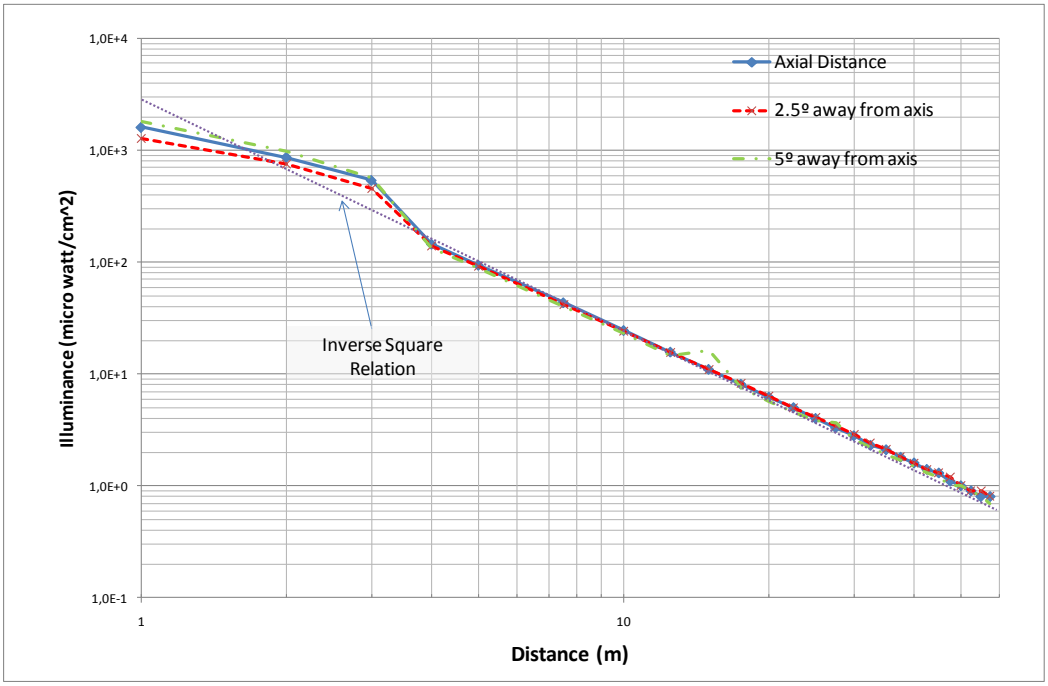

Fig. 3.20: Measured Irradiance (μ w/cm^2) values

3.7 VLC Channel

It is stated that the VLC systems in outdoor applications require LoS propagation. Propagation characteristics of VLC drastically change due to communication environment, especially, the effect of weather conditions is strong and also because of interference caused by other light sources. The received signal power fluctuates due to atmospheric obstacles such as rain, fog and so on, in the propagation channel, while different light sources deteriorate the desired signal intensity. In addition, communication characteristics change with season, time and region [21]. Therefore, it is necessary to evaluate the availability of the optical wireless communication system under various environments. The discussion here presented is restricted to the LoS case since this is the most relevant scenario for the intended application.

3.7.1 Channel DC Gain or Attenuation for LoS Propagation path

If we consider that the transmitter emits an axially symmetric radiation pattern described by the radiant intensity $P_tR_0(\varphi)$ W/sr, a receiver located at distance d and angle φ with respect to

the transmitter senses an irradiance (W/cm^2) value of $I_s(d, \varphi) = P_t R_0(\varphi)/d^2$. The power detected and received by PD with an effective area of A_{eff} is given as: $P_r = I_s(d, \varphi).A_{eff}(\sigma)$; where, σ is the incidence angle. The frequency response of visible light channels are relatively flat near to DC, so commonly the channel is characterized by its dc gain *H(0)*, given by:

$$H(0)_{LOS} = \begin{cases} \frac{A_d}{d^2} R_0(\varphi) T_s(\lambda)\, g(\lambda)\, cos(\sigma), & 0 \le \sigma \le FOV \\ 0 & \psi > FOV \end{cases} \tag{3.31}$$

where, A_d is the detector area, T_s is the optical filter gain, and g is the gain of optical concentrator (if used).

For a transmitter consisting of an array of LEDs, the LoS channel gain is given as [20, 66]:

$$H_T(x, y, z) = A_d\, P(t) T_s(\lambda)\, g(\lambda).E(0) \frac{m+1}{2\pi} \sum_{k=0}^{M-1} \sum_{i=0}^{N_k-1} \frac{\cos^m(\varphi_i) cos(\sigma_i)}{[(x-x_i)^2+(y-y_i-h)^2+z^2]^{\left(\frac{m+3}{2}\right)}}\, rect\left(\frac{\sigma_i}{FOV}\right) \tag{3.32}$$

If the area of the detector, the total transmitted power, the gain of the filter and the gain of concentrator are all normalized to one, the loss on the channel over distance can be drawn. The simulation results (Fig. 3.21) show that a receiver with around 56dB of gain would be necessary for data communication in order to cover 100m distance, ignoring noise effects.

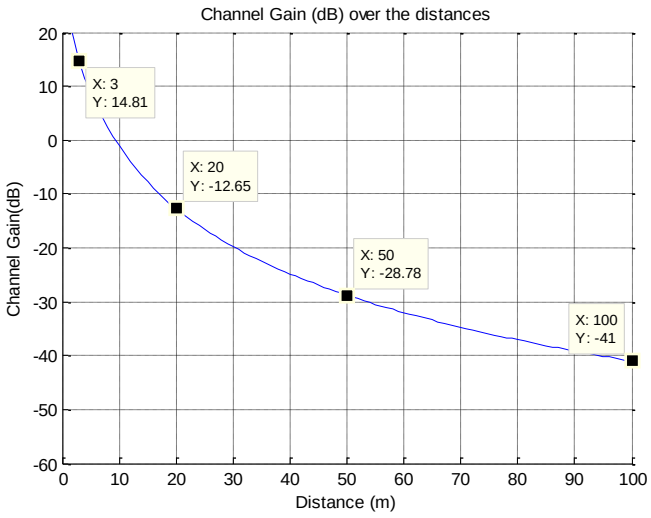

Fig. 3.21: Channel Gain (dB) over Distance

However the noise, especially lights from natural and artificial sources deteriorate signal intensity propagating through optical wireless channel. They also cause interference to the desired signal. In the following sections these effects are discussed.

3.7.2 Channel Behavior under Different Conditions

Atmospheric channel is one of the most complex channels in the communication world. The channel may change its characteristics by more than two orders of magnitude per kilometer, depending on weather conditions [25]. Fog and clouds scatter and absorb optical signals, which cause transmission errors. In the present communication scenario, apart from background and other light sources, it is common to consider fog to have the worst effect on system performance.

3.7.2.1 Channel Behavior in Fog Environment

The atmospheric channel is modeled with fog whose contents are primarily water. Fog particles are spherical in shape and have radii varying between 0.01μm and 15μm, depending on geographical locations [9]. The distribution of particles throughout the channel is assumed to be uniform.

It is possible to identify a fog condition with a visibility range and relate it to the optical attenuation by using the Kruse formula [23] given here in its original form:

$$\Gamma(V,\lambda) = \frac{17.0}{V}\left(\frac{550}{\lambda}\right) 585V^{(1/3)} \quad [\frac{dB}{km}] \tag{3.33}$$

where, V is the visual range in km, λ is wavelength in nanometers, and Γ is the attenuation in dB/km. However, this formula is not adequate for visible light channels, because the wavelength dependence of fog is too small in the visible and infrared range [24]. Therefore it is necessary to specify a fog condition with a parameter that is more general than its visibility range. In one of the models analyzed [25], the parameter that indicates the thickness of fog is the optical depth. The optical depth generally indicates the average number of interactions that light will incur when propagating through a multiple-scatter channel. The optical depth (τ_0) is defined as $\tau_0 = \rho\sigma_t L$, where ρ is the density of fog particles, σ_t is the scattering cross section,

and L is the distance at which fog particles reside. In this study, we specify the distance L to be around 100m and assume that fog covers the whole length of the communication distance. Based on Ref. [22], for transmission range 300m with optical carrier of 670nm wavelength, an optical depth of about 10 corresponds to a visibility of less than 200m. Therefore, a rough idea on wavelength of 630nm can be estimated.

3.7.2.2 Frequency Response of the Channel

Light transmission through dense fog can be analyzed using vector radiative transfer theory (VRTT) [1, 2]. RT theory is based on the assumption of power conservation, and it is applicable for studying multiple-scattering effects. Authors in paper [25] analyzed the ON-OFF keying modulated light transmission through dense fog using this theory and solved RT equations for a band-limited signal to obtain the specific intensity of a received signal in the frequency domain. The received signal consists of two components: the coherent intensity and diffused (incoherent) intensity. The coherent intensity is the function of angular frequency (ω) and the optical depth ($\tau_0 = \rho\sigma_t L$),

$$J_{coh} = I_{coh}(\omega, \tau_0)\, exp(-\tau_0) \tag{3.34}$$

while, the diffused intensity also depends on scatter angle (θ), and given as:

$$J_{diff} = \pi I_d(\omega, \tau_0)\, \theta^2 \tag{3.35}$$

where, the diffused intensity is considered to be uniform for small scattering angles ($\Delta\theta$).

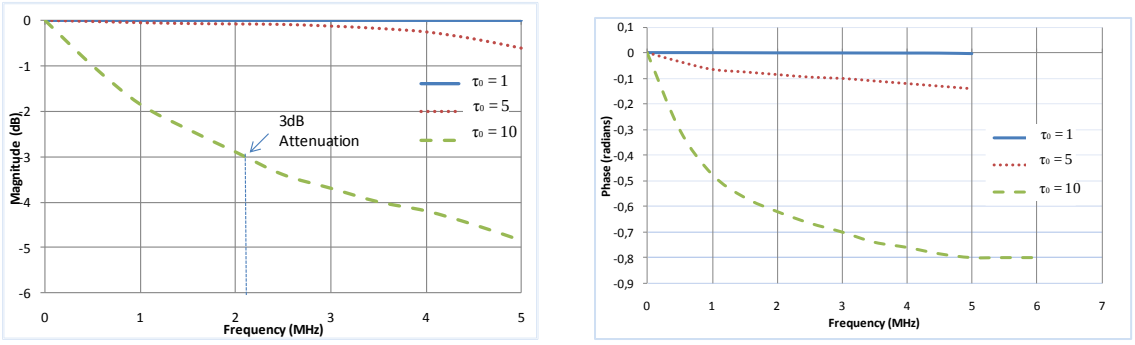

(a) (b)

Fig. 3.22: Frequency Response for Optical depth = 1, 5, 10: (a) Magnitude; (b) Phase

Therefore, the total intensity can be given as:

$$J_t = J_{coh} + J_{diff} = I_{coh}(\omega, \tau_0) exp(-\tau_0) + \pi I_d(\omega, \tau_0)\, \Delta\theta^2 \quad (3.36)$$

For each calculated frequency, the magnitude and the phase of total intensity (J_t) are derived to obtain the frequency response. The frequency response represents the characteristics of the channel as a function of frequency shown in Fig. 3.22. Fig. 3.22(a) shows that the frequency response of the channel has the characteristics of a low pass filter. The phase response of the fog channel displays nonlinear characteristics at low frequency, and it depends on the optical depth as shown in Fig. 3.22(b). The bandwidth is commonly defined at a −3dB frequency. The received signals of τ_0 = 1 and 5 are always higher than −3dB for the frequency range under discussion. For the τ_0 = 10 case, the bandwidth is limited to 2MHz as shown in Fig. 3.22(a). This translates into higher attenuation on the transmitted signals. (Note: τ_0 has no unit).

Atmospheric conditions affect channel variation. In addition, there are multiple of other interfering sources such as, artificial and natural lights. We briefly discuss their effects.

3.8 Noise and Interference

3.8.1 Additive White Gaussian Noise and SNR

In optical channels, the quality of transmission is typically dominated by shot noise [20]. The desired signals contain a time-varying shot noise process which has an average rate of 10^4 to 10^5 photons/bit. In the channel model, however, intense ambient light striking the detector leads to a steady shot noise having a rate of order of 10^7 to 10^8 photons/bit, even if a receiver employs a narrow-band optical filter. Therefore, we can neglect the shot noise caused by signals and model the ambient-induced shot noise as a Gaussian process [3], [71]. When little or no ambient light is present, the dominant noise source is due to the receiver pre-amplifier noise, which is also signal-independent and Gaussian (though often non-white). Accordingly, the optical wireless channel model, as represented in Fig. 3.23 is given as:

$$y(t) = Rx(t) * h(t) + n(t) \quad (3.37)$$

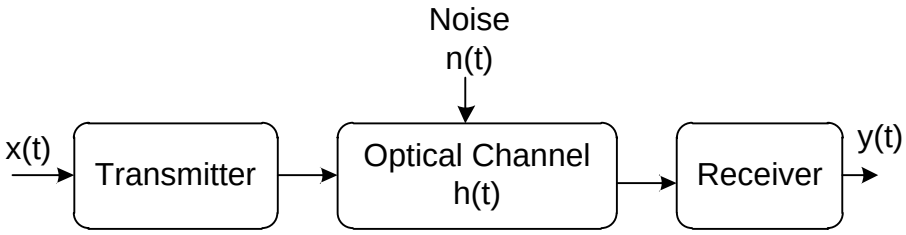

Fig. 3.23: Simple Communication Model

where *y(t)* represents the received signal current, *x(t)* represents the transmitted optical pulse, *n(t)* represents the AWGN noise, and the symbol '*' denotes convolution. *n(t)* is observed in the optical-to-electrical (O/E) converted signal *x(t)*. *R* represents O/E conversion efficiency at a user terminal´s photo detector. The photo detector is the major source of shot noise, its power spectral density is proportional to the detected optical power.

In a LoS path, the received optical power P_s is derived by the transmitted optical power P_t as:

$$P_s = H(0)P_t \tag{3.38}$$

where *H(0)* is the channel gain in LoS path as defined in equation (3.31).

The information bits are transmitted at a bit rate R_b = 1/T bits/sec, where *T* is the symbol period (or symbol interval). The binary sequence emitted by the source *b(t)* represents the signal *x(t)* in Fig. 3.23 can be expressed by:

$$b(t) = \sum_{n=-\infty}^{\infty} a_n g(t - nT) \tag{3.39}$$

where a_n is the information symbols which are binary random variables with the probability of 1/2 for the values of 0 and 1; and *g(t)* is the shaping pulse, normally a square pulse of duration '*T*', the same as the symbol period *T*.

Multipath fading can be neglected in optical wireless channel. In the channel model, the information carrier is a light wave whose frequency is about 10^{14}Hz. Moreover, detector dimension is in the order of thousands of wavelengths, leading to efficient spatial diversity, which also prevents multipath fading. With detector conversion efficiency *R*, the electrical signal is RP_r. The electrical SNR is then defined as [17]:

$$SNR = \frac{\sqrt{2}RP_r}{\sqrt{N_0 B}} \tag{3.40}$$

Assuming that *n(t)* is dominated by a Gaussian component having double-sided power spectral density $N_0/2$ over the desired bandwidth *B*.

The following sections derive the SNR for different conditions and evaluate the performance of the receiver.

3.8.2 Signal to Noise Ratio under Fog Environment

In the fog environment due to optical depth (τ_0), light rays are scattered and therefore, detector's effective FOV gets slightly changed. A detector with area A_d and specified FOV will intercept the light intensity. When the FOV covers only one scatter angle θ, we can replace θ with half-angle FOV. However, when the FOV covers more than one scattering angle, the integration of incoherent intensity from all scattering angles is needed. Following this, the received power was calculated from the specific intensity by solving VRRT equation in [25] with normalized transmitted power of 1W. The received power (P_s) and the background light power (P_{bg}) are defined as:

$$P_s = I_{coh}(\omega,\tau)\{exp(-\tau)\} + \pi\, I_d(\omega,\tau)\, FOV^2 A_d \lambda T_f \tag{3.41}$$

and,

$$P_{bg} = H_{bg}\pi FOV^2 A_d \lambda T_f \tag{3.42}$$

Where, H_{bg} is the background radiance ($Wm^{-2}nm^{-1}sr^{-1}$), λ is wavelength (nm) of the light wave, and T_f is the filter transmittivity.

The received power (P_s) when bit *1* is transmitted (i.e. ON signal) is always higher than the received power when bit *0* is transmitted (i.e. OFF signal). Since, during bit *1* transmission there will also be background power (P_{bg}). If P_1 is the received power during ON state and P_0 is the received power during OFF state. The detector current during ON state (I_1) is:

$$I_1 = RP_1 = RP_s + RP_{bg} \tag{3.43}$$

and, the detector current during OFF state (I_0) is similarly given as (only background power):

$$I_0 = RP_0 = RP_{bg} \tag{3.44}$$

The noise components will have thermal noise (n_{th}), shot noise (n_{sh}), and background radiation (n_{bg}), whose variance is given as:

$$\sigma_{th}^2 = \frac{(4KT_eFB)}{R_L};\ \sigma_{Sh}^2 = 2qRP_sB\ ;\ \sigma_{bg}^2 = 2qRP_{bg}B \tag{3.45}$$

where, K is Boltzman's constant (K = 1.381E-23), q is the electronic charge (q = 1.6E-19 C), T_e is the temperature (290K), F is the circuit noise figure, B is the bandwidth of the detector, R_L is load resistance (ohm), and R, the responsivity of the detector (amperes per watt), defined as:

$$R = \eta q\lambda/hc \tag{3.46}$$

where, η is the quantum efficiency of the photo detector, h is Planck's constant (h = 6.6E-34 J/s), and c is the velocity of the light wave (c = 3E8 m/s).

The detector noise variance during ON and OFF state is given as:

$$\sigma_1^2 = \sigma_{Sh}^2 + \sigma_{th}^2 + \sigma_{bg}^2 \tag{3.47}$$

and,

$$\sigma_0^2 = \sigma_{th}^2 + \sigma_{bg}^2 \tag{3.48}$$

Therefore, SNR can be given as:

$$SNR = \frac{RP_S}{\sqrt{\sigma_0^2} + \sqrt{\sigma_1^2}} \tag{3.49}$$

Substituting P_s from equation (3.41) yields:

$$SNR = \frac{R\left[I_{coh}(exp(-\tau)) + I_d\pi Fov^2\right]A_d\Delta\lambda T_f}{\sqrt{\sigma_{th}^2 + \sigma_{bg}^2} + \sqrt{\sigma_{Sh}^2 + \sigma_{th}^2 + \sigma_{bg}^2}} \tag{3.50}$$

Table 3-8: Simulation Parameters and Settings

Parameters	Value	Parameters	Value
Bolzmann's Constant (k)	1.381e-23	Area of the Detector	1 cm^2
Planck's Constant (h)	6.6e-34 J/s	Responsivity of Detector	0.46 A/W
Electronic Charge (q)	1.6e-19 C	Detector Electronic Bandwidth (B)	10 MHz
Velocity of Light (c)	3e8 m/s	Wavelength (λ)	600e-9 m
Equivalent Temperature (Te)	290 K	Load Resistance	100 Ohm
Circuit Noise Figure	4	Background radiance	0.2 W/m^2 nm sr
Filter Transmissivity (T_f)	0.5	Peak Power	1 W

3.8.3 Receiver Performance under Fog Environment

3.8.3.1 Effect of field of view

It is stated above that the received power also depends of FOV of the detectors. Wider FOV results in increased signal power as well as noise power. Consider the parameters in Table 3-8 which are typical for existing light source and the detector in the specified wavelength range. Noise performance for receiver's FOV is illustrated in Fig. 3.24. From Fig. 3.24, it can be seen that the shot noise is dominant when the optical depth is 1. In this case, the signal is rarely scattered by the fog particles. For the normalized peak power (1W), the shot noise is much more than the background radiation. However, at the optical depth of 10 (extreme case) the signal is scattered, resulting in a variation of the effective FOV and hence, the shot noise is reduced. The information on dominant noise is important to understand the characteristics of the receiver.

Fig. 3.25 illustrates the effect of the effective FOV as a function of optical depth when the received power considered from 1E-12 to 1E-3W. It is seen that the variation in angle is almost 0 (rad) when optical depth is below 7. However when optical depth is increased from 7, the variation of the effective FOV is noticeable. This is because for small values of the optical depth the signal is hardly scattered.

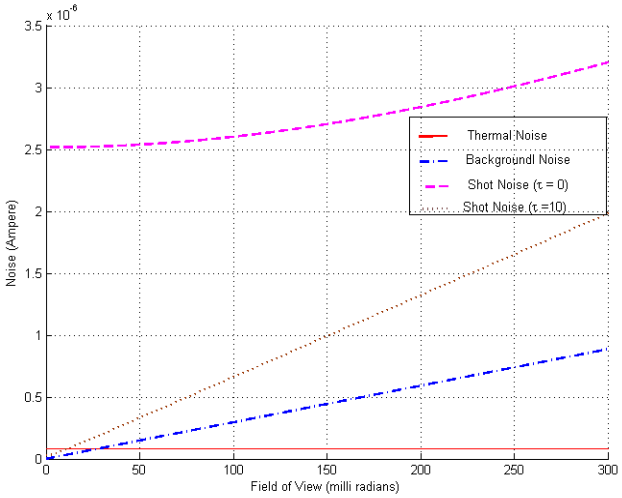

Fig. 3.24: Receiver Noise for Variation of FOV

3.8.3.2 SNR Performance under Fog Environment

SNR variation dependence on FOV is shown in Fig. 3.26(a). It shows that SNR value is almost constant for optical depths near 1. Since, the coherent intensity is independent of the FOV while the incoherent intensity is affected by the FOV as it depends on the scattering angles. However, the variation is very small in terms of milli radians. The SNR increases for increasing FOVs, when optical depth is 10. When optical depth is 5, the variation is much smaller than that of optical depth value 10 for 150 milli radian of FOV and then it follows the behavior of optical depth 10. Moreover, it is also observed that FOV can not be extended and even with slight increase, SNR remains constant.

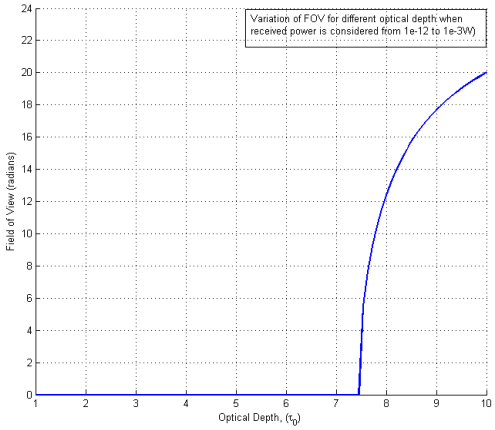

Fig. 3.25: Variation of FOV for Different values of Optical depth

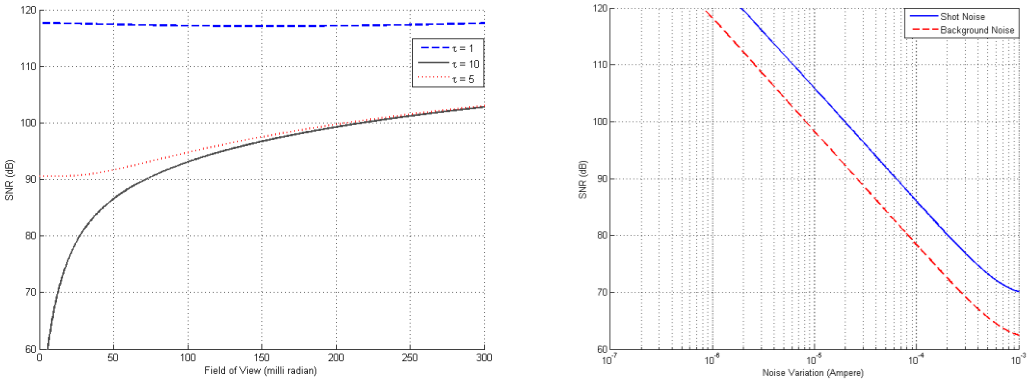

(a) (b)

Fig. 3.26: (a) SNR over FOV for Optical depth of 1, 5 and 10; (b) SNR variation for Variation in Noises

Background noise increases with increase in artificial or natural lights. The effect of variation of noise (shot noise and background noise) is shown in Fig. 3.26(b). It can be seen that there is sharp decay in the SNR value when noise increases.

Thus from the above results it is interpreted that channel behavior deteriorates greatly because of atmospheric conditions. Sun lights are found to be IR sensitive and it has been observed that IR filter improves the performance of the receiver. At the same time, it is also advisable to keep the detector unexposed to direct sun light. Both of these techniques have greatly improved the performance of VLC system.

It has also been discussed that the channel condition is heavily affected by different light sources degrading the performance of the systems. In the following sections, we discuss various sources of light noise.

3.8.4 The Light Interference

The noise is directly proportional to the amount of light incident on the photo-detector, therefore, it is a function of the average optical power. Natural and artificial light sources produce very high levels of irradiance. The average optical power (background) P_{bg} that impinges on the photo detector produces shot noise with power proportional to P_{bg}. Both

natural (sun and moon) and artificial light sources contribute to this effect, but sun light is by far the source with higher impact. The noise caused by sunlight can be considered steady with slow intensity variations over time. Also, fast variations in irradiance caused by artificial light sources produce an interfering signal which is added to the transmitted signal. Artificial ambient light comes from several light sources: lights from cars arriving from opposite direction, fluorescent lamps driven by conventional ballasts and fluorescent lamps geared by electronic ballasts.

3.8.4.1 SNR in presence of Shot Noise

The steady background irradiance produced by natural and artificial light sources is usually characterized by the d.c. current it induces on the receiver PD since the resulting shot noise power is directly proportional to that current [6]. This current is usually referred as the background current (I_{bg}) [26].

This parameter can be easily included in the system models to account for the shot noise produced by the background light. This background irradiance can be measured directly for shiny sun light or fluorescent road lights. Normally, direct sun light is expected to give a maximum current value. We consider that noise elements are from ambient sky light [69] (the spectrum is shown in Fig. 3.27), circuit shot noise and shot noise from the received power

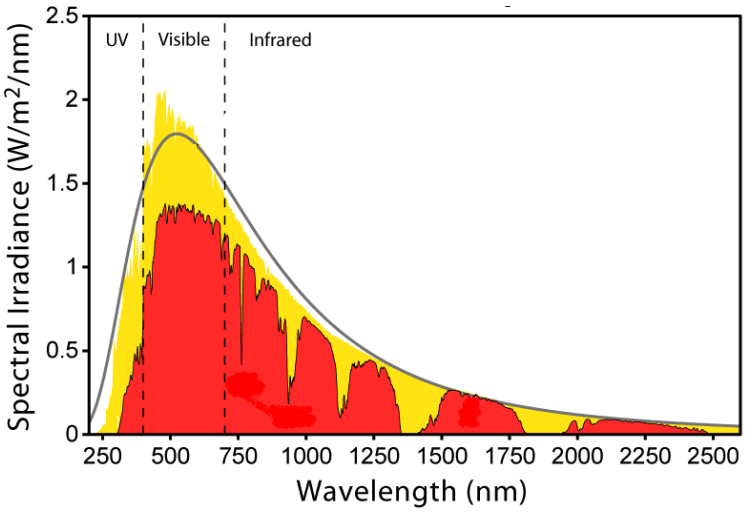

Fig. 3.27: Spectrum of Sun Light [4]

itself. Noise variance of ambient skylight and circuit thermal noise is considered to be the same as in (3.45).

$$\sigma^2 \approx 2qRP_sB + 2qRP_{bg}B + \frac{(4kT_eFB)}{R_L} \tag{3.51}$$

Therefore, the SNR is given as:

$$SNR = \frac{RP_s}{\sqrt{\left[2qRP_sB+2qRP_{bg}B+\frac{(4kT_eFB)}{R_L}\right]}} \tag{3.52}$$

3.8.4.2 Different Light Sources and Interference

Many kinds of street and road lights that are in use today cause interference on VLC systems. However, incandescent lamps and fluorescent lamps equipped with electronic ballasts can induce significant interference, if not filtered out. The average optical power that impinges the photo detector, due to natural and artificial ambient lights, induces very high levels of shot noise posing stringent limitations on the performance of the transmission system [5]. In addition, artificial light sources produce a time varying irradiance, resulting in an optical signal that interferes with the transmitted signal [26, 27]. This interfering signal is periodic and deterministic [26]. The interference induced by artificial lights is characterized through extensive measurements and a simple model was proposed by authors in [26]. Techniques to estimate the model parameters along with some typical values are presented. The model can be used to estimate the optical power penalty induced by this type of interference in VLC systems. Some of the important light sources are:

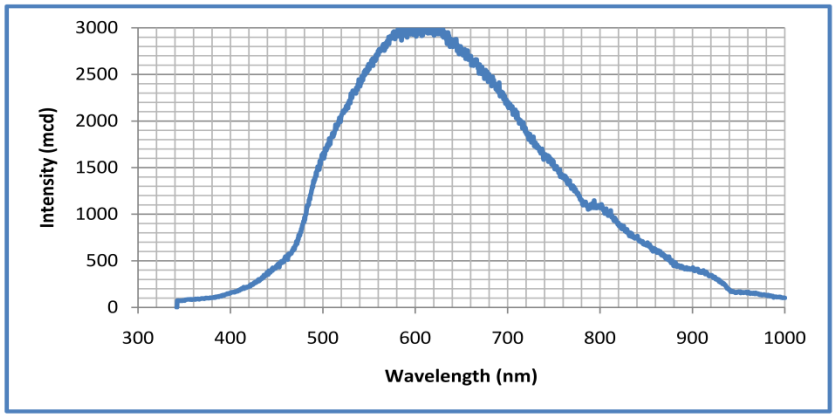

Fig. 3.28: Measured Spectrum of Incandescent Lamp (Philips)

Incandescent and Halogen Lamps – Fig. 3.28 shows the measured spectrum for an incandescent lamp. A sinusoid from approximately 100Hz to 2kHz carry a significant amount of energy and frequency higher than around 800Hz contains component below 60dB from the fundamental.

Fluorescent Lamps – Spectrum of CFL is shown in Fig. 3.29. Though there are many types of fluorescent lamps being used, their waveforms and spectra are quite similar. The interference produced by a conventional fluorescent lamp is a kind of distorted sinusoid and has frequency components over 25kHz. For frequencies higher than 5kHz, the interference power spectral density exceeds 50dB the observed value at 100Hz component. However, interference

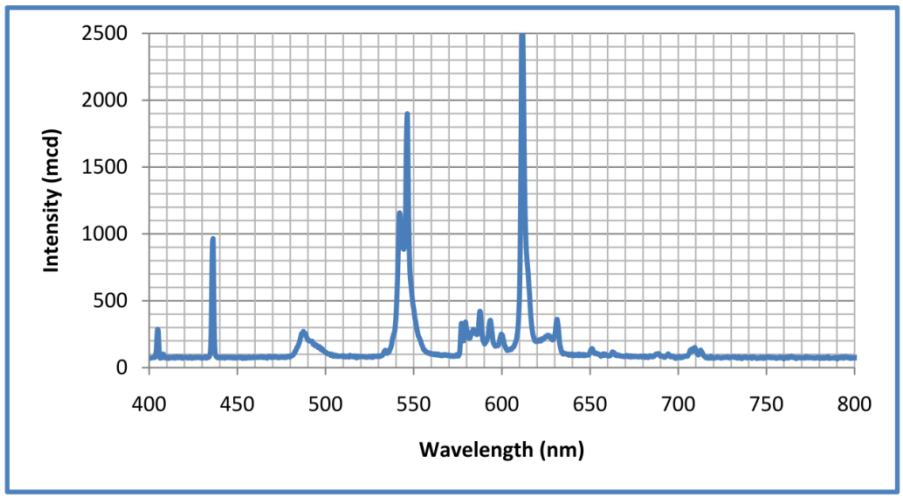

Fig. 3.29: Measured Spectrum of Conventional Fluorescent Lamp (from OSRAM)

produced because of fluorescent lamps driven by electronic ballasts have in addition higher frequency component in the region of 1MHz.

3.8.4.2.1 Interference Model

Sometimes, very high frequency light interference such as fluorescent lamp with electronic ballasts may interfere with VLC system. This can deteriorate the performance. A thorough study was under taken by authors in [26] [64] and models were developed for different artificial light sources. We use the same model in our study. The model is given as:

$$i_m(t) = RP_m + \frac{RP_m}{F_1 A_1} \sum_{k=1}^{10} a_k cos(2\pi(100kt) + \varphi_k) + \frac{RP_m}{F_2 A_2} \sum_{k=1}^{20} b_k cos(2\pi(100k - 50)t + \varphi_k) + c_k cos(200\pi kt + \omega_k) + \frac{RP_m}{F_3 A_4} [d_0 cos(2\pi f_h t + \theta_0) + \sum_{j=1}^{11} d_j cos(2\pi f_h jt + \theta_j)] \quad (3.53)$$

where, P_m is the average optical power of the interfering signal, R is the responsivity of the detector, A_1, A_2, A_4 are the constants that relate the interference amplitude with background current (I_{bg}), F_1, F_2 and F_3 is the optical filter attenuation factor, b_k, c_k are the parameters can be inferred through experiments [26], d_j, Θ_j are highly dependent on the type of electronic ballast, f_h is taken around 40kHz, φ_k are the relative phases of each harmonic of 50Hz and ω_k are phase of the odd harmonics.

The typical values are given in Table 3-9 and Table 3-10.

Table 3-9: Average values for Incandescent Light Interference

k	1	2	3	4	5	6	7	8	9	10
a_k	1	1.72e-2	1.5e-2	5.51e-3	2.85e-3	4.37e-4	8.17e-4	1.28e-3	8.3e-4	6e-4
φ_k	0	1.30	-1.28	-2.98	1.07	-1.08	1.34	-1.37	2.09	-1.8

3.8.5 Minimizing the Effect of Noise

Optical channel in outside environment is dynamic. As stated above it depends on atmospheric conditions, on natural and artificial lights. We can have very little or no control over these. In such situations, either we design high intensity directive emitter or avoid exposure of receiver from interfering sources. The emitter has been designed following this necessity. However for the receiver, during the experiments it was found that if detector is kept directly exposed to bright lights like sun, data reception is practically inhibited. But when the receiver is not allowed to be exposed to direct sun light, the performance of the same receiver is greatly improved. In terms of coverage distance, it was observed that, under direct sun light exposure (receiver facing directly to the sun on shining day at noon) data reception is possible up to a distance of 5-7m, however, the same receiver in the same condition but with the detector not

Table 3-10: Values for the Phase Parameters

k	1	2	3	4	5	6	7	8	9	10
b_k	3.56e-26	1.44e-40	2.93e-47	1.14e-51	5.85e-55	1.37e-57	8.92e-60	1.19e-61	2.73e-63	9.53e-65
C_k	2.05e-5	7.83e-20	2.88e-28	2.99e-34	6.81e-39	1.11e-42	6.86e-46	1.14e-48	4.06e-51	2.62e-53
φ_k	4.61	2.86	5.43	3.9	2.0	5.98	2.38	4.35	5.87	0.70
ω_k	0	0.08	6.0	5.31	2.27	5.7	2.07	3.44	5.01	6.01
k	11	12	13	14	15	16	17	18	19	20
b_k	4.66e-66	2.99e-67	2.42e-68	2.38e-69	2.75e-70	3.68e-71	5.58e-72	9.47e-73	1.77e-73	3.62e-74
C_k	2.72e-55	4.23e-57	9.13e-59	2.62e-60	9.64e-62	4.38e-63	2.40e-64	1.55e-65	1.16e-66	1.01e-67
φ_k	1.26	1.29	1.28	0.63	6.06	5.49	4.45	3.24	2.07	0.87
ω_k	6	6.17	5.69	5.37	4.0	3.69	1.86	1.38	5.91	4.88

directly exposed, is able to receive 90% of data over a distance of around 40m and around 50% of data at 50m distance. The experimental results are presented in chapter six.

The technical approach to reduce the effect of noise is the type of robust modulation that can be used. Different modulation schemes will be discussed in the next chapter.

3.9 Concluding Remarks

This chapter discussed LED-based traffic lights emitter for VLC systems and develops models for arrays of LEDs. More focused was given to co-centric LED array as it resulted in higher performance. LED-based traffic system set-up was also described. Different scenarios were considered and the most suitable model was developed and designed. In this chapter, the propagation path i.e. the channel was also discussed in detail and effects of most prominent atmospheric elements were considered. We have also classified and discussed various sources of noise and their effects on light waves propagating channel. The SNR performance was analyzed and important results were presented.

CHAPTER 4: MODULATION TECHNIQUES FOR VLC SYSTEMS

Summary

There are many technical issues that need to be addressed when designing VLC systems. The most important one is the modulation technique. Background from IR suggests the use of L-PPM while inverted form of this i.e. I-LPPM can also be used depending on lighting arrangements. Similarly, use of equalization can increase the data rate in VLC systems but at the cost of complexity. However, in the outdoor applications, performance of VLC systems suffers from many environmental issues. To minimize these effects different modulation methods become apparent for different data rates and transmission ranges. In this chapter, various possible modulation techniques are discussed. Based upon the comparative performance, direct sequence spread spectrum (DSSS) based on sequence inverse keying (SIK) modulation technique is recommended for noisy environment such as road safety applications. In this chapter DSSS SIK technique is analyzed and important results are presented. A Matlab/Simulink model for VLC system is developed and analytical results are verified.

4.1 Introduction

The previous chapter showed that the performance of VLC systems is likely to be impaired by the significant high path loss and the noise induced by external lights. High path loss leads to the use of considerably high optical power levels. In addition, they also suffer from the speed of optoelectronic devices (LEDs and PIN photodiodes). System performance varies depending on the environment conditions, data rate, technical solutions and implementation of a particular system.

In the application of traffic information broadcast system, data is received by the receiver installed on moving vehicles. In the case of uniform motion assumption, the amount of data received will depend on the data transmission rate, velocity of the vehicle and the road length (service area) in which data can be received. This is given by the relation:

$$Received\ data[bit] = \frac{Transmission\ Rate[bits/sec]\ X\ Service\ Area[m]}{Velocity\ of\ Vehicle[kmph]} \tag{4.1}$$

That is, the received data increases with the distance (increase in service area). However, the possibility of interference also increases with distance. Assuming, a vehicle approaching traffic point at a speed of 60kmph that is, covering 16.6m of distance each second. Considering a data rate 100kbps, and a service area between 2.5m to 70m of road length, the amount of received data comes to be approximately 150kbits to 420kbits. Furthermore, a text message of around 10kbits (more or less the amount of data in an A4 page) of displayed data can be easily viewed or read by drivers using car built-in radio displays or intended computers. This means that each second 15 to 42 times, 10kbits of data can be sent by VLC broadcast transmitter and receiver is expected to reliably receive the information. If the transmitted information is repeated a number of times, the driver will have little over 4 seconds to read the message before crossing the service area when green signal remains on (the worst case condition). However, if the vehicle needs to stop for red signal there will not be a problem in receiving and reading the information. Also, Doppler effect [6] which is given in its simple form as:

$$f_r = \left(\frac{c+v_r}{c}\right) f_s \tag{4.2}$$

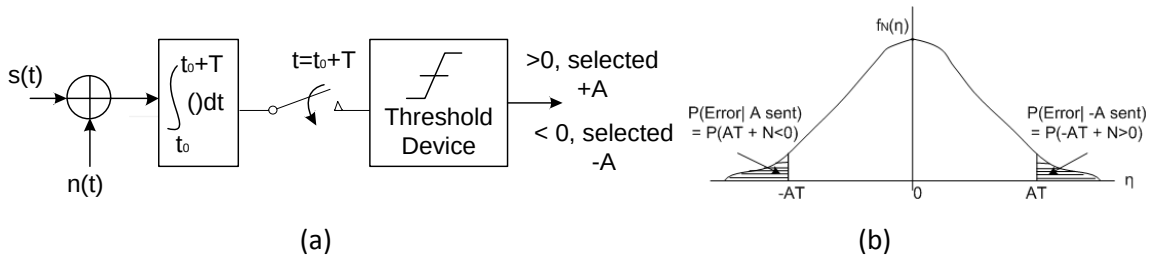

Fig. 4.1:(a) Integrate-and-dump Receiver; (b) Illustration of Error Probabilities for Binary Signaling

where, f_r is the receiver's frequency, f_s is the source frequency, c is the velocity of light wave, and v_r is the velocity of receiver. Thus, for the above parameters there is a shift, or delay, of less than 5.556E-15s, which can be ignored.

The above scenario is applicable in normal conditions i.e. when LoS channel is free from other disturbances such as fog, rain and dense dust. But under these conditions the channel behavior will vary and thus the service area will be affected. Therefore, a robust modulation technique is required for this system. DSSS based modulation has been widely used in radio systems and considered robust especially in noisy environments. However, the requirements of transmission bandwidth increase thereby affecting data rate. But, in traffic information broadcast in road safety applications the data rate is not an important issue. Minimizing the main effect of external noise is the most important.

In this chapter, we focus on one of the most robust modulation techniques based on DSSS. The choice for the method is also supported for low data rate applications. The primary measure of system's performance for digital data communication system is the probability of error (P_E) [5] [28]. Therefore, we derive a generic expression for P_E and SNR for baseband data transmission on AWGN channel.

4.2 Baseband Data Transmission in White Gaussian Noise

Consider the binary digital data communication system with transmitted signal consisting of a sequence of constant amplitude pulses of either A or $-A$ units in amplitude and T seconds duration. Considering a detector with an Integrate and dump architecture (Fig. 4.1a), its

performance can be evaluated with probability of error of the received signal. The output of the integrator at the end of a signaling interval is:

$$V = \int_{\tau_0}^{\tau_0+T} [s(t) + n(t)]\ dt \tag{4.3}$$

where, *s(t)* is the incoming signal and *n(t)* is the noise signal with double sided power spectral density $N_0/2$. That is:

$$V = \begin{cases} +AT + N, & if + A\ is\ sent \\ -AT + N, & if - A\ is\ sent \end{cases} \tag{4.4}$$

where *N* is a random variable defined as:

$$N = \int_{\tau_0}^{\tau_0+T} n(t)\ dt \tag{4.5}$$

Since *N* results from a linear operation on a sample function from a Gaussian process, it is a Gaussian random variable. It has the mean:

$$E\{N\} = E\{\int_{\tau_0}^{\tau_0+T} n(t)dt\} = \int_{\tau_0}^{\tau_0+T} E\{n(t)\}dt = 0 \tag{4.6}$$

since *n(t)* has zero mean. Its variance is therefore,

$$var\{N\} = E\{N^2\} = E\left\{\left[\int_{\tau_0}^{\tau_0+T} n(t)dt\right]^2\right\}$$

$$= \int_{\tau_0}^{\tau_0+T}\int_{\tau_0}^{\tau_0+T} E\{n(t)n(\sigma)\}dt\ d\sigma$$

$$= \int_{\tau_0}^{\tau_0+T}\int_{\tau_0}^{\tau_0+T} \frac{1}{2}N_0\ \delta(t-\sigma)dt\ d\sigma \tag{4.7}$$

Using the shifting property of the delta function, we obtain:

$$var\{N\} = \frac{1}{2}\ (N_0\ T) \tag{4.8}$$

Thus, the probability density function (pdf) of *N* is:

$$f_N\ (\eta) = \frac{exp^{-\frac{\eta^2}{N_0 T}}}{\sqrt{\pi N_0\ T}} \tag{4.9}$$

where η is used as the dummy variable for *N* to avoid confusion with *n(t)*.

4.2.1 Probability of Error and Signal-to-Noise Ratio

The probability of error and SNR are two of the most important performance parameters of a communication receiver. The probability of error is defined as the probability of making a wrong decision, resulting in a different value for each type of error. For transmission of +*A*, an error occurs if AT + N < 0, that is if N < -AT. The probability of this event is:

$$P(error|A\ sent) = P(E|A) = \int_{-\infty}^{-AT} \frac{exp^{-\frac{\eta^2}{N_0 T}}}{\sqrt{(\pi N_0\ T)}}\ \mathrm{d}\eta \tag{4.10}$$

which is the area to the left of $\eta = -AT$ in Fig. 4.1(b). Letting:

$$u = \frac{-\sqrt{2}\,\eta}{\sqrt{N_0 T}} \tag{4.11}$$

we can write as:

$$P(E|A) = \int_{\sqrt{\frac{2A^2T}{N_0}}}^{\infty} \frac{exp^{-\frac{u^2}{2}}}{\sqrt{2\pi}} du \triangleq Q\left(\sqrt{\frac{2A^2T}{N_0}}\right) \tag{4.12}$$

where Q is an error function[1]. The other way in which an error can occur is, if –A is transmitted and –AT+N > 0. The probability of this event is the same as the probability that N > AT, which can be written as:

$$P(E|-A) = \int_{AT}^{\infty} \frac{exp^{-\frac{\eta^2}{N_0 T}}}{\sqrt{\pi N_0 T}}\ d\eta \triangleq Q\left(\sqrt{\frac{2A^2T}{N_0}}\right) \tag{4.13}$$

which is the area to the right of $\eta = AT$ in the Fig. 4.1(b). The average probability of error is:

$$P_E = P(E|+A)P(+A) + P(E|-A)P(-A) \tag{4.14}$$

Substituting (4.12) and (4.13) into (4.14) and assuming that P(+A) = P(-A) = 0.5, we obtain:

$$P_E = Q\left(\sqrt{\frac{2A^2T}{N_0}}\right) \tag{4.15}$$

We can interpret the ratio A^2T/N_0 in two ways. First, since the energy in each signal pulse is:

[1] $Q(z) = \int_z^{\infty} \frac{1}{2\pi} exp^{-\frac{y^2}{z}}\, dy$, and also, $Q(z) = \frac{1}{2}\left[1 - erf\left(\frac{z}{\sqrt{2}}\right)\right] = \frac{1}{2} erfc\left(\frac{z}{\sqrt{2}}\right)$

$$E_b = \int_{t_0}^{t_0+T} A^2\, dt = A^2\, T \tag{4.16}$$

We see that the ratio of signal energy per pulse to noise power spectral density is:

$$SNR = \frac{A^2\, T}{N_0} = \frac{E_b}{N_0} \tag{4.17}$$

where, E_b is called the energy per bit because each signal pulse (+A or –A) carries one bit of information. Second, we know that a rectangular pulse of duration T seconds has amplitude spectrum ($AT\ sinc\ Tf$) and that $R_b = 1/T$ is a rough measure of its bandwidth. Thus,

$$SNR = \frac{A^2}{(N_0\, R_b)} \tag{4.18}$$

can be interpreted as a function of bandwidth (data rate).

Next, we examine the performance of various modulation techniques.

4.3 Basic Modulation Techniques

The choice of modulation technique in the design of VLC systems remains one of the most important technical issues. Background from IR technology suggests the use of modulation techniques such as OOK, L-pulse position modulation (L-PPM), subcarrier phase shift keying (SC-PSK) and these have been discussed and proposed [20], [29], [70]. Utilization of equalization techniques for IR as well as indoor short range VLC has also been proposed by authors in [71, 72]. The use of equalizers substantially increases the receiver complexity while OOK and L-PPM though simple to implement are affected by interference due to artificial light sources.

In the following sections, we discuss various modulation techniques. OOK technique which forms the basic standard for evaluation is discussed below.

4.3.1 On-Off Keying – Non Return to Zero (NRZ)

On-Off-Keying is the simplest form of amplitude-shift keying (ASK) modulation that represents digital data as the presence or absence of a carrier wave. In its simplest form, the

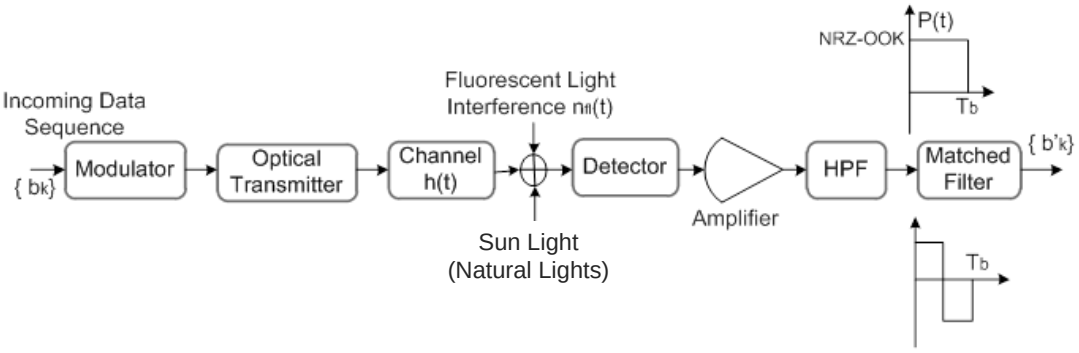

Fig. 4.2: Block Diagram of a Typical IM/DD Receiver

presence of a carrier for a specific duration represents a binary one, while its absence for the same duration represents a binary zero. Some more sophisticated schemes vary these durations to convey additional information. OOK is analogous to unipolar line code [5, 20].

The block diagram of a typical receiver system employing IM/DD is shown in Fig. 4.2. Information bits are the inputs to the modulator (NRZ or Manchester) at a bit rate of R_b (bit per second (bps)). Pulse waveforms produced by the modulator for each bit drive the optical transmitter. The intensity-modulated optical signal passes through a time-dispersive multipath channel that is fully characterized by its impulse response $h_c(t)$. The incoming optical signal is converted to an electrical signal by the photodiode, using direct detection.

This electrical signal consists of a distorted replica of the transmitted signal, shot noise, $n_{sh}(t)$, as well as fluorescent lights periodic interference, $n_{fl}(t)$. The high pass filter (HPF) at the receiver front end, after the photodiode, is modeled as a first-order RC filter with a cut-off frequency of f_o. Matched filtering using Integrate and dump filter is assumed for all modulation schemes. In the absence of fluorescent light and inter symbol interference (ISI), this corresponds to the optimum maximum-likelihood (ML) receiver [28].

The peak amplitude of the received signal pulses is A, and is directly proportional to the optical power, i.e., $A= 2RP_s$, where R is the photodetector responsivity and P_s is the average received optical power [28]. The power spectral density (PSD) of the Gaussian shot noise $n_{sh}(t)$ is denoted by N_0. The shot noise PSD is dependent on the total DC-generated photocurrent,

i.e., $N_0 = 2q(I_B + i_b)$, where I_B is the DC photocurrent generated by stationary ambient lighting, i_b is the average level of the fluorescent light interference and q is the charge of one electron.

The transmitted signal waveform can be described as an infinite series of time delayed replicas of the basic pulse waveform *p(t):*

$$S(t) = \sum_{k=-\infty}^{\infty} a_k \, p(t - kT_b) \tag{4.19}$$

where *p(t)* is the rectangular pulse of duration $T_b = 1/R_b$ and a_k is the information bearing amplitude. If the signal is Manchester, *p(t)* is an alternating pulse of the same duration with mid-bit transition. Ignoring noise components, the received signal pulse *r(t)* at the input of the matched filter will be:

$$r(t) = h_F(t) * p(t) \tag{4.20}$$

where $h_F(t)$ is the impulse response of the HPF and $'*'$ denotes convolution.

4.3.1.1 Bit Error Rate for OOK Modulation

On-Off-Keying transmitter emits a rectangular pulse of duration $1/R_b$ and of intensity $2P$ to signify a one bit, and no pulse to signify a zero bit. The bandwidth required by OOK is roughly R_b [30]. BER is given in terms of minimum distance. In this type of receiver design, the receiver will choose a signal from the set of known signals which is the closest to the received signal. Since the receiver observes which of the possible signals is closest to the received signal, it stands to reason that it is less likely to make an error due to noise. That is, one important measure of the noise immunity of a given signal set is the minimum-distance between signals, defined as:

$$d_{min} = \min_{i \neq j} \|x_i - x_j\| \tag{4.21}$$

Or

$$d_{min}^2 = min \int_{i \neq j} \left[x_i(t) - x_j(t)\right]^2 dt \tag{4.22}$$

where d_{min} is the minimum Euclidean distance. Fig. 4.3 shows a graphical illustration of Euclidean minimum distance between two signals.

For the OOK case, the minimum distance in terms of energy per bit is derived to be:

$$d^2{}_{ook} = 2E_b \qquad (4.23)$$

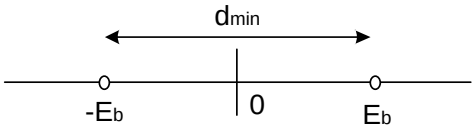

Fig. 4.3: Illustration of Minimum Distance

where, E_b is the energy per bit. The BER is then given in terms of minimum distance as:

$$BER = Q\left(\frac{d_{min}}{\sqrt{2N_0}}\right) \qquad (4.24)$$

and, the BER for OOK system is therefore:

$$BER_{OOK} = Q\left(\sqrt{\frac{E_b}{N_o}}\right) = Q\left(\sqrt{\frac{2R^2P_S^2T_b}{N_o}}\right) \qquad (4.25)$$

where, R is the responsivity of the detector, P_s is the average power, and T_b is the bit interval. Also, in terms of error function, it is given as:

$$BER_{OOK} = \frac{1}{2}\, erfc\left(\sqrt{\frac{R^2P_S^2T_b}{N_o}}\right) \qquad (4.26)$$

The power required by OOK to achieve a given BER is:

$$P_{OOK} = \frac{1}{R}\sqrt{\frac{N_0\, R_b}{2}}\; Q^{-1}(BER) \qquad (4.27)$$

For any other modulation scheme to achieve the same error probability, the required power is approximately:

$$P_{req} = \left(\frac{d_{OOK}}{d_{min}}\right) P_{OOK} \qquad (4.28)$$

4.3.2 Pulse Position Modulation (PPM)

Higher average power efficiency can be achieved by employing pulse modulation schemes in which a range of time dependent features of a pulse carrier may be used to convey information.

PPM has been used widely in optical communication systems. It is a scheme where pulses of equal amplitude are generated with signal's information modulated on pulse position. During PPM transmission, signal pulses have fixed width and amplitude, the information is represented by the pulse position in time.

L-PPM utilizes symbols consisting of *L* time slots (chip). A constant power *LP* is transmitted during one of these chips and zero during remaining *(L-1)* chips. Hence, encoding $log_2 L$ bits in the position of the high chip. If the amplitude of transmitted waveform is *A*, the average transmitted power of 2PPM is *A/2*, that of 4PPM is *A/4*, and for L-PPM is *A/L*. For any *L* greater than 2, PPM requires less optical power than OOK. In principle, the average optical power requirement can be made arbitrarily small by making *L* suitably large, at the expense of increased bandwidth.

For a given bit rate, L-PPM requires more bandwidth than OOK by a factor of $L/\log_2 L$ i.e. 16-PPM requires four times more bandwidth (BW) than OOK. The bandwidth required by PPM to achieve a bit rate of R_b is approximately the inverse of one chip duration, B = L/T [20, 30]. In addition to the increased bandwidth requirement, PPM needs (as compared to OOK) more transmitted peak power and both slot and symbol-level synchronization [31].

In the absence of multipath distortion, L-PPM yields an average–power requirement that decreases steadily with increasing *L*; the increased noise associated with a $(L/\log_2 L)$-fold wider receiver noise BW is out weighted by the *L*-fold increase in peak power.

Fig. 4.4 shows the block diagram of the L-PPM system. Input bits, at rate R_b, enter a PPM encoder, producing L-PPM symbols at rate $R_b/Log_2 L$. Each symbol contains a single

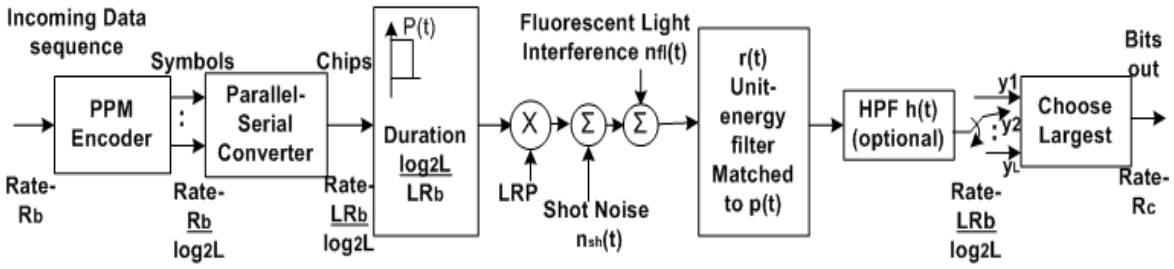

Fig. 4.4: Block Diagram of L-PPM System

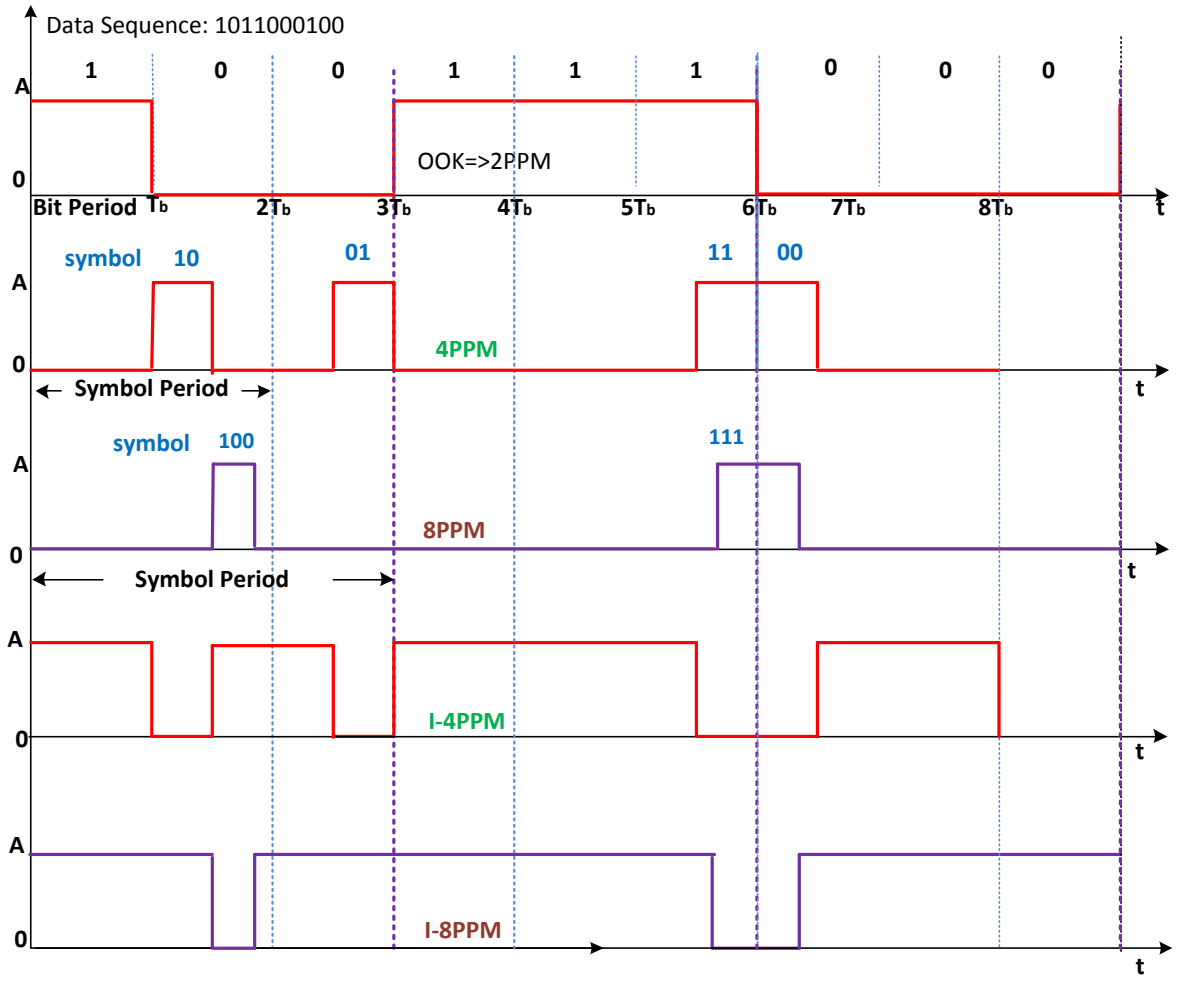

Fig. 4.5: Illustration of L-PPM and I-LPPM Waveforms

sample of unit amplitude and *(L-1)* samples of zero amplitude as shown in Fig. 4.5. The PPM symbols are converted to a serial sequence of chips at rate $LR_b/\log_2 L$ and passed to a transmitter filter whose impulse response *p(t)* is a unit-amplitude rectangular pulse of duration $\log_2 L/LR_b$. The chips are scaled by LRP, shot noise *n(t)* and fluorescent-light interference $n_{fl}(t)$ are added. The receiver employs a unit energy filter *r(t)*, matched to *p(t)*, which is followed by high pass filter of response *h(t)*. The filtered signal is sampled at rate $LR_b/\log_2 L$ and passed to a comparator that determines which sample in each L-length block has the largest value thus yielding the output bit sequence. Without fluorescent light and high pass filtering, the receiver is ML receiver.

For this type of receivers, the set of PPM symbols is orthogonal, of the form:

$$X_m = [0,0,\dots.,b_m,0,0] \tag{4.29}$$

where the non-zero term is in the *m-th* position. Thus, every symbol has the same distance to the others.

4.3.2.1 Bit Error Rate of L-PPM

For *L* orthogonal signals, there are *(L-1)* other signals at minimum distance, and the error probability is independent of which signal is transmitted. Assuming that the information is random with uniform distributions. The minimum distance in this case is given as:

$$d_{min}^2 = 2E_b log_2 L \tag{4.30}$$

In terms of average power the minimum distance is:

$$d_{min}^2 = 4R^2 P_s^2 T_b \log_2 L \tag{4.31}$$

So that,

$$BER_{L-PPM} = Q\left(\sqrt{\frac{E_b}{N_o}}\sqrt{\log_2 L}\right) = Q\left(\sqrt{\frac{2R^2 P_S^2 T_b}{N_o}}\sqrt{\log_2 L}\right) \tag{4.32}$$

The average optical signal power required to achieve a given BER for an L-PPM system can be found by solving for P_s:

$$P_{req-LPPM} = \frac{1}{R}\left(\frac{N_o R_b}{2\log_2 L}\right) Q^{-1}(BER) \tag{4.33}$$

The power penalty in terms of P_{ook} is given as:

$$P_{req-LPPM} = \frac{P_{OOK}}{\sqrt{log_2 L}} \tag{4.34}$$

That is, L = 2 yields a sensitivity for 2-PPM that is identical to OOK. We see that, for any *L* greater than two, the optical power required by L-PPM is smaller than that required by OOK.

It can also be noted that, 2-PPM has the same power efficiency as OOK but requires twice the bandwidth. It is apparent that 4-PPM is particularly attractive because it has the same bandwidth requirement as 2-PPM but requires 3.8dB less optical power. As *L* increases from 4

to 16, the bandwidth requirement increases from $2R_b$ to $4R_b$, while the sensitivity (required power, from equation 4.33) increases from 3dB to 7.5dB better than OOK.

For a given transmitter power, background illumination power, and bit rate, it is desirable to maximize the coverage area between transmitter and receiver, which is equivalent to maximizing the power efficiency.

4.3.3 Inverted – PPM (I-PPM)

In the case of conventional PPM, we set only one pulse among *L* sub intervals. Average transmitted power, i.e. LED brightness, falls to *1/L* when the peak amplitude is not changed. Of course, LED brightness can be made to equal with other modulation methods if we increase the amplitude *L* times (practical limitation with power constraint). I-PPM yields higher brightness than conventional PPM. Inverting the pulse position of conventional PPM, we obtain I-PPM. The optical intensity is 'off' during the 1-th sub-interval and 'on' everywhere else as shown in Fig. 4.5. For example, in case of 4-PPM light is 'on' equivalent to 3-chip duration, making the LED three times as bright as conventional 4PPM. When amplitude of the transmitted waveform is *A*, average transmitted power of I-4PPM is *3A/4*. That is, the average transmitted power of I-L-PPM is *(L-1)A/L*.

4.3.3.1 Bit Error Rate of I-LPPM

In the case of I-LPPM, the minimum distance is given as:

$$d_{min}^2 = \frac{2E_b \log_2 L}{L-1} \tag{4.35}$$

and, the BER is:

$$BER_{I-LPPM} = \sqrt{\frac{E_b}{N_o}} \sqrt{\frac{\log_2 L}{L-1}} = Q\left(\sqrt{\frac{2R^2 P_s^2 T_b}{N_o}} \sqrt{\frac{\log_2 L}{L-1}}\right) \tag{4.36}$$

The average optical signal power required to achieve a given BER for an I-LPPM system can be found by solving for P_s:

$$P_{req-ILPPM} = \frac{1}{R} \sqrt{\frac{N_o R_b}{2}} \sqrt{\frac{L-1}{\log_2 L}}\, Q^{-1}(BER) \tag{4.37}$$

and, power penalty in terms of P_{ook} is:

$$P_{req-ILPPM} = \sqrt{\frac{L-1}{\log_2 L}}(P_{OOK}) \tag{4.38}$$

The simulation results are given in section 4.4.3. From the simulation results it is observed that L-PPM forms of modulation are power efficient and can increase the data transmission rate. However, that may result in inter-symbol interference and increased bandwidth. On the other hand, I-LPPM is suitable for the scenario where power is not a constraint that is required illumination remains to be in place. This means, they are not power efficient. However, the effect of noise on the systems remains an issue and in VLC systems the noise effect needs to be minimized. This implies that a different approach must be considered. From the background on RF technology we know the bandwidth spreading can minimize the effect of noise on the channel. In the next section, this issue is discussed in detail using DSSS technique.

4.4 Direct Sequence Spread Spectrum

4.4.1 Basic Operation

In a direct sequence spread spectrum communication system [5], the spectrum spreading is accomplished before transmission through the use of a spreading code that is independent of the data sequence. The same spreading code is used in the receiver (operating in synchronism with the transmitter) to de-spread the received signal so that the original data may be recovered. The information-bearing signal is multiplied by a spreading code so that each information bit is divided into a number of small time slots. These small time slots are commonly referred to as chips. In this process the narrow bandwidth of the information-bearing signal is spread over a wide bandwidth with a factor *N* which is equal to the length of the spreading sequence.

Spread-spectrum communication techniques may be very useful in solving different communication problems. The amount of performance improvement that is achieved through the use of spread-spectrum, relative to an unspread system, is described in terms of a so-called

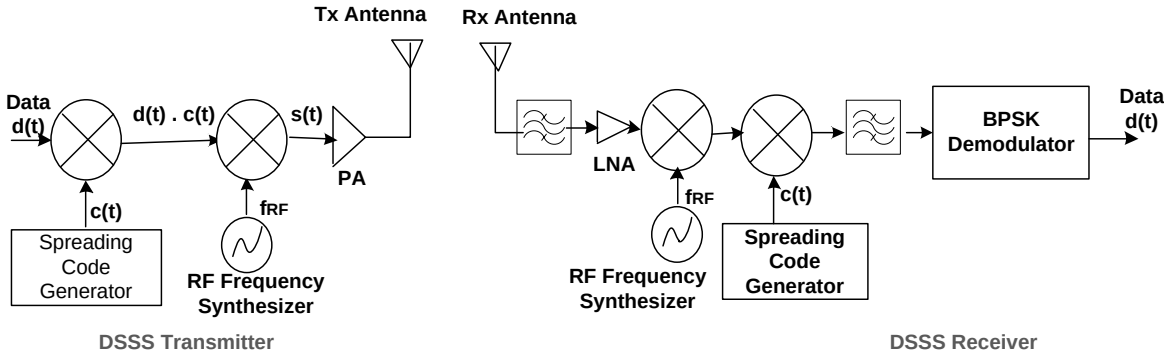

Fig. 4.6: Conceptual Block Diagram of DSSS Transmitter and Receiver

processing gain (PG) factor. In spread-spectrum modulation an information signal is transformed into a transmitted signal with a much larger bandwidth. The transformation is achieved by encoding (spreading) the information bearing signal with a spreading code signal. This process spreads the power of the original data signal over a much broader bandwidth, resulting in a lower power spectral density than the unspread information signal. When the spectral density of the resultant spread spectrum signal starts to merge with or fall below the background noise level, the DSSS communication signal enters a state of low visibility or perception, making it hard to locate or intercept. This communication mode is commonly referred to as low probability of interception (LPI), and offers a form of security, which was previously exploited for military applications [5], but is presently applied to a host of commercial applications. The PG of the spread-spectrum system can be defined as the ratio of transmission bandwidth to information bandwidth:

$$PG = \frac{B_T}{B_B} = \frac{T_b}{T_c} = \frac{R_c}{R_b} = N \tag{4.39}$$

where B_T is the transmission bandwidth, B_B is the bandwidth of information-bearing signal, T_b is the bit period of the data signal, T_c is the chip period of the spreading code, R_c is the chip rate of the spreading sequence, R_b is the bit rate of the data signal and N is the length of the spreading code.

The receiver correlates the received signal with a synchronously generated replica of the spreading code signal to recover the original information-bearing signal. This implies that the receiver must know the spreading sequence or code used to spread or modulate the data.

The basic spreading process in a direct sequence spread-spectrum system is illustrated in the conceptual block diagram of a DSSS transmitter and receiver in Fig. 4.6. The information-bearing signal *d(t)* is multiplied by the spreading code *c(t)* and modulated onto a RF carrier frequency to obtain a final spread output signal *s(t)*;

$$s(t) = d(t)c(t)cos(2\pi f_{RF}\, t) \tag{4.40}$$

where, f_{RF} is the carrier frequency.

The incoming signal is received by the RF front-end consisting of basically a noise reject band pass filter, a low noise amplifier (LNA) and a mixer to down-convert the RF signal to intermediate frequency (IF). This DSSS IF signal is de-spread and band pass filtered, where after the de-spread signal is demodulated by means of a binary phase shift keying (BPSK) demodulator, to recover the original information-bearing signal *d(t)*. The process of spreading and de-spreading signal in frequency domain is depicted in Fig. 4.7.

A DSSS system employing complex spreading sequences may include several advantages, such as offering perfectly constant envelope output signal including the possibility to generate a single side band (SSB) DSSS signal with theoretically up to 6dB more PG than offered by conventional double side band (DSB) system while exhibiting comparable auto and

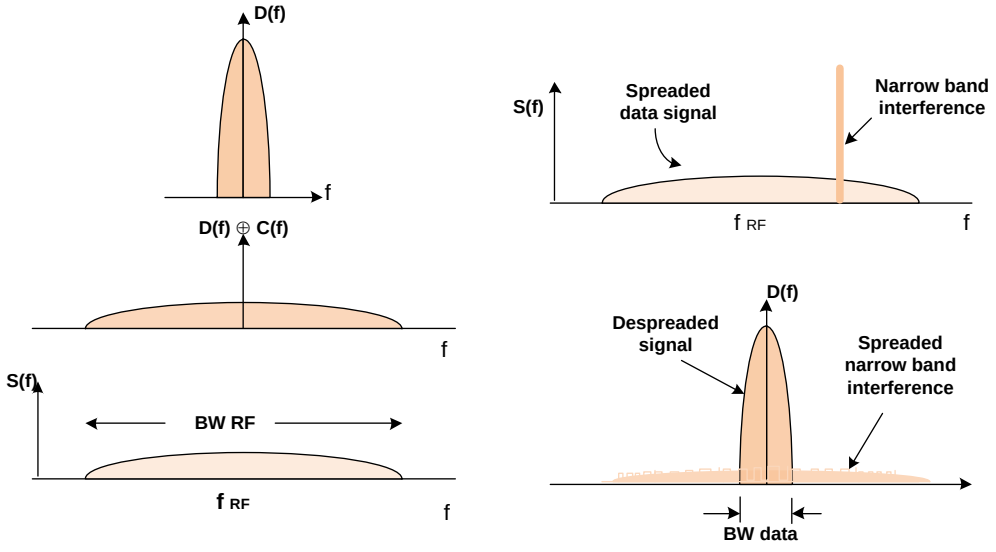

Fig. 4.7: Spreading/de-spreading Process of Signal in Frequency Domain

improved cross correlation properties compared to any other binary (DSSS) presently employed [7].

4.4.2 DSSS Modulation in VLC System

Spread spectrum modulation technique can minimize the effect of interference according to the processing gain advantage. While the additional bandwidth requirement of a spread-spectrum modulation scheme reduces the system bandwidth efficiency, the processing gain of the spread spectrum technique helps to combat artificial light interference effects and multipath dispersion (if any) without the need for extra circuitry such as equalizers. A form of DSSS technique called sequence inverse-keying (SIK) [16] is able to combat these two important channel impairments and is a potential modulation method for low data rate VLC in outdoor applications.

4.4.2.1 Basic Principle

The use of DSSS in optical wireless (OW) system is based on the basic principle of unipolar-bipolar correlation [32]. In radio systems, DSSS uses bipolar spreading sequences that cannot be used as such in the all-positive (unipolar) optical medium. Because in optical medium there is no negative going pulses and when there is no light pulse, the signal has to be represented by zero level. Therefore, a technique called unipolar-bipolar sequencing, allows the same spreading codes of radio systems to be used in optical systems, is employed instead. Unipolar-bipolar sequencing, involves transmission of a unipolar spreading sequence and correlation with a bipolar version of the same spreading sequence, preserves the correlation properties of bipolar-bipolar sequencing although with the introduction of a fixed dc offset.

At the transmitter, a unipolar spreading sequence is modulated by binary data such that the sequence is transmitted for a binary ‘1’ while the inverse (complement) sequence is transmitted for a binary ‘0’. This type of modulation is called as SIK. The resulting spread spectrum signal uses a rectangular NRZ chip waveform to modulate the intensity of the visible light source (LEDs). At the receiver, the optical signal is detected and processed. The spread signal may be AC coupled prior to de-spreading, in order to remove the unwanted DC signal

components introduced by the optical channel. AC coupling does not alter the correlation properties of the spreading sequence, thus de-spreading can use the bipolar version of the unipolar spreading sequence. For a single correlator detection, the de-spread signal is integrated over the data bit period T_b and sampled at intervals of $t = T_b$. The sample value at the correlator output is zero-threshold detected such that either a positive or a negative sample results in a binary '1' or '0' estimate of the transmitted data bit, respectively.

4.4.2.2 Sequence Inverse Keying Modulator

Fig. 4.8 shows the schematic diagram of the transmitter and receiver of SIK system. The modulator part basically performs digital operation of XNOR where incoming data bit is modulated by a pseudo noise (PN) random data with a bit rate higher than the data bit. Thus, the transmitted data is said to be spread. A similar operation is needed at the receiver to de-spread the incoming sequence from the channel.

Consider the unipolar binary data *b(t)* from traffic information source given as:

$$b(t) = \sum_{k=-\infty}^{\infty} b_k(t) \tag{4.41}$$

for $b_k \in \{0,1: -\infty \leq k \leq \infty\}$. b_k is XNORed with unipolar spreading sequence *s(t):*

$$s(t) = \sum_{n=0}^{N-1} s_n(t) \tag{4.42}$$

where, $s_n \in \{0,1: n = 0,1, \ldots..N-1\}$, with *N* being the sequence length, T_c is the chip duration and $T_b = NT_c$. The duration of *N* chips in one period of the spreading sequence is equal to the bit duration. In fact, the XNOR function realizes the SIK modulation format. The spread data is then used to modulate the intensity of the LED light source. The optical signal is characterized by an average optical power *P* and a peak pulse power *2P*. The light propagates through free space channel, get added with noise and then, detected by photodiode.

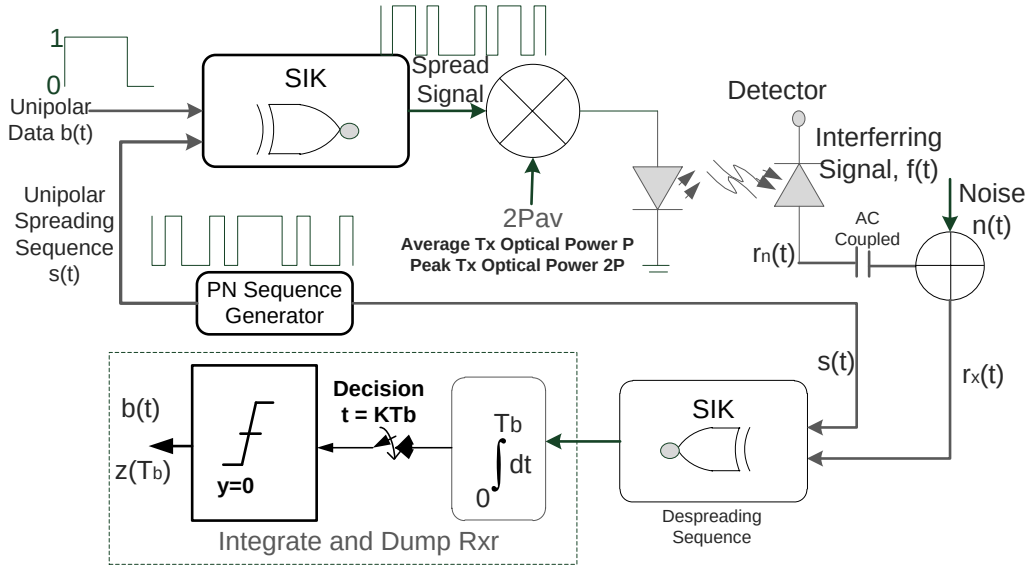

Fig. 4.8: SIK Modulation for VLC

The photodiode responsivity is R=A/W. The detected photocurrent for the LoS case can be given as:

$$r_n(t) = 2RP_s b(t) \oplus s(t) + f(t) + n(t) \tag{4.43}$$

where, P_s is the mean optical power of the desired LoS signal impinging the photodiode, *f(t)* is the interfering signal at the output of the photodiode due to ambient light, *n(t)* is the channel noise process (including amplifier thermal noise and shot noise, considered additive white Gaussian noise with power spectral density $N_0/2$). *b(t)* is the sequence of unit amplitude rectangular data bits each of duration T_b. *s(t)* is the periodic PN sequence of unit amplitude rectangular chips each of duration T_c. The operator '⊕' represents the SIK function given as:

$$b(t) \oplus s(t) = \frac{[1+b'(t)s'(t)]}{2} \tag{4.44}$$

where, *b'(t)* and *s'(t)* are the bipolar version of *b(t)* and *s(t)* respectively.

The *f(t)* as discussed in [33] has the DC component RP_f and AC component $RP_f f'(t)$ with P_f as the average interfering power from other sources of light. Substituting these values in received signal results in:

$$r_n(t) = 2RP_s\, b(t) \oplus s(t) + RP_f + RP_f f'(t) + n(t) \tag{4.45}$$

This received signal is AC coupled and so the DC term will be removed. The signal is then given as:

$$r_x(t) = 2RP_s\, b(t) \oplus s(t) + RP_f\, f'(t) + n(t) \tag{4.46}$$

This signal is now multiplied by *s'(t)* [de-spread] and then integrated over one data bit duration and zero threshold detected. Therefore, the correlator output becomes:

$$z(T_b) = \frac{1}{T_b}\int_0^{T_b} 2RP_s\, b(t) \oplus s(t)s'(t)dt + \frac{1}{T_b}\int_0^{T_b} RP_f\, f'(t)s'(t)dt$$

$$+ \frac{1}{T_b}\int_0^{T_b} n(t)s'(t)\, dt \tag{4.47}$$

Since *f'(t)* varies slowly with respect to the spreading code *s'(t)* over the integration period T_b, then *f'(t)* can be approximated by *f'(T_b)* which is sample value of *f'(t)* made at time $t = T_b$ and is constant over integration period. So, the above equation becomes:

Or $$z(T_b) = b_k RP_s + \frac{RP_f}{N}\, f'\,(T_b) + \, n(T_b) \tag{4.48}$$

where, $b_k \in \{1, -1\}$ denotes the present data bit which is desired signal term. The second term is the interference caused by light sources while the third term is the additive white Gaussian noise.

4.4.2.3 SNR and BER of SIK Modulator

The mean (μ_z) and the variance σ_z^2 of *z(T_b)*, at the correlator output from equation (4.48) can be given as:

$$\mu_z = b_k RP_s \tag{4.49}$$

$$\sigma_z^2 = \left(\frac{\sigma_m\, RP_f}{N}\right)^2 + \frac{N_0}{2T_b} \tag{4.50}$$

where b_k is the data bit sequence of unit amplitude, σ_m is the standard deviation of *f'(T_b)* and the same as the RMS value of *f'(t)*. The value given in [28] is around 0.3593. In μ_z, b_k is the data bits either 1 or -1. In equation (4.50), the first term is the variance produced by light sources, while the second term is the variance produced by the channel noise process. We see

that the variance produced by light interference is reduced by processing gain *N*. The SNR at the correlator output can be obtained as:

$$SNR_{sik} = \frac{(mean)^2}{(variance)} = \frac{\mu_z^2}{\sigma_z^2} \tag{4.51}$$

Or

$$SNR_{sik} = \frac{R^2 P_s^2}{\left(\frac{\sigma_m R P_f}{N}\right)^2 + \frac{N_0 R_b}{2}} \tag{4.52}$$

Or

$$SNR_{sik} = \frac{1}{\left(\frac{\sigma_m P_f}{N P_s}\right)^2 + \left(\frac{\sqrt{N_0 R_b}}{\sqrt{2}\, R P_s}\right)^2} \tag{4.53}$$

where P_s is the mean optical power of the desired signal impinging the PD. If $\sqrt{(N_0 R_b/2)} = RP_n$, where, P_n denotes a noise equivalent optical power. The second term in the denominator of equation (4.53) can also be written as $1/SNR_{opt}$, where SNR_{opt} is the optical signal-to-noise power ratio. Thus equation (4.53) can be written as:

$$SNR_{sik} = \frac{1}{\left(\frac{\sigma_m P_f}{N P_s}\right)^2 + \left(\frac{1}{SNR_{opt}}\right)^2} \tag{4.54}$$

We also define signal-to-interference ratio (SINR) as:

$$SINR = \frac{P_s}{P_f} \tag{4.55}$$

Substituting this in above equation results in:

$$SNR_{sik} = \frac{1}{\left(\frac{\sigma_m}{N.SINR}\right)^2 + \left(\frac{1}{SNR_{opt}}\right)^2} \tag{4.56}$$

when we assume data bit '+1' and '-1' to be equiprobable, the BER is defined in terms of SNR as:

$$BER = Q\left(\sqrt{SNR}\right) = Q\left(\sqrt{\frac{E_b}{N_0}}\right) \tag{4.57}$$

which is the same as in equation (4.25). Therefore, BER for the DSSS SIK system can be expressed as:

$$BER_{sik} = Q[\sqrt{(SNR_{sik})}] \tag{4.58}$$

The average optical signal power required to achieve a given BER for a SIK system can be found by solving for P_s which is expressed as:

$$P_{req-sik} = \frac{1}{RN}\sqrt{\left(R^2\sigma_m^2\,P_f^2 + N^2R_bN_0\right)/2}\;\;Q^{-1}(BER_{sik}) \tag{4.59}$$

where, R is responsivity of the PD, N is the processing gain, P_f is the light interference, σ_m is the standard deviation of interfering signal, R_b is the data rate, and N_0 the noise power density. In terms of P_{ook}, the required power for DSSS SIK is expressed as:

$$P_{s-sik} = \frac{1}{N}\left(\sqrt{\frac{R^2\sigma_m^2P_f^2}{N_0R_b} + N^2}\right)P_{ook} \tag{4.60}$$

The performance parameters in terms of BER and SNR, data rate and power requirements are analyzed and simulated which is presented in next section.

4.4.3 Performance of Modulation Schemes

In this section, results from modulation analysis described previously are presented. First we

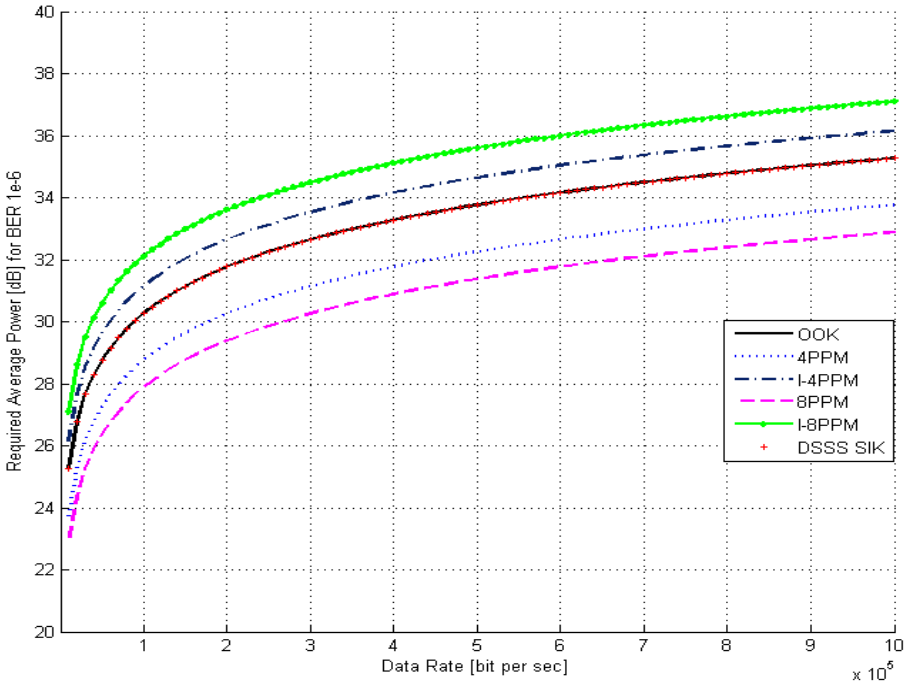

Fig. 4.9: Required Average Power for Different Data Rate when BER is 1e-6

considered the AWGN channel. A BER of 10^{-6} is considered good for reliable data transmission. We assume data rate on the range of tens of kbps is enough for the intended applications. Therefore, 28 to 34dB of power is required (Fig. 4.9) under this condition for all the modulation schemes. If data rate increases, the power requirement also increases (Fig. 4.9). It is also observed that power requirement increases when *L* increases for I-LPPM, while it decreases for L-PPM. Power efficiency however, remains the same in both DSSS SIK and OOK. That is, unlike L-PPM or coded schemes which increase their power efficiency over OOK with the introduction of redundancy; DSSS has the same power efficiency as OOK. This property originates from the fact that in DSSS a single codeword is used and hence it is not possible to exploit the minimum Hamming distances between each codeword. Instead, the redundancy or bandwidth expansion in DSSS is used to mitigate multipath ISI and narrowband light interference.

Fig. 4.10(a) and Fig. 4.10(b) show BER versus SNR curves for all modulation schemes. For these results data rate is fixed at 1MHz for all the modulation techniques. It can be seen that SIK performs better even with small interference (Fig. 4.10.b). Comparing between L-PPM and I-LPPM, L-PPM performance is better. However, applications where average power

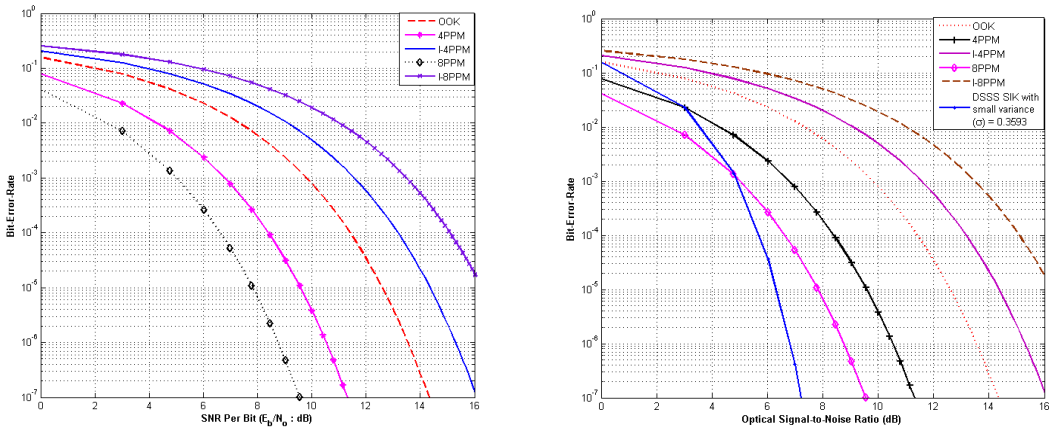

(a) (b)

Fig. 4.10: BER Performance: (a) Different Modulation; (b) Includes DSSS SIK with Small Noise Variance.

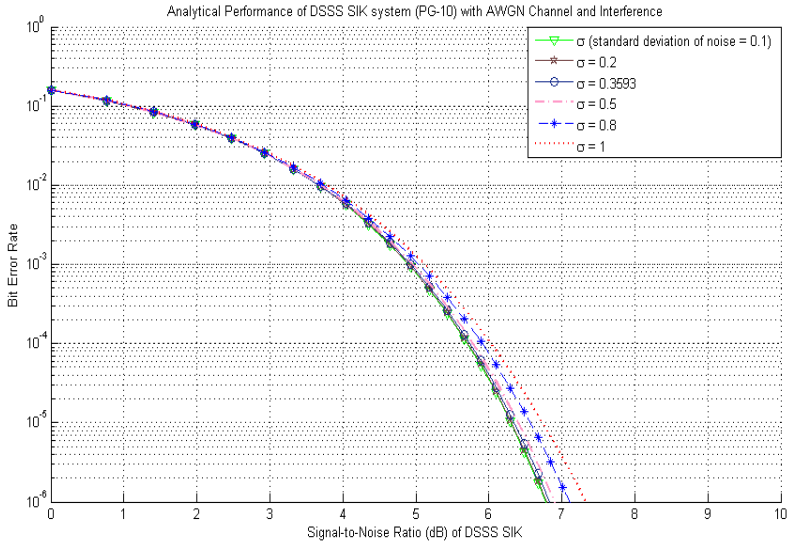

Fig. 4.11: BER Performance of SIK with Different values of Standard Deviation when SINR is 1

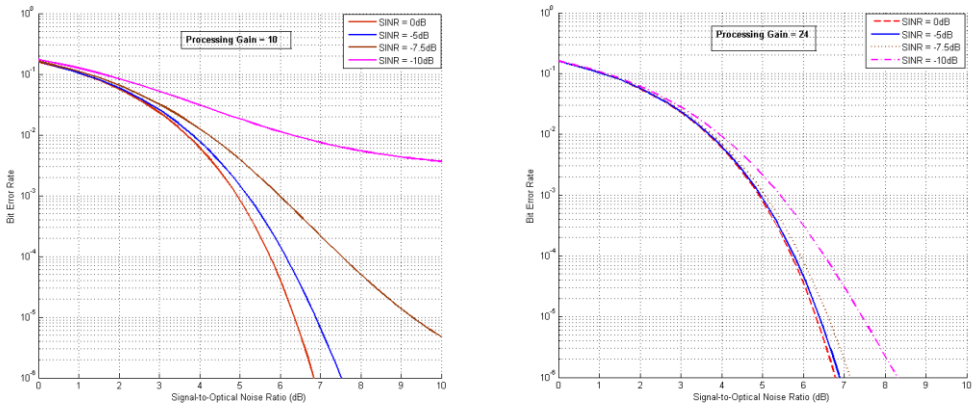

(a) (b)

Fig. 4.12: (a) BER Performance for various Signal to Interference Noise ratio (SINR) when PG = 10; (b) BER vs Signal to Optical Noise ratio (SNR_{opt}) (dB) for PG=24.

is not a constraint and light remains ON for most of the pulse duration, I-PPM can offer high data rate transmission as lights remain ON for most of the pulse duration.

Fig. 4.11, Fig. 4.12 and Fig. 4.13 show the analytical simulation results of DSSS SIK modulation. The effect of standard deviation of noise interfering signal (σ) with processing gain (PG) of 10 is shown in Fig. 4.11. It is seen that there is no significant difference in SNR

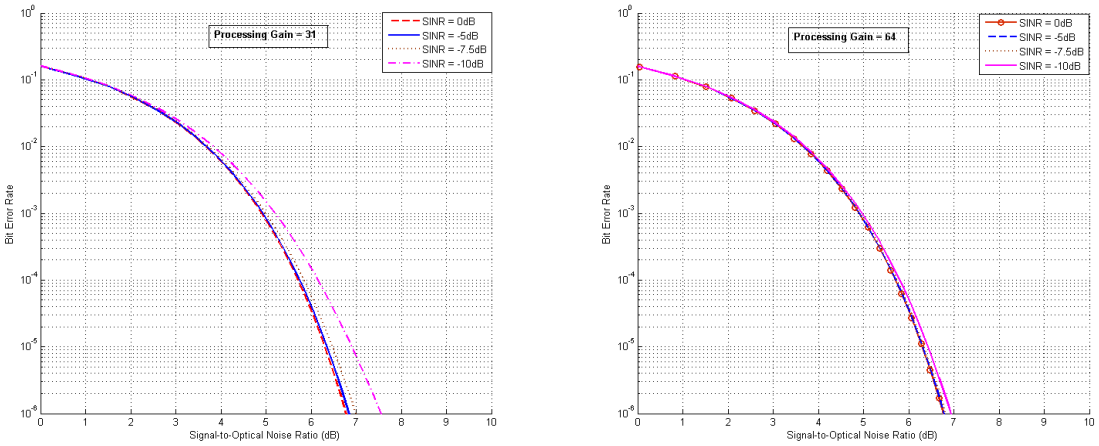

(a) (b)

Fig. 4.13: (a) BER Performance for various Signal to Interference Noise ratio (SINR) when PG = 31; (b) BER vs Signal to Optical Noise ratio (SNR_{opt}) (dB) for PG=64.

from σ =0.3593 taken as standard value from [26], [30] to any other values between 0 to 1. Similarly, Fig. 4.12(a) illustrates the effect of signal-to-interference ratio (SINR) for PG of 10. It is observed that when interference increases, the BER performance decreases. At -10dB, the performance is highly deteriorated.

Fig. 4.12(b) shows the effect of interference (SINR) when PG is increased from 10 to 24, which is expected. Similarly, Fig. 4.13(a) and Fig. 4.13(b) depict the effect of interference when PG is further increased to 31 and 64 respectively. It is seen that increase in PG enhances the performance of SIK system. At PG = 64, system's performance with -10dB of interference reaches closer to the performance at 0dB interference.

In the next section, we model VLC systems in Matlab/Simulink and verify the analytical results.

4.5 VLC System Matlab/Simulink Model

The theoretical and numerical analysis relies on various approximations which may not perform accurately when a model is implemented in simulation tools such as Matlab/Simulink. To verify this, we have implemented our model in Simulink and examined the results.

As simulation exercise, two Matlab models were developed in Simulink. Two decorrelator receiver architectures have been developed for de-spreading spread spectrum signals: Integrate and dump filter, also called as active correlator and PN matched filter. They are optimum from a SNR point of view. The motivations behind the study are: (i) to compare the performance of DSSS SIK using both of these receiver architectures, and (ii) implement the architecture that is most suitable for FPGA. A brief detail is given for both the receiver architectures before presenting the simulation results.

4.5.1 Integrate and Dump Decorrelator Receiver

This receiver operates correctly when the local PN sequence is accurately matched and correctly timed, with respect to the spreading code within the received signal. Synchronization becomes difficult too and it is a very slow process. Fig. 4.14 shows the basic structure of Integrate and dump filter decorrelator [8]. The Integrate and dump block creates a cumulative sum of the discrete-time input signal, while resetting to zero according to a fixed schedule. When the simulation begins, the block discards the number of samples specified in the *Offset* parameter. After this initial period, the block sums the input signal and resets the sum to zero every *N* input samples, where *N* is the Integration period (one data bit). The reset occurs after the block produces its output at that time step. This block also results in a delay of one bit. Parameters settings are shown in Table 4-1.

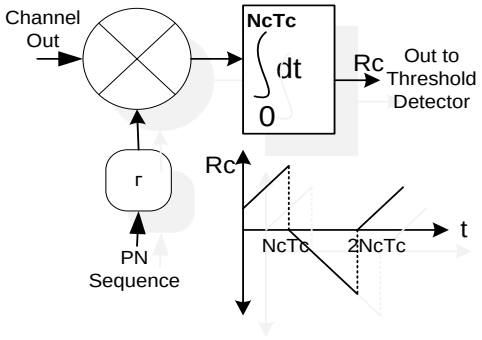

Fig. 4.14: Active Decorrelator Receiver

4.5.2 PN Matched Filter Correlator Receiver

A typical PN matched filter decorrelator [90] is shown in Fig. 4.15. This filter implements convolution using a finite impulse response (FIR). The FIR coefficients are a time reverse replica of the PN sequence. For example, the PN sequence (p_{ni}) and filter coefficients (Fc_i) can be given as:

pn_i = [pn0 pn1 pn2 pn3 pn4 pn5 pn6] = [-1 +1 +1 +1 -1 -1 +1],

Fc_i = [Fc0 Fc1 Fc2 Fc3 Fc4 Fc5 Fc6] = [+1 -1 -1 +1 +1 +1 -1].

The output of the FIR is the convolution of the received (incoming) signal b_c with the FIR coefficients Fc_i. Because of time reversion, the output of the filter is the correlation of b_c with the PN sequence, given by:

$$R_c(\tau) = \sum_{k=0}^{N_c-1} b_c(t - kT_c)\, F_c k = \sum_{k=0}^{N_c-1} b_c(t - kT_c) P_{N_c-1-k} \tag{4.59}$$

If the receiver is not synchronized, then the received signal will propagate through the matched filter, which outputs the complete correlation function. In Fig. 4.15, the large peak confirms that the correct code is indeed being received and provides accurate timing information for the synchronization of the received signal. The peak output of FIR PN matched filter is the decorrelated data and the polarity of the large correlation peaks indicates the data value.

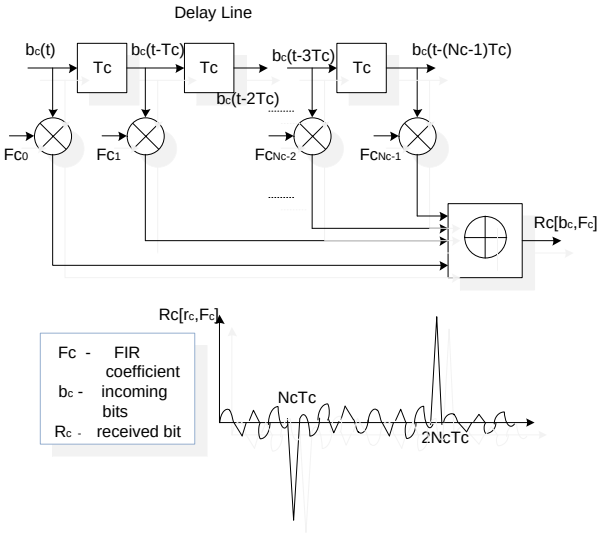

Fig. 4.15: PN Matched Filter Decorrelator using FIR

4.5.3 Simulink VLC Systems Model Common Blocks

In the Simulink model structure of Fig. 4.16, the receiver block connected by dashed lines is the Integrate and dump decorrelator while the receiver block connected by solid lines shows the discrete FIR based PN matched decorrelator. Detail model is shown in the Fig. 4.17 with FIR decorrelator receiver architecture. Different functionalities were achieved using different blocks. Here both the conditions; DSSS SIK with AWGN channel only and with additional noise in the model are considered. The model consists of Bernoulli binary generator as data source, PN sequence generator as spreading code, SIK subsystem to obtain the SIK function, data format converters, AWGN channel, noise generator, Integrate and Dump filter, threshold detector and error detection block.

Table 4-1: Simulink VLC Systems Model Simulation Parameter Settings

Block	Parameter(s) and Value	Block	Parameters and Values
Bernouli Binary Random Generator	-Probability of a P(0) =P(1) = 0.5, -Sample Time = 1	Integrate and Dump Filter	-Integration period (number of samples): 10, -Offset (number of samples):0 -Output intermediate value
Pseudo Noise Generator	-Generator Polynomial: [1 0 0 1 1], -Sample Time : 1/10, -Output mask vector : 0	Error Rate Calculation	-Receive delay: 1, -Computation delay: 1
Additive White Gaussian Noise	-Signal-to-Noise Ratio (Eb/No) : 1-16dB, -Number of bits per symbol: 1, -Input signal power, referenced to 1 ohm (watts): 1, -Symbol Period: 1/10	Simulation Time	10^7 Seconds
Noise Generator and low pass filter	-Sample Time: 1/100 -3dB cut off frequency 35KHz	Free running Up Counter	-Counting from 0 – 9 -Output : count and hit -Samples per output frame : 1
Signum	-Output 1 for positive input, -1 for negative input, and 0 for 0 input, y = signum(u)	Discrete FIR Filter	-Direct form structure -Numerator coefficients : [1 -1 -1 1 -1 -1 -1 1 1 1] -Initial state: 0 -Sample time : 0.1
		Delay Network	-Delay unit: Sample -Delay: 1 sample -Initial condition: 0 -Gain: 0.25

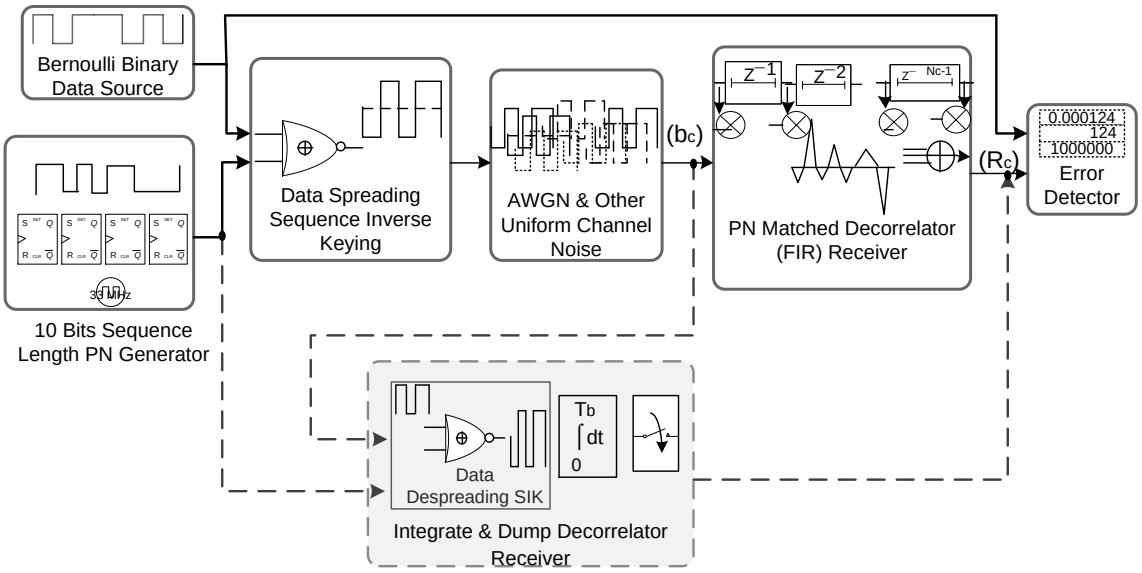

Fig. 4.16: Simulink Model for DSSS Based VLC Systems

4.5.3.1 Data Source

A Bernouli Binary Generator is used to generate binary sequence at a specified data rate. It is a random data generator with probability of 0 and 1 being equal. Different parameters are set according to specifications in the Table 4-1.

4.5.3.2 SIK Modulator and Transmitter

This subsystem performs SIK function which is nothing more than XNOR operation where the PN sequence is transmitted when data bit is '1' while inverse of PN sequence is transmitted for data bit '0'. The system receives both the inputs: one from data source and the other from PN sequence. The block also uses data conversion system suitable for channel, such as, unipolar to bipolar conversion.

4.5.3.3 The AWGN Channel and Noise

In the simulation model we considered two situations: VLC system with AWGN channel where Additive White noise affects the system and in addition to AWGN the system is highly

influenced by external noise (artificial light) sources. A noise generator source with low pass filter is also included to simulate the effect of additional noise in the system. The filter characteristic is also changed to band pass with frequency band of 15- 40kHz. The subsystem also includes sign/threshold detector to provide output data pattern acceptable to the DSSS SIK receiver.

4.5.3.4 DSSS SIK Demodulator and Receiver

Apart from performing SIK function, this important subsystem encloses Integrate and dump filter. This block creates a cumulative sum of the discrete-time input signal, while resetting the sum to zero according to a fixed schedule. When the simulation begins, the block discards the number of samples specified in the *Offset* parameter. After this initial period, the block sums the input signal and resets the sum to zero every *N* input samples, where *N* is the Integration period (one data bit) parameter value. The reset occurs after the block produces its output at that time step. This block adds a delay of one bit.

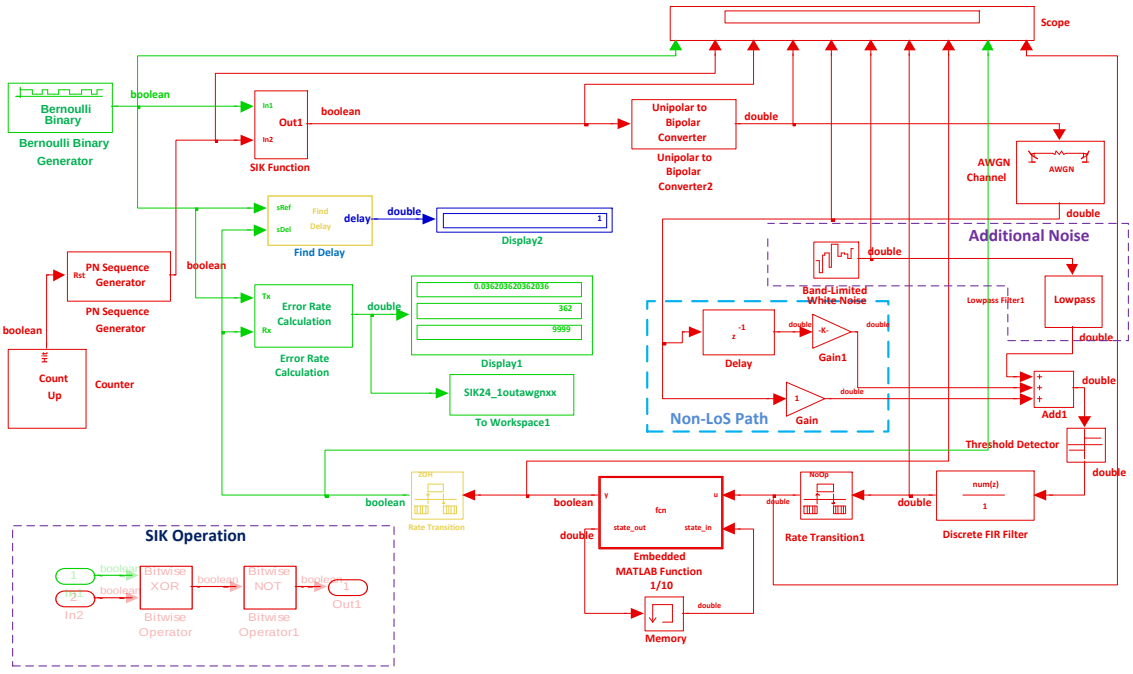

Fig. 4.17: Simulink Model for FIR Decorrelator Architecture with Non-LoS and Subsystem of SIK operation

4.5.3.5 Error Rate Calculation

The block calculates the number of bits in error from that of transmitted bit. This ascertains the minimum performance requirement of a system. The performance is recorded using monitors.

4.5.3.6 PN Code Generator

The PN code is characterized by its process gain and the overall complexity. To have a compromise between spectrum spreading and processing gain, a PN sequence length of 10 was developed and used. It offers almost the same autocorrelation properties as of Barker code [10] of length 11.

4.5.3.7 Noise generator and Low Pass Filter

The blocks are used to induce additional noise in the channel which is filtered with a cut off frequency of around 35kHz. This is the maximum noticeable noise component from light sources using a ballast circuit. With the filter characteristic of band pass in the range of 15-40kHz, no noticeable difference is found in performance.

Based on the parameter settings and simulation set-up as summarized in Table 4-1, the simulation is performed for various conditions. The results are presented in the following section.

4.5.4 VLC Systems Model Performance Results

This section presents the results of both the receiver architectures developed in Matlab/ Simulink model for DSSS SIK system. We have considered AWGN channel and a noise generator for considering external and interferring sources. The effect of one non-LoS path is also considered, though it is assumed that we have normally LoS path in VLC design.

Fig. 4.18 illustrates the performance of two receiver architectures. It can be seen that they perform approximately the same. Meaning, if we make any changes to the model such as addition of interfering sources, the performance will remain the same. However, in the FIR

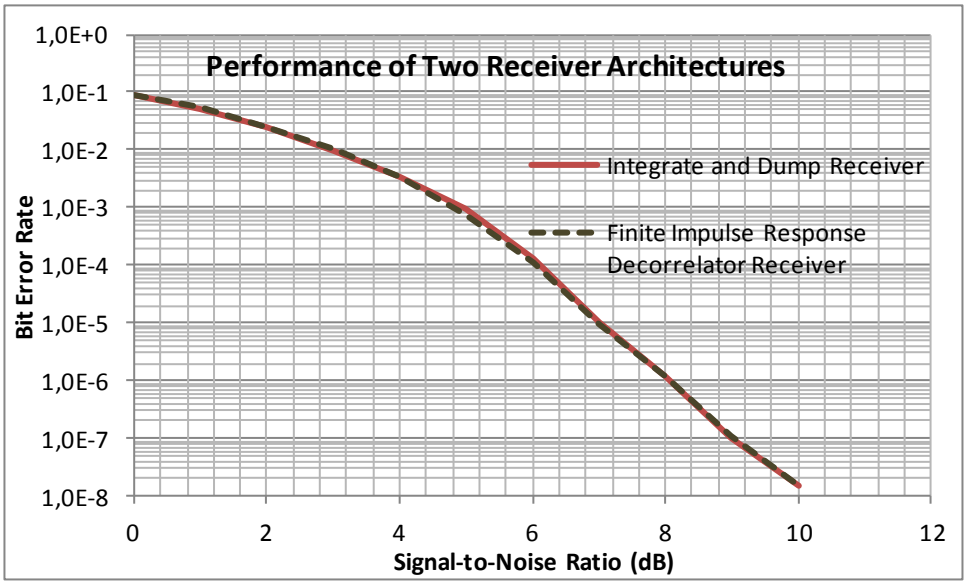

Fig. 4.18: Performance of two Receiver Architectures without Interference

architecture, the synchronization time is much less as compared to the Integrate and dump based. It is also seen that the result matches with the mathematical analysis. We can interpret that a SNR over 8dB would be necessary to provide a BER of 10^{-6}. However, again the performance will depend on the distance of transmission range. Light intensity decreases inversely of the square of the distance.

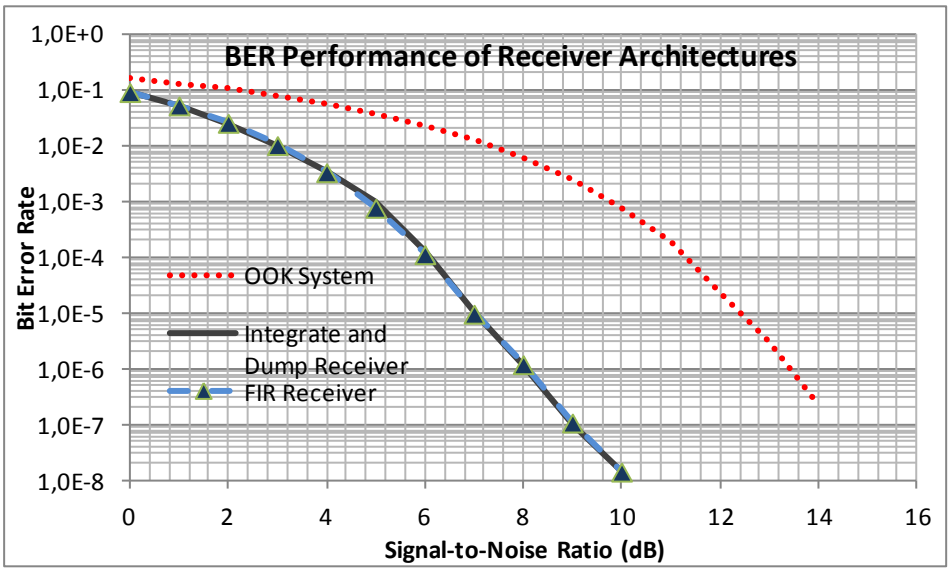

Fig. 4.19: BER Performance of Receiver Architectures

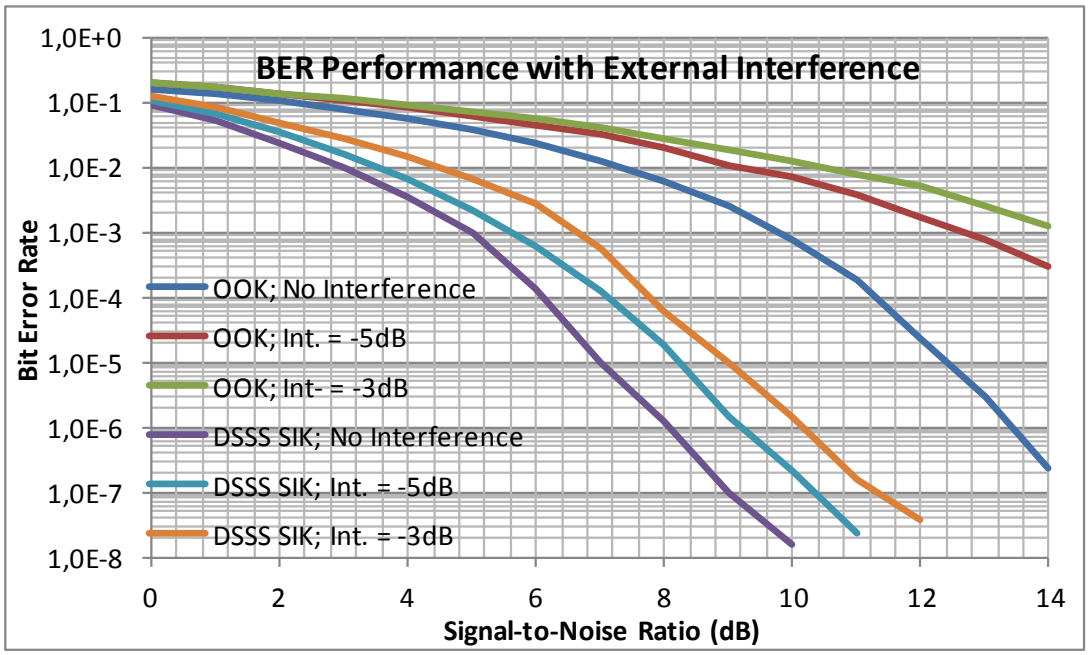

Fig. 4.20: Effect of Additional Noise (Interference) on Simulink model of Receiver Architectures

Fig. 4.19 shows the performance of receiver architectures including OOK system. This shows that SIK performs better than OOK based receiver. The effect of additional noise is illustrated in Fig. 4.20. Additional noise produced is low pass filtered. The cut off frequency is selected to be 35kHz which simulates the interference from light sources using ballast circuit. It is seen that effect of interference deteriorates the performance of DSSS SIK as well as OOK based systems, however, OOK based system is more affected as compared to SIK system. We have also seen that the effect of such interference can be minimized using higher length of PN sequence, i.e. processing gain.

Analytical and system simulation results presented above, offer the expected behavior of VLC systems. They present significant valuable information before actual hardware prototype is designed. However, behavior and function of hardware designed systems may drift slightly. Moreover, to fully examine the performance, a system has to be designed and implemented. Next chapter discusses in detail the implementation of the VLC system.

4.6 Concluding Remarks

Different modulation techniques which can be used in VLC systems have been discussed and analyzed in this chapter. BER and SNR performance parameters for PPM and DSSS SIK techniques were discussed in detail. Based upon the simulation results, it was observed that the L-PPM which was a suitable method for IR do not offer significant improvement in VLC systems. Therefore, a robust method based on DSSS SIK system was investigated and discussed for VLC systems. The analytical results were verified using Matlab/Simulink model. The performance of the system especially in road safety applications in outdoor is expected to be improved using the technique of DSSS SIK. Detail implementation will be discussed in next chapter 5.

CHAPTER 5: VLC SYSTEMS DESIGN AND IMPLEMENTATION

Summary

Designing VLC systems is a multidisciplinary task. A complex system like this makes the task even more difficult to achieve. It requires the knowledge of optoelectronic parts to protocol design. This chapter presents overall system design and implementation. Optoelectronic parts of VLC emitter and receiver architecture are designed and their response curves are presented in brief. Software and signal processing parts of emitter and receiver are implemented in FPGA. In the final implementation of the VLC receiver, we have used FIR decorrelator architecture which offers faster synchronization as compared to integrate and dump receiver architecture. Performance of Matlab/Simulink VLC model implementation and FPGA VLC is also compared. Their performance is nearly the same.

5.1 Introduction

Designing VLC systems is a complex task. It is even harder to design for applications such as ITS. It involves from physical layer design through the application layer. It requires the knowledge of optoelectronic devices and circuits, road traffic settings to protocol development. A broad area of knowledge becomes necessary to fulfill the requirements. This chapter deals with complete system design and prototype development.

In the first part of the chapter, the optoelectronic blocks of the emitter and receiver are discussed. Important simulation results are also presented. In this section, receiver optoelectronic parts such as characteristics of photo detector, transimpedance front end amplifier topology, and associated blocks are discussed. Overall receiver circuit configuration is discussed and response results are presented.

The later part of the chapter provides details on FPGA implementation. FPGA emitter and receiver architecture based on FIR decorrelator are discussed. The main building blocks, their functionalities and implementation details are presented. Important simulation results are presented and compared with Simulink VLC system model. We first discuss in detail the overall system architecture and main building blocks.

5.2 VLC System Architecture and Design

An extended illustration from chapter two Fig.2.6 of overall VLC systems architecture [73] is shown in Fig. 5.1. The blocks shown are supported on a FPGA and discrete components. The optoelectronic parts on the emitter sides are necessary to drive the LED-based traffic lights, which are switched on/off at a modulating frequency decided by the digital clock manager (DCM), on the FPGA. On the other hand, signal processing blocks on the FPGA, process the received information bits, assemble them into frames. Many control signals and protocols are needed in the process. Modulated and processed information bits are transmitted as light pulses using the free space optical channel. These light pulses are detected by a photo-diode and amplified in the VLC receiver installed on vehicles. The photo-diode converts light pulses

into electrical signals, which are then AC coupled to remove DC components, amplified and processed in the signal processing blocks of FPGA. The end result is the received information signal which may have errors depending on channel conditions. The following sections provide a detailed description of the major blocks of overall VLC system.

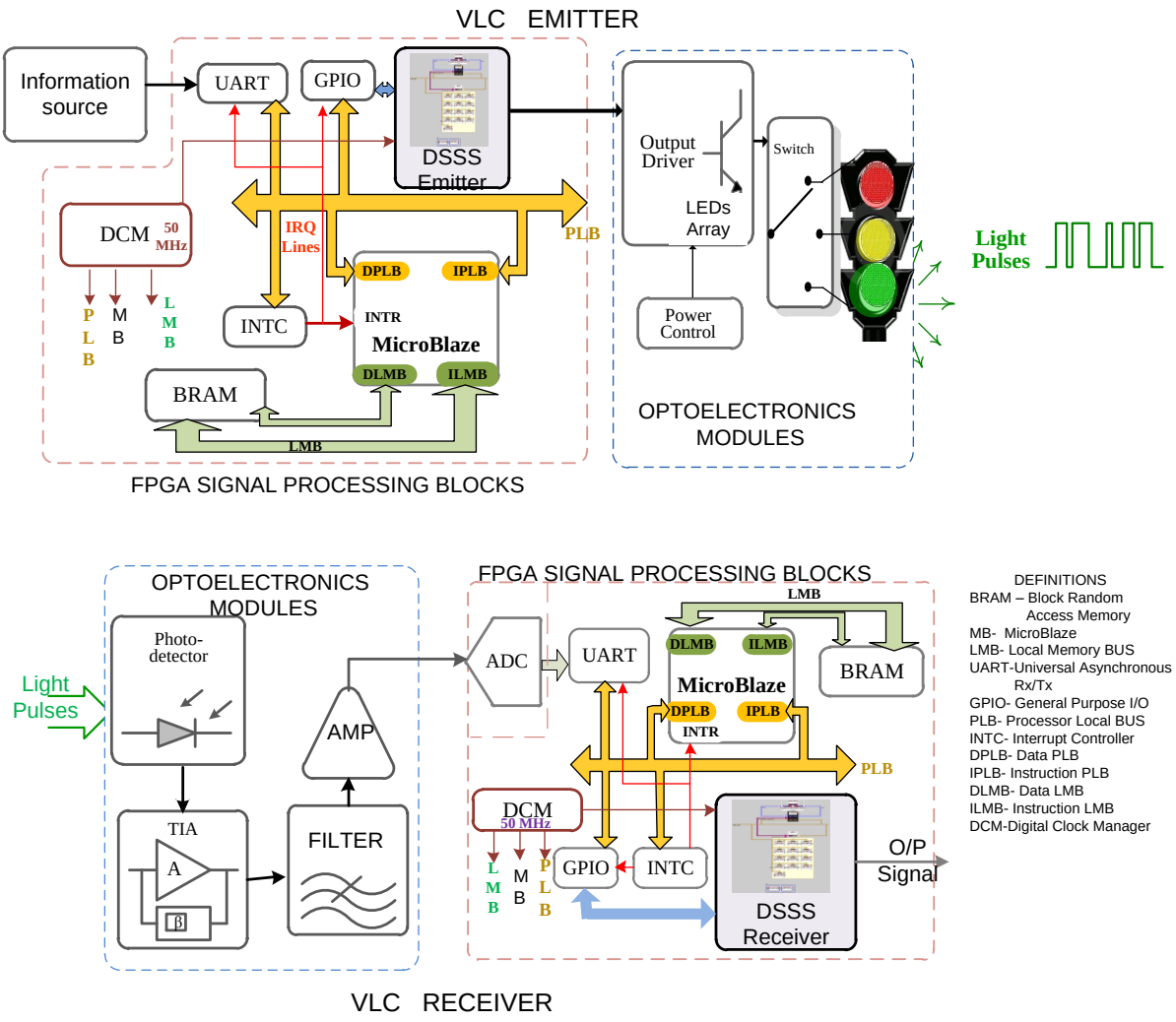

Fig. 5.1: VLC System Architecture

5.2.1 VLC Emitter Design

This section describes design of optoelectronic parts of VLC emitter and evaluates its performance.

5.2.1.1 Optoelectronic parts of The VLC Emitter

The emitter is necessary to provide both traffic control signaling and data transmission. Measurements and characterization are necessary to evaluate the design and assess its performance.

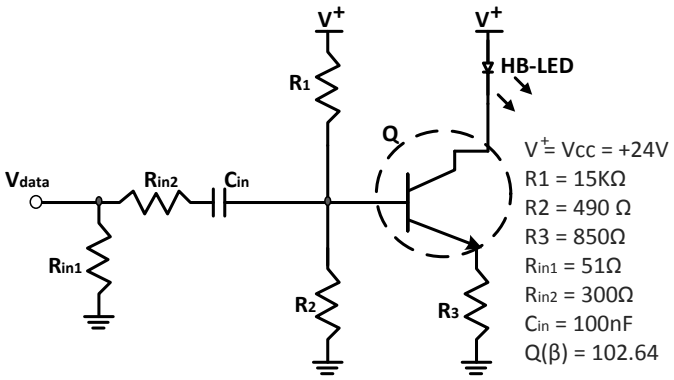

Fig. 5.2: Discrete Current-sink Optoelectronic Emitter Topology

The emitter consists of a discrete electronic circuit able to drive an array of LEDs. A discrete transistor topology (typically current sink) as shown in Fig. 5.2 is used. Fast switching transistors allow to explore faster switching frequencies, which is an important requirement in the current application. A digital signal (V_{data}) controls the transistor's (Q) ON/OFF state, enabling current flow through the HB-LEDs. This was achieved using a fast NPN transistor (BFR92A). Resistors R_1 and R_2 set the operating point.

In traffic broadcast applications, the traffic lights need to work even if the data signal is disconnected. The operating point of Q is set so that transistor remains ON and a current of around 35mA (in active region) flows. However, V_{data} is applied (V_{data} = 0 or 3V) and the transistor switches between OFF and ON, that is, cut off and saturation. When the signal is 0V, the minimum threshold operating point voltage is dropped to 0V. When the signal is 3V, a maximum peak saturating current (I_D) of approximately 40mA is recorded. If V_{data} is disconnected, the transistor will drive a steady current around I_D = 35mA.

The base voltage of Q is given by:

$$V_B = V_{BE} + (I_{Ddc}\, R_3) \tag{5.1}$$

Table 5-1: Values of Electrical Current through the HB-LED

I_D@ different Frequency		(a)@ 100KHz	(b) @ 1 MHz	(c) @ 10MHz	(d) Constant Value
V_{data}	Logic high (3v)	38.1 mA	39.0 mA	40.0 mA	34.6. mA
	Logic Low (0V)	10.4 µA	12.6 µA	42.9 µA	

where, V_{BE} = 0.73V. In order to keep *Q* in the cut-off region when V_{data}= 0V, the transistor's base-emitter junction have to be below V_{BE}, which means that V_B cannot go over 0.7V.

Neglecting the base current of *Q* and the effect of R_{in2}, when V_{data}=0V, V_B is approximately:

$$V_B = V_{CC}\ \frac{R_2}{R_1+R_2} - \frac{V_{data_{pp}}}{2} \tag{5.2}$$

Considering that this value has to be less than 0.7V and choosing R_1= 15kΩ, the value of R_2 has to be approximately 470Ω. Resistor R_3 can be obtained from equations (5.1) and (5.2) when V_{data} is disconnected:

$$V_{BE} + (I_{Ddc}\ R_3) = \left(V_{CC}\ \frac{R_2}{R_1+R_2}\right) - \frac{V_{data_{pp}}}{2} \tag{5.3}$$

In these condition, replacing the previously obtained values results in R_3= 850Ω.

5.2.1.2 Performance of the Emitter

Simulation results are presented in Fig. 5.3 and Table 5-1. Plots "a", "b" and "c" represent the current through the HB-LEDs for V_{data} frequencies of 100kHz, 1MHz and 10MHz respectively. Plot "d" represents the constant current that flows through the HB-LEDs when V_{data} is disconnected. The current values obtained are consistent with the projected values in a wide range of frequencies.

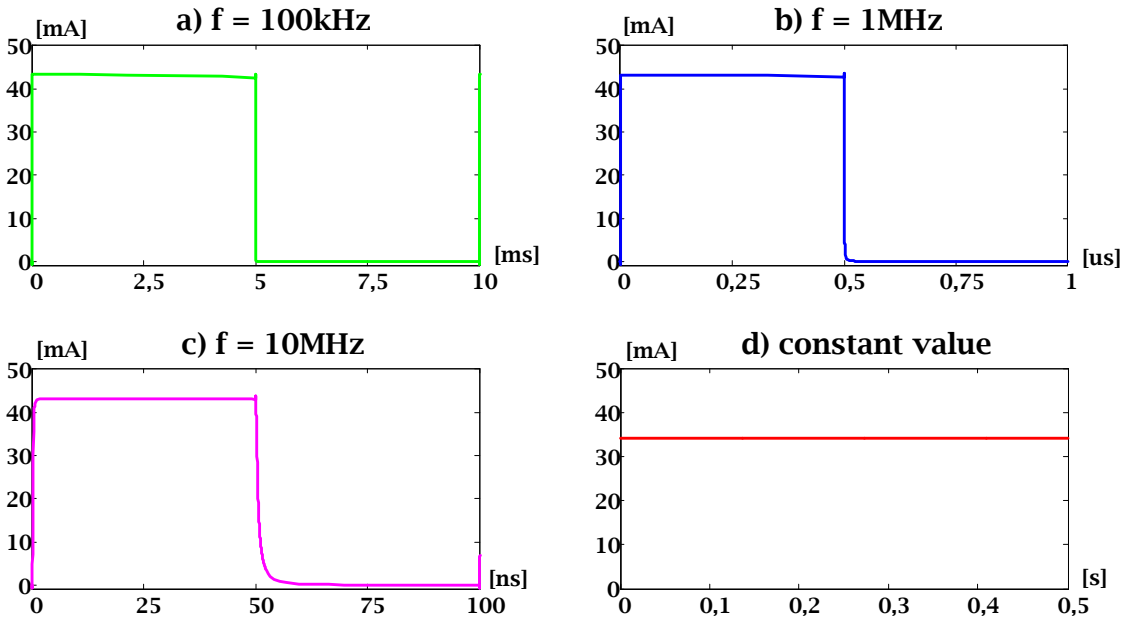

Fig. 5.3: Optoelectronic Emitter- time domain Response at Different Frequencies

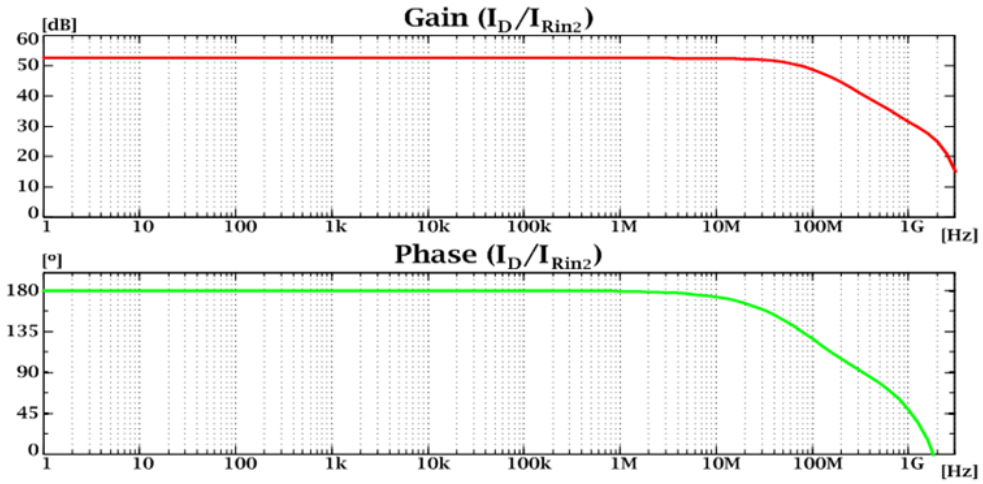

Fig. 5.4: Optoelectronics Emitter- gain/phase Response (I_D/I_{Rin2})

Fig. 5.4 shows the frequency gain-phase response of the current amplification (I_D/I_{Rin2}). It can be seen that the emitter has a large bandwidth, with a 3dB cut-off frequency of 84.92MHz and a steady gain of 52.45dB.

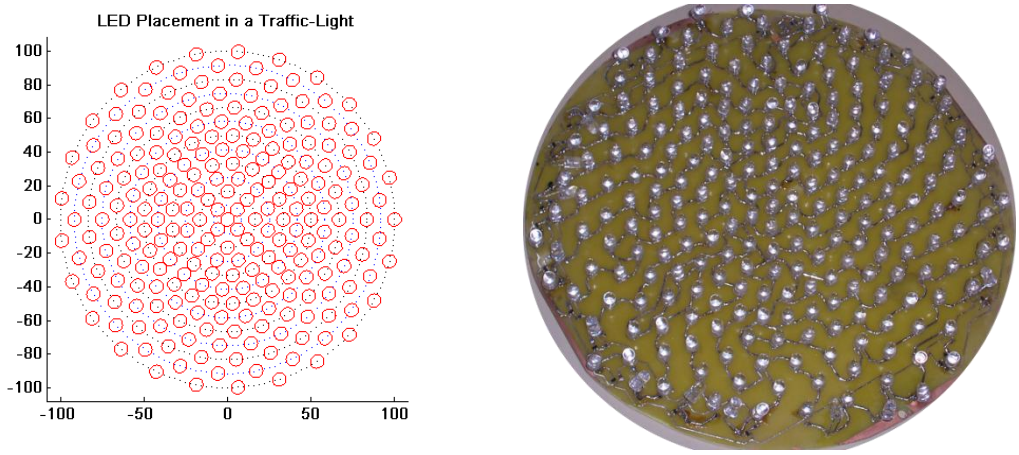

Fig. 5.5: Optimized Placement of LEDs in 200mm Traffic Light case: (a) Simulated layout; (b) Designed/assembled traffic light

5.2.1.3 LEDs Traffic Lights Emitter Design

As stated before, LED-based traffic lights work as VLC emitter in ITS applications. The array of LEDs is made to switch on/off at desired frequency using modulation techniques. Normally, high rate switching is not detectable by human eyes. Human eyes perform a low pass filtering action on the perceived light signals. Continuous switching is perceived with different intensity levels, depending on the duty cycle of light signals. This way, it is possible to have red, amber and green light signals depending on traffic control, and at the same time, broadcasts traffic data information.

In chapter 3, a model for the traffic lights and traffic light system set-up was developed. Based on simulation results, it was recommended the usage of circular arrays. An optimized placement algorithm further suggested high occupancy LED placement in the inner half of the rings while less occupancy in the outer half. The same traffic light has been designed in the standard 200mm diameter traffic light case. The layout is presented in Fig. 5.5(a). The designed traffic light is shown in Fig. 5.5(b).

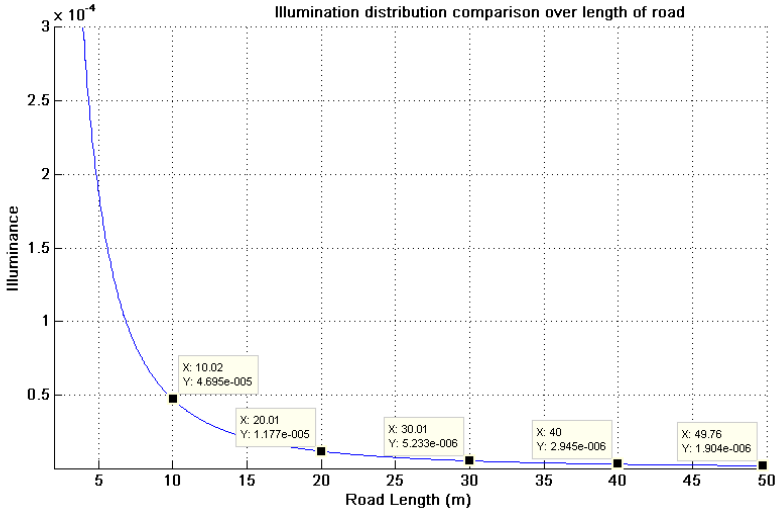

Fig. 5.6: Illuminance over Distance for Designed (fig.5.5b) Traffic Light.

5.2.1.4 Performance of the Traffic Light VLC Emitter

Following the experimental set-up in Fig. 3.16 the Illuminance variation over distance are measured from the designed traffic light. The result is shown in Fig. 5.6. It can be seen that an illuminance value of the order of 2μW/cm^2 is received at a distance of around 50m. A receiver able to detect these small signals would be required.

5.2.2 VLC Receiver Design

Receiver transforms the modulated light pulses into text message. First, the photodiode converts light into an electrical current of very small value. A transimpedance amplifier is used to convert this small current into a voltage signal which is fed to a low-pass filter, thus removing any high frequency noise component. Similar to the emitter, the VLC receiver consists of optoelectronic parts and reconfigurable hardware implemented in FPGA. The optoelectronic parts are discussed next while FPGA implementation is discussed in section 5.3.2.

5.2.2.1 Front-end Amplifier

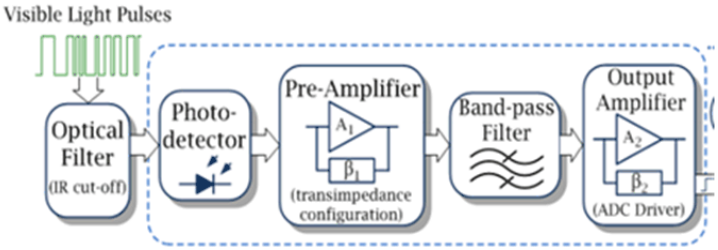

Fig. 5.7: Block Diagram of Optoelectronic VLC Receiver

The front-end amplifier circuitry to use in the VLC receiver employs a photodiode to capture the data signal from the free-space optical medium and converts it into an electrical current. As light impinges on the photodiode's active area, an electrical current is generated. This photocurrent consists of a desired signal current (proportional to the incident optical power of the transmitted signal) and a noise component mostly dominated by shot noise current. Typically, the sum of these contributions is a small amplitude current, which leads to the necessity of several amplifying and filtering stages in order to produce a viable output that can be sampled and further processed at the receiver's FPGA. The main building blocks of the proposed front-end amplifier are depicted in Fig. 5.7. As light signals reach the receiver, an optical IR cut-off filter helps remove unwanted spectral content. A reversely biased PIN photo-diode, operating in the photoconductive mode generates a current proportional to the collected light. A pre-amplifier in a transimpedance configuration provides low distortion and a large gain-bandwidth product. According to several studies performed for IR front-ends, this configuration presents the best compromise between bandwidth and noise, for this kind of applications [18]. The resulting voltage is then applied to a band-pass filter, which was achieved by cascading a low-pass filter with a high-pass filter. Both stages were implemented with resource to active filtering configurations with a Butterworth response. The first stage uses a second order multiple-feedback low-pass configuration and the second stage uses a third order Sallen-Key configuration with a voltage gain of two. The resulting output signal is DC filtered before passing through the output amplifier. This stage provides signal gain when the input is very small. It also provides amplitude limitation, if the input reaches

over a preset value. This makes it easier to adapt the output signal's dynamic range to the input range of the analog-to-digital converter (ADC).

5.2.2.1.1 Photo Detector

A PIN photo-diode can maintain a linear response for input light power ranging from nanowatts up to tens of milliwatts. Although a higher reverse voltage does not influence the induced photocurrent, it reduces the device's junction capacitance allowing for faster switching times. Table 5-2 shows important optical and electrical characteristics [91] of some photo-diodes, from different manufacturers.

5.2.2.1.2 Transimpedance Front End Amplifier

The preamplifier module is of critical importance to the receiver's overall performance. The biggest challenge in front-end amplifier design is to achieve a high-gain, and stable operation with a large bandwidth. These conditions become hard to achieve mostly due to limitations imposed on the gain bandwidth (GBW) by the input circuitry.

Table 5-2: Si photodiodes Electrical Characteristics

Manufacturer	Model	S_λ @ λ_{peak}	I_{dark} @ V_R	C_{PD} @ V_R	t_{SW}	f_{SW}
		[A/W]	**[pA]**	**[pF]**	**[µs]**	**[MHz]**
EG&G VACTEC	VTH2091	0.60	5.000 @ 30V	120 @ 12V	15.000	-
HAMAMATSU	S1133	0.30	10 @ 1V	700 @ 0V	2,5	-
	S3204-09	0.66	6.000 @ 70V	130 @70V	-	20
KODENSHI	SP-101		500.000 @ 5V	17 @ 0V	-	
	SP-1CL3		500.000 @ 5V	50@ 0V	-	
	SP-1KL		100.000 @ 5V	50@ 0V	-	
OSRAM	BP 104S	062	2,00 @10V	48 @ 0V	20.000	-
	BPW 34B	0.20	2,00 @10V	72 @ 0V	25.000	-
	BPW 34S	0.62	2,00 @10V	72 @ 0V	20.000	-
SHARP	BS100C	-	3 @ 1V	500 @0V	200	-

(For quick reference, the photodiodes used in this project are grey shadowed)

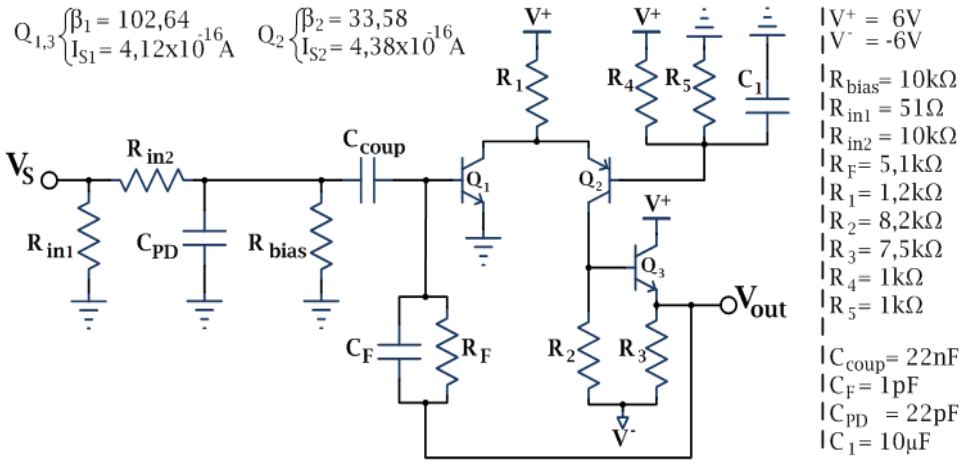

Fig. 5.8: Preamplifier Topology

After analyzing the expected general behavior of the input amplifier and the recommended configurations, three different preamplifier topologies were characterized. The base configuration used is a discrete topology that has been tested for many years, yet it is suitable for a wide range of applications. A transimpedance configuration using shunt-shunt feedback topology is used. The circuit configuration is shown in Fig. 5.8. For the desired application, 1MHz signal frequency is desired. In order to guarantee a proper response of the implemented topologies a minimum of 10MHz should be considered for the high cut-off frequency. Transimpedance gain of 5kΩ is adequate to the desired application. With a low cut-off frequency of 731,92Hz the effect of low-frequency noise from external light sources can be reduced. Also, it has a high cut-off frequency of 33,21MHz, and steady gain of 74,01dB, which corresponds to the expected transimpedance of 5,02kΩ.

The gain/phase responses of the configuration are shown in Fig. 5.9 for different values of R_F and C_{PD}. It can be seen that higher values of resistance increase the gain reducing the frequency range. Fig. 5.9 also shows the effect of PD capacitance at highest gain. It is possible to increase higher cut-off frequency using smaller capacitance values. The gain/phase curves show that for frequencies above hundreds of megahertz, there is still a positive gain, which could lead to high-frequency noise components to be amplified, and it would be convenient to

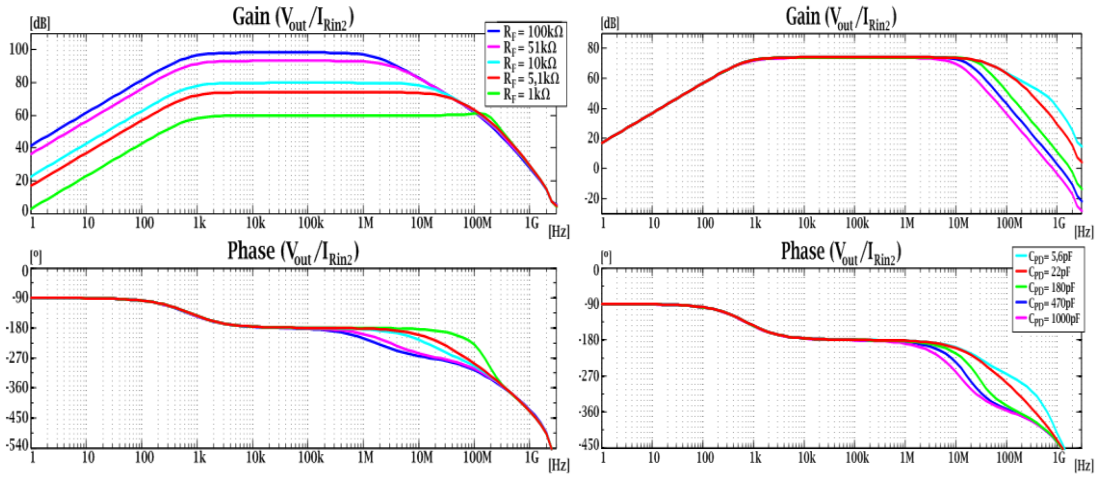

Fig. 5.9: Phase/Gain plot for different values of R_F and C_{PD}

increase the attenuation at these frequencies. A low-pass filter is then included after transimpedance amplifier, in final design.

5.2.2.1.3 Circuit Design

The complete receiver schematic is shown in Fig. 5.10. As shown, the transimpedance amplifier is followed by filters and amplifying stages. The band-pass filter was achieved by cascading a low-pass filter with a high-pass filter. The low-pass was implemented in order to

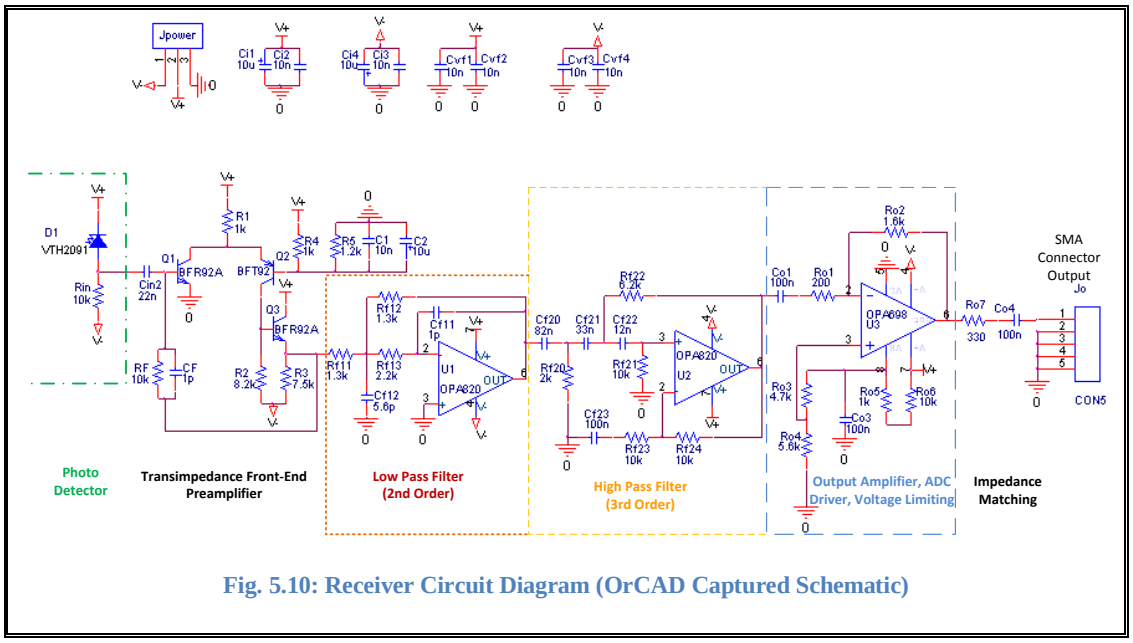

Fig. 5.10: Receiver Circuit Diagram (OrCAD Captured Schematic)

remove the high-frequency signal components that were detected during initial circuit simulation. The high-pass filter was introduced to remove low-frequency signal components such as the 50Hz contribution from the power-grid, 100Hz and the first harmonics (200Hz, 300Hz, etc) from the blinking of fluorescent lamps.

The final stage is a wideband voltage limiting amplifier. This stage adapts the output voltage levels to the ADC input range. Given the wide dynamic range of the input signal it is necessary to guarantee a significant level of amplification for the low level signals, while assuring that the output does not reach over the typical 3.3V of the digital circuitry. The chosen voltage limiting amplifier guarantees both conditions as it operates linearly to within 20mV of the output limit voltages.

Given that the communication system will use square pulses the distortion caused by the limiting amplifier on overdrive signals will not affect signal detection. Amplifier gain and lower and higher cut off frequency are shown in Table 5-3. Fig. 5.11 shows the overall response of the receiver. A total gain of about 100dB is achieved for the frequencies of up to 15MHz.

The analog parts of both the transmitter and the receiver are designed according to the desired application. The frequency response is taken into account in order to evaluate the adequacy of the designed circuits. In the following sections, the FPGA implementation details are presented, simulation results are also compared with Matlab/Simulink results.

Table 5-3: Gain/phase results of the Voltage Amplifier's effect on the Receiver

Circuit	f_L [Hz]	f_H [MHz]	Gain [dB]
Voltage amplifier	11.782,00	69,82	30,03
Preamplifier+filter	728,89	29,84	74,01
Preamplifier+filter+ voltage amplifier	11.822,00	27,56	107,04

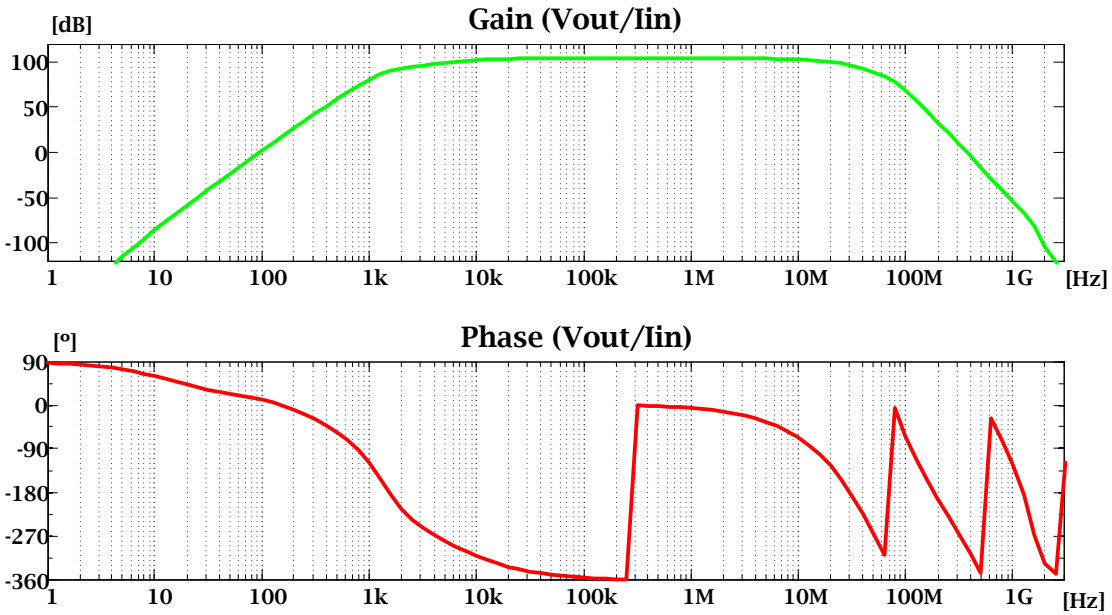

Fig. 5.11: Response curve of Overall Receiver

5.3 FPGA Implementation of VLC System

FPGAs are configurable hardware platforms which provide the flexibility to realize the digital electronic circuits. They are attractive from performance and power consumption points of view. They are also cost effective. Configurable hardware implementation offers some flexibility of adjustment in settings as compared to actual hardware. FPGAs contain programmable logic components called "logic blocks", and a hierarchy of reconfigurable interconnects that allow the blocks to be "wired together"- somewhat like many (changeable) logic gates that can be inter-wired in (many) different configurations. Logic blocks can be configured to perform complex combinational functions, or merely simple logic gates like AND and XOR. In most of the available FPGAs, the logic blocks also include memory elements, which may be simple flip-flops or more complete blocks of random access memory (RAM). In addition to digital functions, some FPGAs have analog features. A few "mixed signal FPGAs" have integrated peripheral ADCs and Digital-to-Analog Converters (DACs) with analog signal conditioning blocks allowing them to operate as a system-on-a-chip (SoC).

Such devices blur the line between an FPGA, which carries digital ones and zeros on its internal programmable interconnect fabric, and analog part, which carries analog values on its internal programmable interconnect fabric.

The output signal from the front-end amplifier is set within the range of the ADC which is the first stage before the FPGA. ADC samples the incoming signal at a rate five times faster than the transmitted signal. When the DSSS receiver detects a valid incoming signal from ADC, i.e. outside a configurable threshold which defines the system "dead zone", it starts processing the incoming signal. This is described in detail in following sections.

A brief description of the PFGA evaluation board and some of the most important associated parts is given first. In the later part, implementation details of major blocks are provided.

5.3.1 Overview of Spartan Evaluation Board

Spartan boards (SP 305 and SP605) from Xilinx [56] were used for implementation. SP605 board enables hardware and software developers to create and evaluate designs targeting the Spartan-6 XC6SLX45T-3FGG484 FPGA. Spartan-6 FPGAs are configured by loading application: (i) specific configuration data, and (ii) a bit stream into internal memory. Spartan-6 FPGAs can load themselves from an external nonvolatile memory device or they can be configured by an external smart source, such as a microprocessor, DSP processor, microcontroller, PC, or board tester. In any case, there are two general configuration data paths:

(i) serial data path that is used to minimize the device pin requirements.

(ii) 8- or 16-bit data path used for higher performance or access (or link) to industry-standard interfaces, ideal for external data sources like processors, or x8- or x16-parallel flash memory.

Like processors and processor peripherals, Xilinx FPGAs can be reprogrammed, in system on demand, an unlimited number of times. Because Xilinx FPGA configuration data is stored in

complementary metal oxide semiconductor (CMOS) configuration latches (CCLs), it must be reconfigured after power down. The bit stream is loaded each time into the device through special configuration pins. These configuration pins serve as the interface for a number of different configuration modes:

- JTAG configuration mode
- Master Serial/SPI configuration mode (x1, x2, and x4)
- Slave Serial configuration mode
- Master SelectMAP/BPI configuration mode (x8 and x16)
- Slave SelectMAP configuration mode (x8 and x16)

The specific configuration mode is selected by setting the appropriate level on the mode input pins M [1:0]. In Master configuration modes, the SP-6 device drives CCLK (clock) from an internal oscillator by default or optional external master clock source GCLK0/USERCCLK. In Slave configuration modes, CCLK is an input.

The SP605 provides board features common to many embedded processing systems. Some commonly used features include:

- DDR3 component memory,
- 1-lane PCI Express interface,
- Tri-mode Ethernet PHY,
- General purpose I/O and a UART (universal asynchronous receive/transmit).

Additional user desired features can be added through mezzanine cards attached to the onboard high speed VITA-57 FPGA Mezzanine Connector (FMC) and low pin count (LPC) connector.

The MicroBlaze™ core is a 32-bit reduced instruction set computer (RISC) Harvard architecture soft processor core with a rich instruction set optimized for embedded applications. With the MicroBlaze soft processor solution, we have complete flexibility to select the combination of peripheral, memory and interface features that gives us the exact system we need at the lowest cost possible on a single FPGA.

MicroBlaze has over 70 configuration options, enabling everything from a very small footprint microcontroller to a high performance embedded computer running Linux. At the heart of this flexibility are the two versions of MicroBlaze, the area-optimized MicroBlaze (with a 3-stage instruction execution pipeline) and the performance-optimized MicroBlaze (with a 5-stage instruction execution pipeline).

The MicroBlaze floating point unit is fully supported by the Embedded Development Kit (EDK). Embedded Development Kit comes with a broad array of soft and hard networking peripherals supporting up to 1G Ethernet. Software drivers for Ethernet peripherals are included with EDK. Networking protocol stacks including IPv4/v6, TCP, UDP, HTTP are provided by many Xilinx Alliance partners [92]. Networking application examples are also provided with various bundled Embedded Boards and Kits [93]. However, many of the features are not necessary for VLC transceiver implementation. The following sections discuss the transceiver implementation details.

5.3.2 VCL Transmitter and Receiver Implementation

The overall system configuration and FPGA architecture was discussed in previous section. In this section, we describe the implementation of signal processing VLC architecture suitable to be used in road safety applications. The transmitter parts are developed to ensure data transmission at the rate of 200kbps (however, configurable) and efficiently drive an array of LEDs. The receiver samples the signal at a maximum sampling rate of 1Msps (limited by the ADC speed in our core) allowing the ADC to sample 5-times higher than the incoming data rate. A novel approach based on sampling frequency was developed to maintain the receiver's synchronization. We have chosen to implement a finite impulse response (FIR) receiver architecture, because this is the most suitable choice for FPGA prototyping. The modulation scheme used for this system is based on direct sequence spread spectrum techniques. The DSSS transceiver developed is based on system on a programmable chip (SOPC) concept.

5.3.2.1 System On a Programmable Chip (SOPC)

SOPC concept is bringing a major revolution in the design and development of integrated circuits in microelectronics technology. With the help of design tools, it is possible to combine several blocks with different functions in a programmable chip. It is an attractive and flexible form of building up a specialized system, containing CPUs, peripherals, interfaces and custom logic. The system was developed using Xilinx design tools taking some of the available advantages of intellectual property (IP) cores. The most important IP cores used were: the MicroBlaze 32-bit microprocessor, buses (PLB-peripheral local bus and LMB-local memory bus), clock manager, UART and finally the general purpose input/output (GPIO) which establishes communication between DSSS emitter/receiver and the remaining system.

5.3.2.2 Pseudo-Noise Sequence

The PN code characterizes the DSSS system process gain. A new 10 bits code was developed. This code has nearly the same characteristic as the popular Barker 11 bits length code. The code is:

PN code = +1 +1 +1 -1 -1 -1 +1 -1 -1 +1.

Both Barker and this code exhibit very good correlation properties avoiding false acquisitions and degradation at DSSS receiver. Fig. 5.12 shows the worst correlation case scenario, which occurs when the sequence finds its complement. Both codes exhibit small partial correlation peaks, however Barker presents a slightly higher peak margin which is the difference between the main peak lobe and side lob (10-2 < 11-1).

The great advantage of Barker code relatively to our 10 bit code is the larger achieved processing gain. In fact, and considering short codes, processing gain is directly related with the length of PN code:

$$Gp = 10\ log\ (PN\ code\ length) \tag{5.4}$$

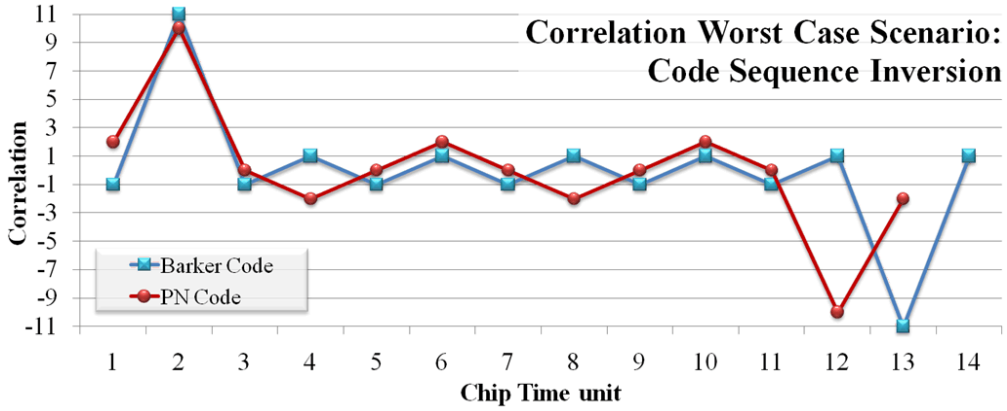

Fig. 5.12: PN Codes Correlation Values Worst Case Scenario

Thus, the code developed has penalty of about 0.4 dB relatively to Barker. A higher processing gain allows a better mitigation of narrowband interference/noise on DSSS system. But the code developed presents advantages relatively to Barker. The first one is that it is balanced, i.e., it has the same number of positive and negative logical levels which reduces the DC component. Also, the number of identical consecutive bits is not more than 3, avoiding voltage drop in analog circuitry. These two characteristics are very important in VLC where the information is carried by intensity modulation and received by direct detection.

Given the low data rate purpose of the developed DSSS system, a shorter code allows a higher data rate input. Furthermore, even length codes simplify the clock relation between chip rate and data rate. The higher processing gain performance obtained by Barker code comes at the cost of logic resources as shown in Table 5-4. It is clear that the new 10 bit code approach uses less logic resources than Barker. Both implementations were performed in two Spartan-xc3s500e-4fg320, the results were obtained with Integrated Software Environment (ISE) tool from Xilinx (Version 12.3) [56].

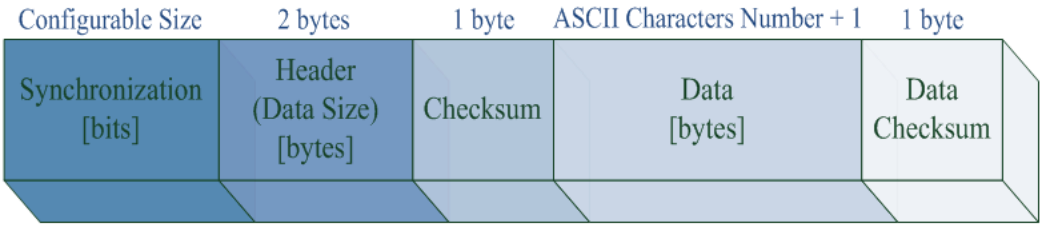

Fig. 5.13: Frame Format for DSSS based VLC transceiver

5.3.2.3 DSSS System Protocol

In order to establish communication between the emitter and the receiver, a frame-based protocol was developed, as depicted in Fig. 5.13. Besides the data message, redundant data is required to be transmitted to allow receiver synchronization and data integrity. The frame is produced in the emitter and translated in the receiver. The frame comprises 5 main fields:

Table 5-4: Comparison of DSSS Transceiver Consumed Resources

Resources	10th length PN Code				11th length Barker Code			
	Emitter		*Receiver*		*Emitter*		*Receiver*	
	Used	*%*	*Used*	*%*	*Used*	*%*	*Used*	*%*
Slices	786	16%	1715	36%	812	17%	2006	43%
Slice Flip-Flops	1159	12%	1222	13%	1185	12%	1386	14%
4 input LUTs	1572	16%	3138	33%	1623	17%	3656	39%
BRAMs	10	50%	4	20%	10	50%	4	20%
MULT18X18SIOs	5	25%	4	20%	5	25%	4	20%
GCLKs	5	20%	2	8%	5	20%	2	8%

1. ***Synchronization*** – this field allows the receiver to achieve synchronization. It consists of an alternate sequence of zeros and ones. By default this sequence has a length of 14 bits, however this number can be adjusted, being a trade-off between time to synchronize and frame overhead. The field ends with a terminator constituted by 16 bits: 1111111100000000. This long sequence avoids false termination acquisitions caused by possible interference or noise;
2. ***Header*** – this field contains the Data size in the frame. With this information the receiver knows in advance the length of the message. There are 2 bytes reserved for this allowing a maximum message length of 65535 (2^{16}) characters. The header can be expanded to transmit other useful information in future implementations;
3. ***Checksum*** – this field contains the complement of the resulting sum of header octets. The receiver uses this field to verify the header data integrity: if the resulting sum of header octets with checksum is all ones (11111111), the header was received successfully, otherwise an error transmission occurred. This field has a fixed size of 1 byte;
4. ***Data*** – this field contains the ASCII code of each character of the message. A message ends with the "enter" key, which has the code 0x0D. This code is used as a data terminator by the receiver. This field has a variable size and depends on the length of message to transmit. The transceiver is able to handle message lengths up to 1024 characters;
5. ***Data Checksum*** – this field contains the complement of the resulting sum of data octets. The receiver uses this field to verify the message data integrity. The process is analogous to the header checksum described above. This field is optional and can be enabled or disabled. If it is enabled, fully received messages will be displayed. This field has a fixed size of 1 byte.

By default the number of frame bits is given by:

$$Frame_{bits-number} = K + 8\,(message\ length) \tag{5.5}$$

where *K* is a constant given by the sum of constant bits contained in frame: 14 (sync) + 16 (sync term) + 16 (hd) + 8 (hd_cks) + 8 (dt_cks). Synchronization bits were considered fixed in order to simplify the calculations. Given that the maximum length of a message is 1024 characters, the maximum number of frame bits is 8254. On the other hand the minimum corresponds to when no character is transmitted and the data field composed only by the data terminator, which results in 70 frame bits. With DSSS techniques all frame bits are multiplied by the PN code; generating the PN code itself, if the frame bit is 1 or its complement, if the frame bit is 0 (sequence inverse keying modulation). Since the PN code has 10 chip bits, the real size of the frame has a multiplicative factor of 10, where each frame bit is considered a packet composed of the 10 chip bits.

Emitter architecture however, contains the main core and other blocks which are discussed in the following sections.

5.3.2.4 Signal Processing parts of The VLC Emitter

The block diagram of the FPGA implementation of the emitter is presented in Fig. 5.14. The proposed system is able to acquire digital data, in this case an ASCII message, modulate and transmit it through visible light medium.

The ASCII message is introduced through an UART terminal and it is stored in the MicroBlaze memory. The data is then transferred to the DSSS emitter core through a simple handshake protocol, using GPIO. The handshake ensures proper transfer of the message sequence. In the DSSS emitter core the message is assembled into a frame as shown in Fig. 5.13. The resulting frame is then modulated with SIK.

In order to simulate the channel behavior for different conditions, the decoded frame is passed to the Xilinx AWGN block [57]. This block allows the evaluation of receiver performance, through addition of bipolar corrupted noise proportional to a defined SNR. However, the output signal must be reformatted back into unipolar so that it can be transmitted by an output pin of the FPGA.

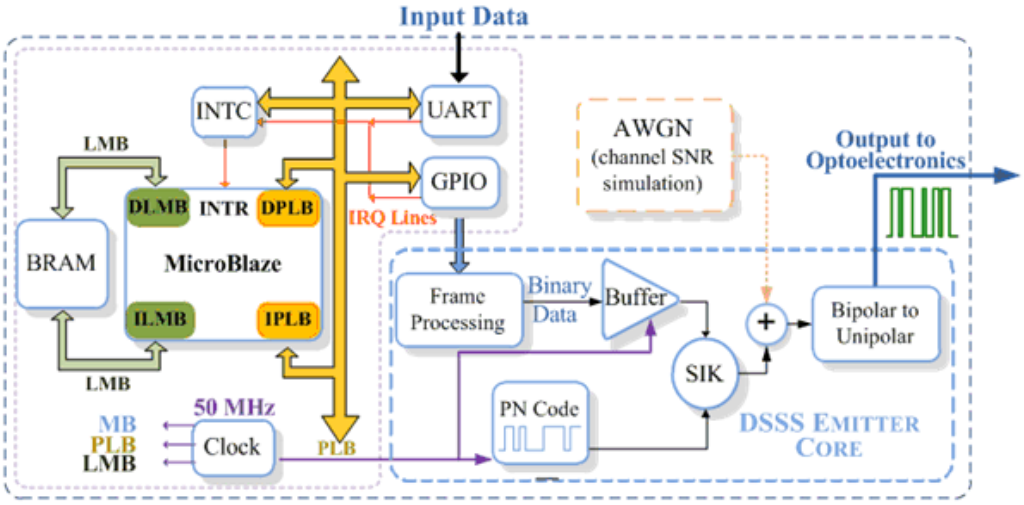

Fig. 5.14: FPGA Implemented VLC Emitter Architecture

During all these operations, the clock manager module generates signals which are applied at different rates to the various blocks. However, data transmission is fixed at 200kbits, which corresponds to chip frequency of 1MHz. This low data rate is considered due to: (i) switching limitation of HB-LEDs at transmitter; (ii) sampling frequency of ADC at receiver. Although, HB-LEDs can switch around 10MHz, [66] the used ADC operates at a maximum of 1.5Msps [56].

5.3.2.4.1 VLC DSSS Emitter Core

This core is the heart of the emitter. Its main tasks are assembling the received message-frame and transmit it in DSSS format. Additionally, it is possible to corrupt the output signal with noise using the Xilinx AWGN core. This core uses two Xilinx tools: ISE projector navigator and system generator.

5.3.2.4.2 ASCII Message Transfer

The first step before making the frame and start the transmission is to transfer the ASCII message from MicroBlaze memory to DSSS emitter core. To ensure the correct data transfer between both units a master/slave handshake protocol was developed. The MicroBlaze

processor behaves as master and DSSS emitter core as slave. Fig. 5.15 shows the simplified slave finite state machine (FSM) implemented in DSSS emitter core.

The data message is transferred in a serialized form using handshake control codes to signal the start of transfer of each ASCII code character and the end of transfer. The basic principle is: when the MicroBlaze is ready to send information, it signals the emitter core and waits for its acknowledgement. The message transfer process is summarized in the following steps:

1) After getting the digitized message, the MicroBlaze initiates the transfer sending the *start* code to emitter core;
2) Emitter core answers with the *start acknowledgement* code and jumps from state *idle* to state *data read*;
3) MicroBlaze replies with the block code signaling the intention of sending the first ASCII code of the message;
4) Emitter core answers with the new block acknowledgement code showing that it is ready to receive the ASCII code message;
5) MicroBlaze sends the first ASCII code from the message;
6) Emitter core stores the ASCII code into a buffer and jumps to the *data read ack* state;
7) Emitter core answers with the block acknowledgment code signaling that the ASCII code was well received and jumps to *data read* state again;
8) Steps (3) to (7) are repeated until the last ASCII code of message is transferred;

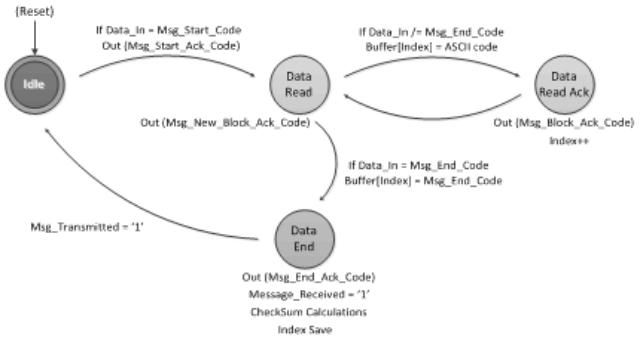

Fig. 5.15: State diagram to Transfer the ASCII Message from MicroBlaze

9) MicroBlaze sends the block code to the emitter core signaling the intention of sending an ASCII code message;

10) Emitter core answers with the new block acknowledgement code showing that it is ready to receive the message ASCII code;

11) MicroBlaze sends the last ASCII code from the message, which corresponds to the *end* code;

12) Emitter core detects the last ASCII code, stores it and jumps to the *data end* state;

13) Emitter core answers with the acknowledgment end code signaling the end of message transfer. At this state several calculations are performed in order to achieve the header and data checksum fields. The last buffer address (index) which points to the last message ASCII code received is saved. In addition the "Message_Received" flag is enabled. The emitter FSM will return to the *idle* state only when the message is fully transmitted. At *idle* state the emitter is able to receive a new message repeating the cycle.

The emitter FSM is controlled by a clock of 100kHz. This frequency allows a safe exchange of data-byte information between MicroBlaze and emitter core. The transfer from MicroBlaze is controlled in software (through GPIO), which is a process that is naturally slower than the FSM realized in hardware.

5.3.2.4.3 DSSS Encoder

The proposed DSSS encoder block was developed using Xilinx System Generator. The developed DSSS encoder is presented in Fig. 5.16. Table 5-5 describes the functions of the input/output ports of the encoder.

When the encoder is enabled (Enabler = '1') each frame bit is modulated in DSSS SIK. The modulation process is simple: if the frame bit is ´1´ the output will be the PN code, otherwise it will be the inverse of the PN code. SIK is easily achieved through the logical port "XNOR". PN code is implemented using a linear feedback shift register (LFSR) with four (n = 4) registers and a counter. The LFSR generates a maximum length sequence (m-sequence) code of (2^n-1) 15 bits. This sequence is truncated to 10 using a counter, resetting the LFSR every 10 times. In order to assure the correct sequence bits, the initial value of the LFSR four registers must be equal to the four initial bits of the PN sequence.

The encoder is managed by a clock of 200kHz, which corresponds to the final rate of the emitter system.

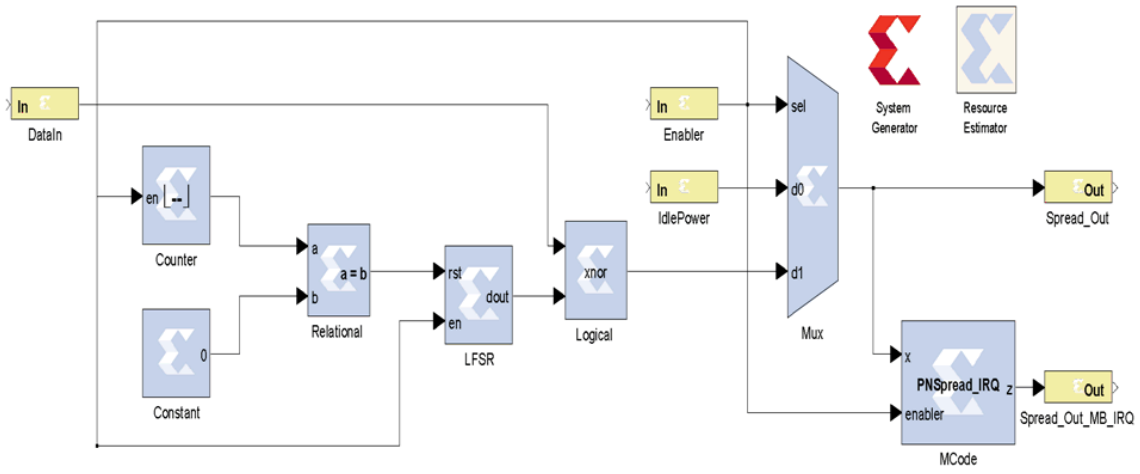

Fig. 5.16: DSSS Emitter Encoder blocks

Table 5-5: Description of the Input/output ports of DSSS Encoder block

Inputs	Description
DataIn	This port is the input to the generated frame bits. Each frame bit is maintained stable during the DSSS SIK modulation process. This is achieved due to the fact that, the FSM responsible to generate the frame bits to managed by a clock 10 times slower than the clock used in DSSS encoder.
Enabler	The enabler port allows activating the DSSS encoder system. This port controls a multiplexer, which allows to choose between the DSSS signal (when the enabler port is activated) and the "IdlePower" port (when the enabler port is deactivated).
IdlePower	This port is the input applied to encoder when it is disabled. In order to maintain a balanced output power on emitter LED's, this port is driven by a constant clock of 200kHz. This is the same clock that controls the encoder block.
Outputs	**Description**
Spread_Out	This is the DSSS output of the encoder. If the AWGN block is deactivated, this port corresponds to the final value of the emitter and is therefore driven by an output FPGA pin to the optoelectronics part.
Spread_Out_MB_IRQ	This port allows driving the DSSS output to MicroBlaze in order to display its values in UART terminal. The "PNSpread_IRQ" block adds a bit to the DSSS output, which is used to force an interruption in MicroBlaze whenever a new DSSS bit is transmitted.

5.3.2.4.4 AWGN Channel Simulator

In order to simulate channel behavior for different conditions, the spread frame is passed through the emitter AWGN channel simulator block (Fig. 5.17). This block allows corrupting the DSSS signal with a specified amount of noise. It is possible to establish a SNR during transmission, which is important to evaluate the receiver performance in different conditions.

The incoming signal from DSSS encoder is corrupted using Xilinx AWGN block as shown in (Fig. 5.18). This block converts the incoming signal in bipolar format and adds white Gaussian noise (through the white Gaussian noise generator). The noise is scaled based on the SNR value in order to achieve the desired noise variance. The AWGN core generates white Gaussian noise using a combination of the Box-Muller algorithm and the central limit theorem [59]. As a result, it is capable to generate a probability density function (PDF) which deviates less than 0.2 percent from the Gaussian, for 4.8σ (standard deviation) from the mean.

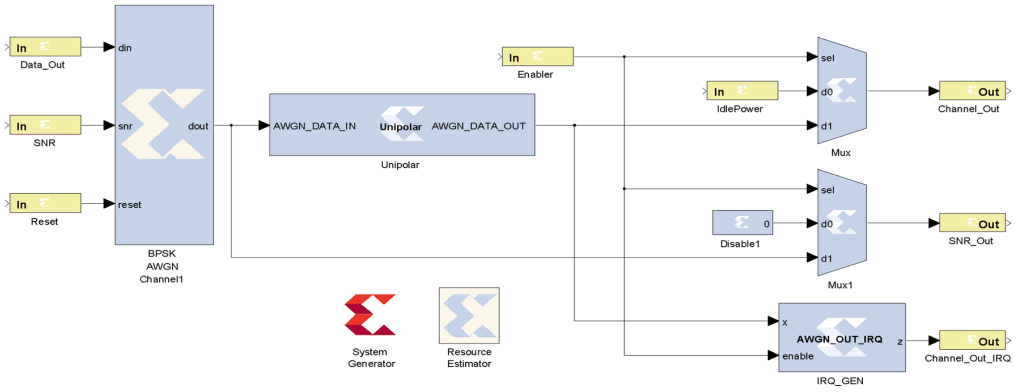

Fig. 5.17: Emitter AWGN channel Simulator block

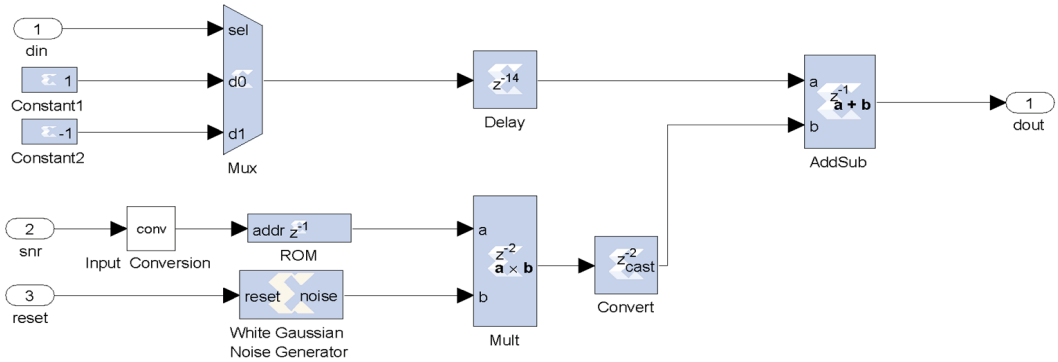

Fig. 5.18: AWGN Channel Subsystem blocks

The signal is reconverted to unipolar format in order to be transmitted through an output FPGA pin. The signal is converted to one or zero, if the corrupted signal is higher or less than zero respectively. The developed receiver samples each DSSS bit five times. Thus this block is managed by a clock 5 times higher (1MHz) than the one used in encoder block (200kHz).

Table 5-6: Description of the Input/output ports of AWGN channel Simulator block

Inputs	**Description**
Data_Out	This port is the input to the generated DSSS bits. Each DSSS bit is maintained stable during the noise corruption process. This is achieved due to the fact of the DSSS encoder be managed by a clock 5 times lower than the clock used in AWGN channel simulator block.
SNR	The noise is scaled based on the SNR value applied to this input. The SNR input range varies from 0.0 to 15.94dB in steps of 62.54mdB.
Reset	When activated, restarts the AWGN block to the default values.
Enabler	The enabler port allows activating the AWGN system. This port controls a multiplexer, which allows choose between the corrupted DSSS signal (when the enabler port is activated) and the "IdlePower" port (when the enabler port is deactivated).
IdlePower	This port is the input applied to AWGN when it is disabled. In order to maintain a balanced output power on emitter LED's, this port is driven by a constant clock of 200kHz.
Outputs	**Description**
Channel_Out	This is the corrupted DSSS output of the AWGN system. When this block is activated, this port corresponds to the final value of the emitter and is therefore driven by an output FPGA pin to the optoelectronics part.
Channel_Out_IRQ	This port allows driving the corrupted DSSS output to MicroBlaze to display its values in UART terminal. The "AWGN_OUT_IRQ" block adds a bit to the corrupted DSSS output, which is used to force an interruption in MicroBlaze whenever a new bit is transmitted.
SNR_Out	This port allows driving the corrupted DSSS output to MicroBlaze before the signal being converted to the unipolar format, i.e., with a precision of 17 bit signed number being 11 of them used after the binary point.

The developed AWGN noise block is optional, i.e., it is possible to activate for simulation and easily deactivate by changing a flag value in MicroBlaze software, for normal transmission operation. The input-output port descriptions are given in Table 5-6.

Apart from these, other blocks were configured using Xilinx EDK tool and SOC based emitter hardware platform was developed and then logically connected using control commands and algorithms to be able to drive optoelectronic emitter. In addition, emitter user UART interface was designed for interactive and easy understanding. Thus, the emitter is able to emit lights at modulated frequency (200kpbs in this case). The modulated light waves pass through the free space medium and photo diode-based detector intercepts the light in the optoelectronic parts of VLC receiver which has been discussed in previous sections. The FPGA implementation of signal processing parts of VLC receiver architecture is presented next.

5.3.3 VLC Receiver Implementation

The photo-detector on the receiver (optoelectronic parts described in previous section) converts the light waves into electrical pulses, which are digitalized, demodulated and reconverted into the original ASCII message. The block diagram of implemented VLC receiver is shown in Fig. 5.19.

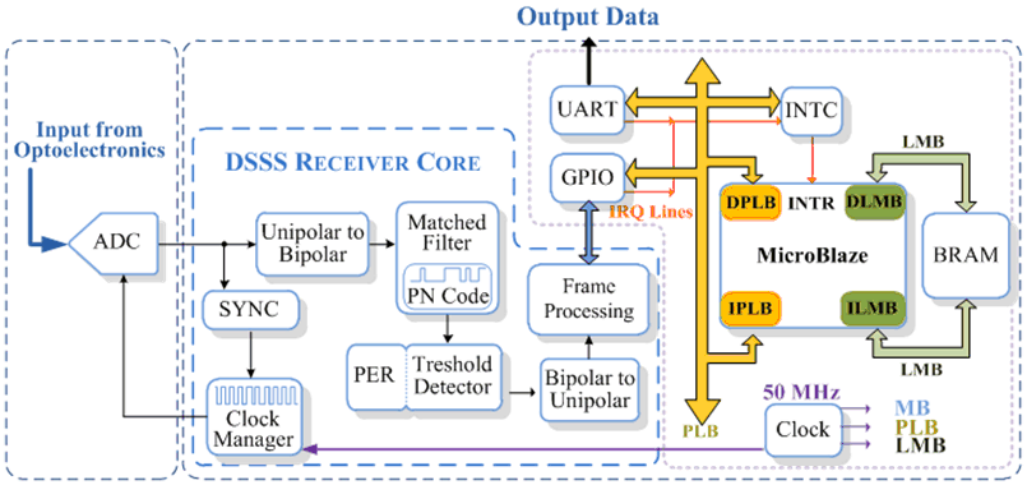

Fig. 5.19: FPGA Implemented VLC Receiver Architecture

The DSSS receiver core is operated at 1MHz which is 5 times higher than the emitter. This allows the ADC to sample 5-times per bit from the receiver's optoelectronics output. Each sample is then analyzed and compared with a reference value. If the sample value is higher than the reference, the data is considered to be '1', otherwise it is a '0'. After performing 5 samples, the final value is then decided by majority samples and converted to bipolar format. The discrete PN matched FIR calculates the correlation between the incoming data and the chosen PN code. Every chip time a correlation value is delivered to a threshold block which decides upon the synchronization of the receiver. A peak correlation value of 10 or -10 means that the PN code of the receiver is perfectly aligned with incoming sequence, i.e., the system is synchronized and it is ready to demodulate the data. The polarity of large correlation peaks indicates the final data value. A short time is required to achieve DSSS receiver synchronization given that correlation is performed every chip (PN bit) time as incoming sequence is correlated with FIR coefficients. The demodulated data frame is then analyzed and processed. If the header and checksum fields were correctly received the ASCII data is passed to the MicroBlaze through GPIO in order to be displayed on a PC terminal, otherwise the receiver loses synchronization and restarts the cycle.

To ensure reliability, the DSSS receiver considers synchronization only if it maintains alignment for two consecutive PN sequences. Synchronization is lost when the correlation value falls to a number lower than eight. This value means that the received sequence differs only by one bit from the expected PN code. Thus the receiver tolerates one bit error in normal operation, however, it loses synchronization when two or more error bits are detected. This in fact, increases the receiver performance making it more immune to noise but requires higher SNR values.

In order to measure the receiver's performance a packet error rate (PER) calculation block was also developed, based on the matched filter correlation values. Each packet corresponds to the 10 length chip bits of the PN code. Upon synchronization, the receiver starts counting every packet received. A packet is considered lost *(amiss)* if at least one bit error is detected. When the receiver loses synchronization the PER counting is stopped.

A novel approach was developed to maintain synchronization of the receiver. Usually, a fine clock phase tune is performed based on early, at time and delayed correlation values. Phase clock is delayed or advanced if a large correlation peak is obtained sooner or later respectively. The developed receiver uses a new concept based on ADC sampling history for the last 5 samples. This technique is independent of synchronization acquisition. Whenever a change of sampled logical state is detected, the *SYNC* block evaluates if the clock is advanced or delayed and adjusts the clock phase to neutralize the undesired offset. For instance, if a change of sampled logical state from zero to one occurs and if the sampling history is '11000', this means that phase clock is advanced and need to be delayed. Thus, due to the nature of PN code the system is able to adjust the phase clock in the worst case after 3 consecutive identical logical states. This enables increment or decrement the receiver system frequency by 42kHz. Before we discuss the synchronization, a brief description of ADC is given.

5.3.3.1 ADC Unit

This section will focus on the implementation of the analog-digital converter of the receiving system. The receiver's prototype was implemented in a Xilinx Spartan-3E development kit [56]. This is a low cost board, which contains a medium scale FPGA and several user interfaces, which can be used for both prototyping and debugging. Moreover, this board includes on-board devices that allow the sampling of external analog signals. The ADC implementation was carried out using these devices, avoiding the use of external components. Fig. 5.20 depicts the analog sampling and conditioning unit, included on the Xilinx Spartan-3E board. This circuit consists of a Linear Technology LTC6912-1

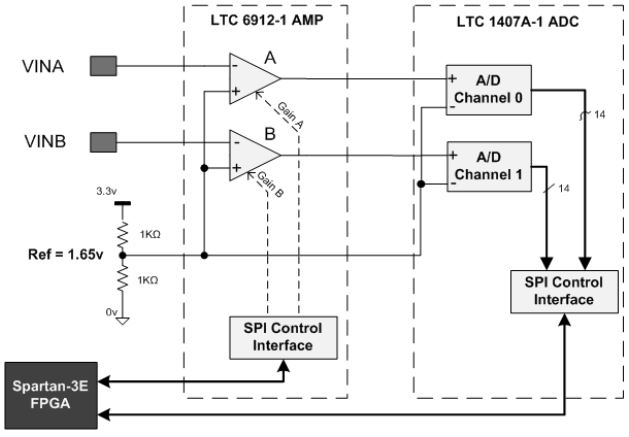

Fig. 5.20: Analog Signal capture and ADC blocks

programmable preamplifier that scales the incoming analog signal from the transimpedance front end amplifier, followed by LTC1407A-1 ADC. Both the pre-amplifier and the ADC are controlled by the FPGA.

The LTC6912-1 provides two independent inverting amplifiers with programmable gain. The purpose of the amplifier is to scale the incoming voltage on VIN_A and VIN_B in order to maximize the conversion range of the ADC. The gain of each amplifier can be adjusted from -1 to -100 which enable signals as small as ±12.5mV to apply full scale inputs to the A/D converters.

The LTC1407A-1 is a 14-bit, 3Msps ADC with two 1.5Msps simultaneously sampled differential inputs, suitable for low/medium speed and portable applications. The ADCs analogue input range is ±1.25V (V_{scale}) relative to 1.65V (V_{ref}). The analog capture circuit converts the analog voltage on VIN_A or VIN_B and transform it to a 14-bit digital representation, D[13:0], expressed by the following equation [56]:

$$D[13:0] = G\ \frac{(V_{in}-V_{ref})}{V_{scale}}\ 2^{N-1} \tag{5.6}$$

where, *G* is the current setting loaded into the programmable pre-amplifier (G [gain] from -1 to -100 with ±12mv can be programmed), V_{ref} is the reference voltage of the amplifier and the ADC, V_{scale} is the maximum range supported by ADC (±1.25V centered on the reference voltage), and *N* is the ADC resolution. The LTC1407A-1 has a 14-bit two's complement digital output, which allows representing values between -2^{13} and $2^{13}-1$.

5.3.3.2 DSSS Receiver Core

This core is the heart of the receiver and it is responsible for decoding the DSSS signal transmitted by emitter. To accomplish this, several blocks were developed in order to be possible to control the ADC, synchronization, DSSS demodulation and frame decoding.

5.3.3.3 Receiver FSM Control Unit

The receiver consists of several blocks with different functionalities. This fact makes the system more flexible and error free, since each block can be separately simulated and tested. However, to build a final system it is crucial to have a control unit responsible to manage the other blocks. Fig. 5.21 depicts a simplified FSM diagram of the control unit, used in receiver. The control unit starts by activating the block that configures the amplifier. This is the first step since the chosen gain of the amplifier, constrains the sampling input range of ADC. The signal "*Amp_Done*" is enabled after the amplifier has been configured and the system initializes the sampling process. Each ADC sample takes 34 cycles of the clock. In order to force the receiver to operate at 1MHz, and given that the unit control is managed by a clock of 50MHz, it is important that a sample occurs at 50 cycles. Thus "sync" and "delay" states were design to take the remaining clock cycles. Whenever a sample ends the signal "*Conv_Done*" is enabled. The system will only consider a valid sample if its value is higher than a pre-defined threshold. This threshold allows a dead zone to receiver, where all the values within this range will be ignored. The flag "*Dead_Zone_Out*" is enabled every time a sample is out of non-operating zone. When the receiver detects, the first time valid sample jumps to "*sync*" state. Otherwise jumps to "*delay*" state, maintaining the sampling frequency. The "*sync*" state uses the last 5 samples to adjust the clock delay relative to DSSS incoming signal and to generate the final sample value ("*Spread_Bit_Value*"). The sample will be considered one, if in the last 5 samples there were more ones than zeros and vice versa. This final sample corresponds to a spread bit that will be further processed in DSSS decoder block. The system will keep the *sample* and *sync* states until 5 samples within the dead zone are collected, or until some

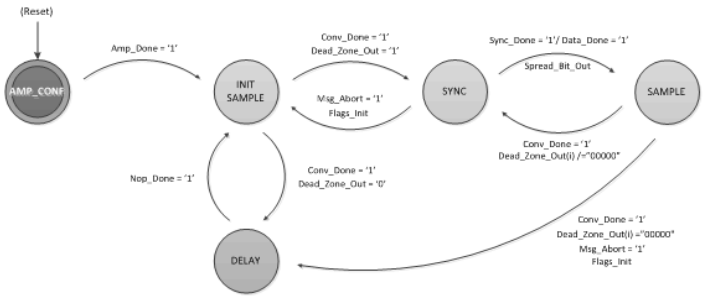

Fig. 5.21: State diagram of Receiver Control Unit

frame checksum failure occurs, or DSSS synchronization is lost. In this case the message receive will be aborted (*Msg_Abort* = '1'), all the flags initialized and the system returns to "*init sample*" (initial sample) state.

5.3.3.4 Synchronization Unit

The synchronization unit is the most complex block of the system. Besides achieving synchronization and track the emitted signal, this block handles the de-spread code from DSSS decoder block. In other words, it is responsible to decode the entire emitted frame and send the message to MicroBlaze UART terminal.

The synchronization process is based on last 5 samples from ADC and is independent of modulation. The technique consists of looking directly to the sample logical states changes. For instance, if a change occurs from state one to zero, and the last five samples history are:

1) "1,1,1,1,0": this means that the clock of the system is slightly advanced relative to transmitted signal. To correct this offset the clock phase needs to be delayed;
2) "1,1,1,0,0": the clock of the system is more advanced relative to transmitted signal than the last and therefore needs to be delayed;
3) "0,1,1,1,1": this means that the clock of the system is slightly delayed relative to transmitted signal. To correct this offset the clock phase needs to be advanced;
4) "0,0,1,1,1": the clock of the system is more delayed relative to transmitted signal than the last situation and needs to be advanced;
5) "1,1,1,1,1": this means that the system clock is perfectly aligned with the transmitted signal.

The same analysis is applied when a change occurs from logical state zero to one. The system is "*blind*" to phase differences when identical logical states are sampled sequentially. Due to nature of the used PN code, the worst case in system is three consecutive equal states, which corresponds to the worst time without synchronizing. This approach is a very good to

perform synchronization. This novel method is independent of synchronization and even any type of modulation. The standard method performs phase tuning based on early, at time and delayed correlation values. These techniques adjust the phase only at the end of PN code and acquire receiver synchronization.

The system uses two distinct techniques to perform the system clock phase adjustment:

1. ***Fine Tune***: the developed block acts directly on Xilinx digital clock manager (DCM) [59] through the "dynamic fine phase shifting" feature. DCM block allows delaying or advancing the phase up to one clock cycle time. The clock phase is dynamically controlled allowing phase shifts in steps of 78ps making up 256 shift points (256 x78ps = 20ns = Tckl). All DCM clock are equally affected by phase adjustment assuring the reliability of the system. The receiver is initially configured to a middle phase point (0) and then it is advanced (up to point 128) or delayed (up to point -128) accordingly with the last 5 samples history. This is a fine tune because the DCM core only allows increment or decrement the phase point-by-point, i.e., shifting one single position;
2. ***Coarse Tune***: in order to extend the tuning to one more clock cycle time, a new technique was developed in synchronization unit. As seen in FSM control unit (in first sub-section) the receiver was designed to work at 1MHz, which corresponds to usage of 50 clock cycles in *sample* and *sync* states (using a reference clock of 50MHz (50M/50 = 1M)). The idea is to increase or decrease one clock cycle (to 51 cycles or 49 cycles respectively) in control unit when the fine tune itself is not sufficient, i.e., when it reaches its limits of ±128 steps points. It works as an extra shift point (±129) based on last 5 samples history.

The use of these two techniques allows accommodating variances of +42kHz (50M/48 =1,0416M) and -38kHz (50M/52 = 0.9615M) around 1MHz.

5.3.3.5 Frame Demodulator

The second task of *synch* block is to demodulate the frame field bits, store the ASCII message in a buffer and if all goes as expected, transfer the message to MicroBlaze to be displayed in UART terminal. It is important to note that the sync block handles directly with the decoded

DSSS bits. In fact, there is a First-In-First-Out (FIFO) between DSSS decoder and *sync* block, which isolates the data rate of the two blocks and delivers the decoded DSSS bits to *sync* block. Fig. 5.22 presents a simplified version of FSM that controls the frame decoding and its delivery to MicroBlaze UART terminal.

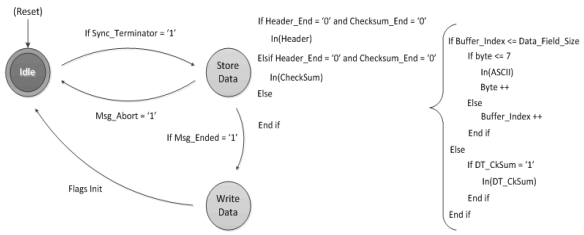

Fig. 5.22: State diagram for Frame Decoding

The FSM remains at *idle state* until synchronization terminator bits is detected. When it happens the "*Sync_Terminator*" flag is enabled and the system jumps to store *data state*. First the header bits are captured which contains the data size field. Then header checksum bits are decoded. At this point, verification to the received header bits is made. If these sequences are passed the system is able to collect the ASCII message, otherwise the message collection is aborted (*Msg_Abort* = '1'). The message is grouped in bytes, which are stored in a byte-addressable buffer.

The number of bytes to be collected was given by header field a-priori during transmission. If the checksum flag is disabled the message is sent to MicroBlaze UART terminal even with transmission errors. On the other hand, if the checksum flag is enabled, the data field is verified and the message will be displayed only if the integrity check is passed, otherwise it is bypassed and the process is aborted.

5.3.3.6 DSSS Decoder

The DSSS decoder block transforms the sampled PN bits in frame bits and store them into a FIFO. This FIFO establishes a bridge between DSSS decoder and sync block. Fig. 5.23 presents the designed DSSS encoder, while Table 5-7 describes its respective input and output ports functionalities. The sampled DSSS bits are first converted to bipolar format through bipolar block. Bits with value of one maintain its value, while bits with value of zero are converted to -1. This bipolar version of sampled spread code is delivered to the matched filter

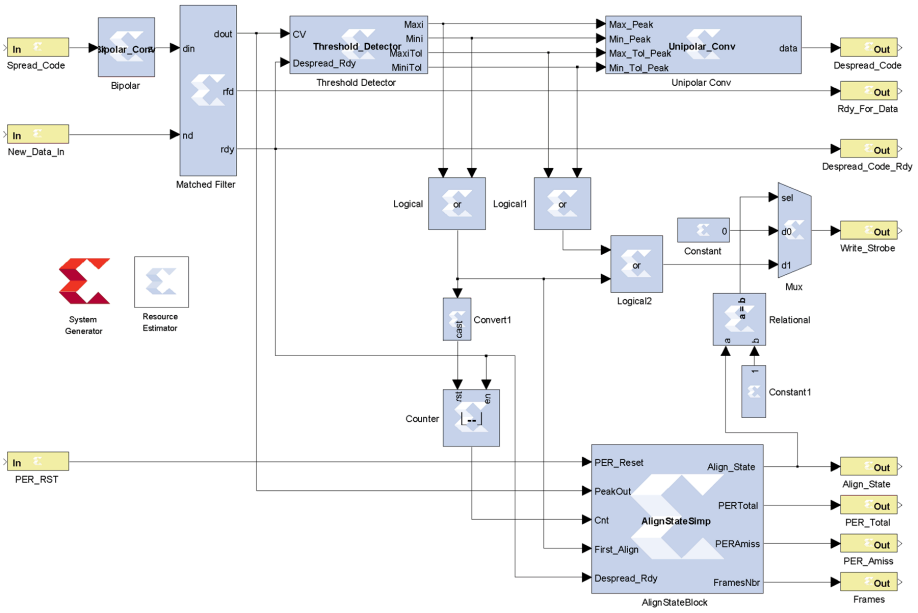

Fig. 5.23: DSSS Receiver Decoder blocks

core, which performs the correlation (at each cycle clock) between the incoming code and its own version of PN code. The match filter is in fact a finite impulse filter, where each coefficient is one bit of the bipolar version of PN code.

Fig. 5.24 illustrates the DSSS synchronization and the main input/output ports involved. When a valid sequence is detected, a large peak of 10th correlation value is obtained and the respective data bit is demodulated (*despread_code*) by signal value. A positive peak corresponds directly to a frame bit value of one, while a negative peak corresponds to a frame bit value of zero. However, the receiver only acquires synchronization (*align_state_out*) if it maintains alignment for two consecutive incoming PN sequences. The demodulated data is validated by the *write_strobe* signal. The receiver achieves synchronization in a very short

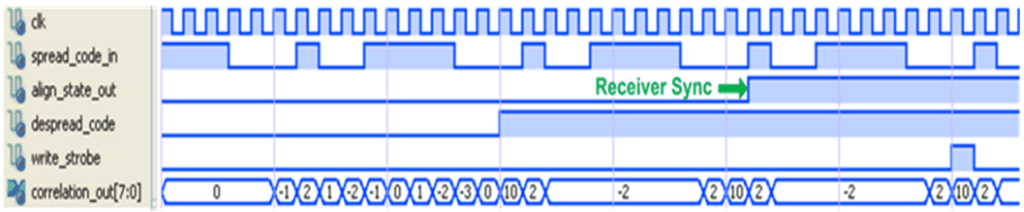

Fig. 5.24: Waveform showing the Synchronization Process

time requiring only 20 clock cycles.

In order to evaluate the receiver performance, a statistic block (Align_State_Block) was

Table 5-7: Description of the Functions of Input/output ports of DSSS Encoder block

Inputs	**Description**
Spread_Code	This port is the input to the ADC sample bits.
New_Data_In	When this signal is asserted, the bipolar version of spread code sample presented to the *din* port and accepted into the matched filter core.
PER_Rst	When this signal is asserted all packet error rate statistics stored in align state block are initialized (PER_Total, PER_Amiss and Frames outputs).
Outputs	**Description**
Despread_Code	This is the final output of the decoder corresponding to the demodulated frame bits. Each frame bit is further stored in a FIFO.
Ready_For_Data	This signal signalizes that the matched filter is ready to accept a new spread code sample.
Despread_Code_Ready	This signal indicates that a new de-spread bit is available on the *dout* port of matched filter.
Write_Strobe	This is a strobe that validates the de-spread bit output. Whenever a new de-spread bit is available this signal is activated in order to validate the respective output.
Align_State	When this signal is enabled means that the incoming PN code is aligned with receiver's PN code, i.e., the receiver is DSSS synchronized.
PER_Total	This output gives the total number of packets collected in receiver at the moment. The signal is constituted by 28 bits; possible count until 268435456 (2^{28}).
PER_Amiss	This output gives the total number of packets loss (*amiss)* collected in receiver at the moment. The signal is constituted by 28 bits; possible count until 268435456 (2^{28}).
Frames	This output gives the total number of DSSS synchronization losses collected in receiver at the moment. If the receiver is in a very low noise environment, the number of synchronization lost coincides with the number of frames/messages received. The signal is constituted by 28 bits; possible count until 268435456 (2^{28}).

developed, which works on the correlation values produced by matched filter. A correlation value of 10 means that the packet received has no error, i.e., the 10 PN codes bits were all received successfully. However a correlation value of 8 means that one DSSS bit among the 10 transmitted was wrongly received producing a packet loss (*amiss)*. The counting is performed since the receiver is DSSS synchronized (*Align_State enabled*).

It is possible to collect the packets statistics at any time through the UART terminal as well as its initializations. The Align State block also controls the alignment of the receiver. The system tolerates one DSSS bit error, but loses synchronization when two or more DSSS error bits are received in same packet. When the receiver loses synchronization it needs two consecutive well received PN sequences to align again.

SOPC receiver's hardware platform is thus built using EDK tool. Algorithms and command controls are designed to logically connect to be able to extract the information bits at the same time calculating packet error, if any.

On successful FPGA implementation, performance of VLC systems is compared from Matlab/Simulink model. This was performed to understand the difference (if any) and reason out the differences. Next section presents the comparative result of VLC systems developed and implemented in Simulink as well as FPGA.

5.4 Implementation Performance of VLC Systems through Simulation

Different approaches were followed in order to design and implement the VLC system. Before, actual hardware implementation, systems were analytically analyzed and simulation results were presented [74]. Matlab/Simulink model was developed based on two receiver architectures to finally decide on best approach for implementation. FIR based approached was implemented due to its fast synchronization characteristics. On implementation, it becomes necessary to examine the performance of the systems from Simulink model to that of FPGA implementation.

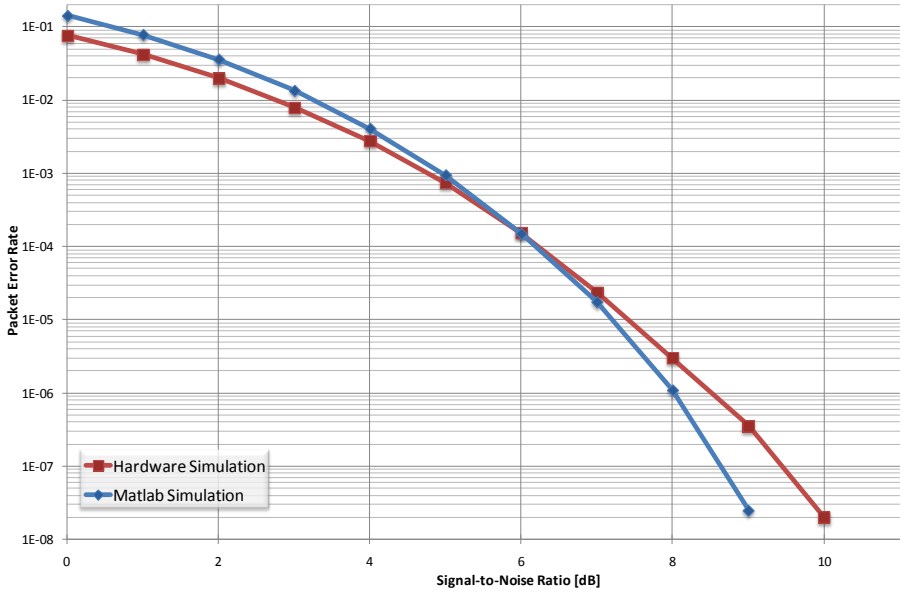

Fig. 5.25: Comparison of Matlab/Simulink VLC model with FPGA Implementation.

Fig. 5.25 presents the simulation result from both implementations. It is observed that Simulink based implementation performance is fare as compared to FPGA hardware implementation. The main reason of small difference may be the synchronization loss due to increase in signal propagation delay in the hardware implementation of FPGA as compared to Simulink in which all blocks are directly connected.

In the next chapter, experimental results are presented which have been performed in different conditions and environments.

5.5 Concluding Remarks

This chapter presented brief hardware design and implementation of VLC systems. Optoelectronic parts of VLC emitter and receiver design were presented with their responses. A receiver with reasonable good sensitivity is obtained. Signal processing and software parts implementation of system in FPGA were discussed. Function and implementation detail of important blocks were explained. Result from Simulink implementation from previous chapter and FPGA hardware implementation was also shown. Their performances were recorded to be nearly the same.

CHAPTER 6: VLC SYSTEMS PERFORMANCE EVALUATION

Summary

The performance evaluation of the VLC prototype is discussed in this chapter. The system was tested in different atmospheric conditions and environments. The results achieved are encouraging and well matched with simulation results in most cases.

6.1 Introduction

Analytical and simulation results from previous chapters confirm the operational behavior of VLC system in laboratory simulation environments. Our system is able to achieve the required behavior. However, its performance may not be the same in real environments. There are many limitations in the settings, for example working temperature, operating voltage, physical interconnections and so on, and these parameters are bound to bring deviations from the expected results. However, our aim always remains to achieve real results under real set-up conditions, as close as possible to traffic control scenario.

In this chapter, the VLC prototype performance is evaluated. The prototype is tested in controlled environments as well as in real environments. The system has been tested for reliability and consistency by running continuously for many hours. Its performance in different environments and atmospheric conditions is given and discussed. The results are encouraging and the performance fulfils our expectations. However, there are possibilities to enhance the performance of the system which will be highlighted in the final chapter. Our first experimental set up and associated results are discussed in the following sections. Many experiments were done, both indoors and outdoors. Naturally, only a subset of these is reported here.

6.2 Indoor Experiments

System's performance was evaluated in different environments and locations. In this section we present the experimental set-up for evaluating the VLC system in different environments.

The emitter is configured to transmit data at a maximum of 200kbps. Different length messages (25 characters, 50 characters, 100 characters, 256 characters and 1024 characters) were used. In this setting we describe two experiments carried out in the laboratory. They are:

(i) Workbench, and

(ii) Laboratory/office setting.

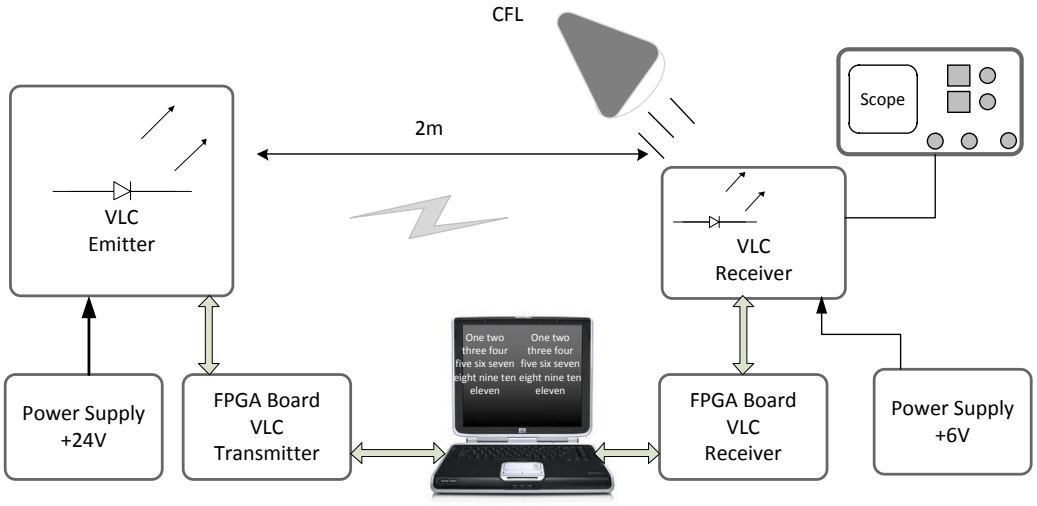

Fig. 6.1: Workbench Experimental Set-up Scenario

6.2.1 Workbench

The first experiment was accomplished in the laboratory work bench. The system was set-up on the work bench in the laboratory as shown in Fig. 6.1. A snap shot of the set-up can also be seen in appendix-I Fig. II. In this case, a high intensity CFL (20W) table lamp was also focused directly into the receiver in order to produce close distance interference.

In the laboratory setting the distance between the emitter and the receiver was very close, the result on packet loss was negligible. The *packet loss* is the difference between the total number of sent packets and total collected packets. The receiver is then subjected to external light noise from the table lamp. It was observed that if the distance between the lamp and receiver is maintained around 0.30m and more, receiver still receives all the messages. Similarly, if the emitter direction is changed, and the emitted light is made to be reflected from walls (non LoS), the receiver still receives over 80% of messages when reflected lights travel for a distance of over 6m. These tests were done to examine the robustness of systems from interference and external noise which was expected for VLC system.

In order to decide what would be the most adequate message length, a set of experiments were made for different message lengths. System's performance for messages with different

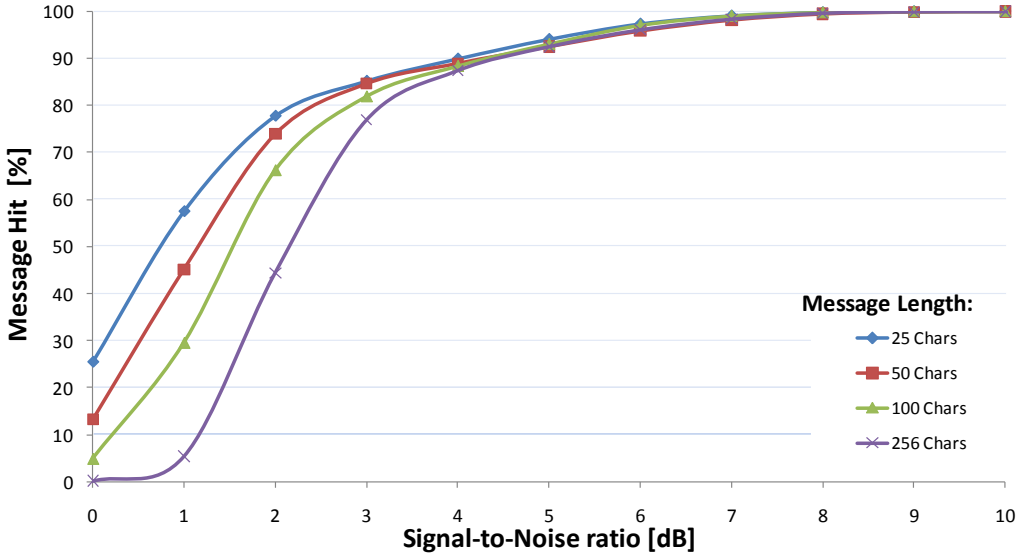

Fig. 6.2: Received Message for Different SNR values

lengths is shown in Fig. 6.2. This figure illustrates the percentage of received messages (message hit) for different SNR values. It is observed that as the length of message increases, the received message rate decreases. Similarly, increase in message length causes synchronization loss. Fig. 6.3 shows the synchronization loss for different character lengths. It is observed that when higher number of characters is sent the losses in synchronization are higher. These tests are performed for wired connected scenario where SNR values are set in AWGN block of FPGA.

6.2.2 Laboratory/Office Setting

Robustness and reliability of the system was further validated using other setting as shown in Fig. 6.4. The real illustration and snap shot image is presented in Fig. III of appendix-I. In this setting, we examined two different scenarios: (i) ideal setting (wired connected-simulation) where the influence of the communication channel was not considered, and (ii) real setting, where the channel effect was taken into consideration. The system was made to run for 6 days continuously.

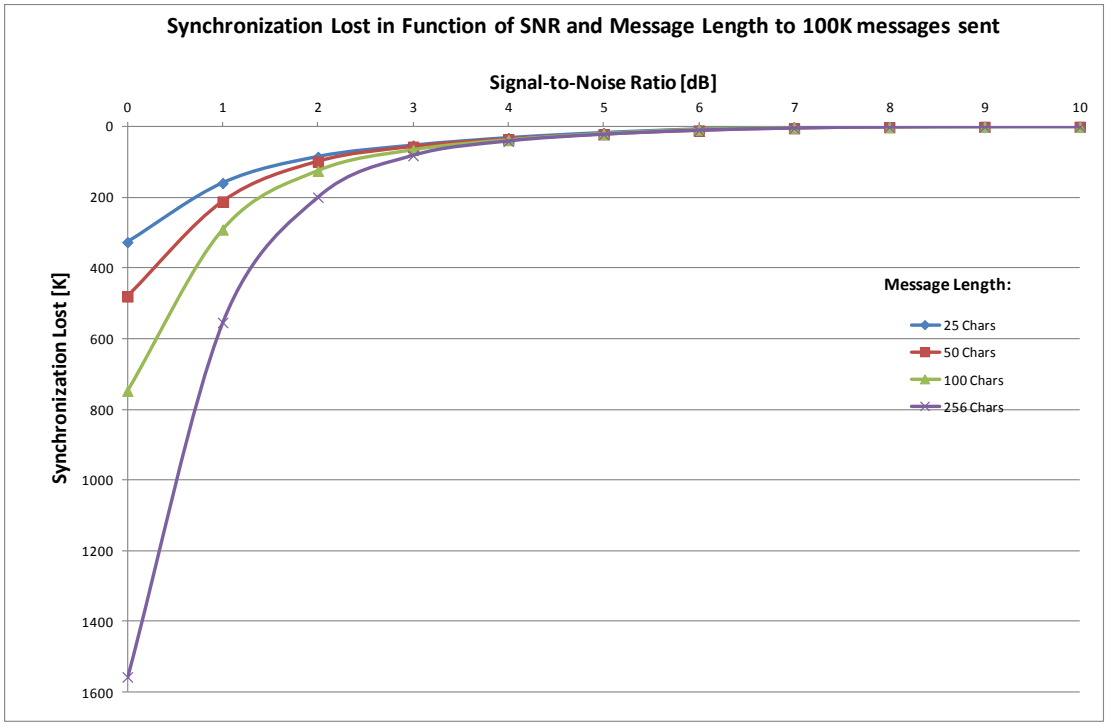

Fig. 6.3: Synchronization Losses for Different Message Lengths

For the real set-up, the distance between emitter and receiver was set to 2.5m. We considered both a dark environment, where room lights were OFF and in the presence of room

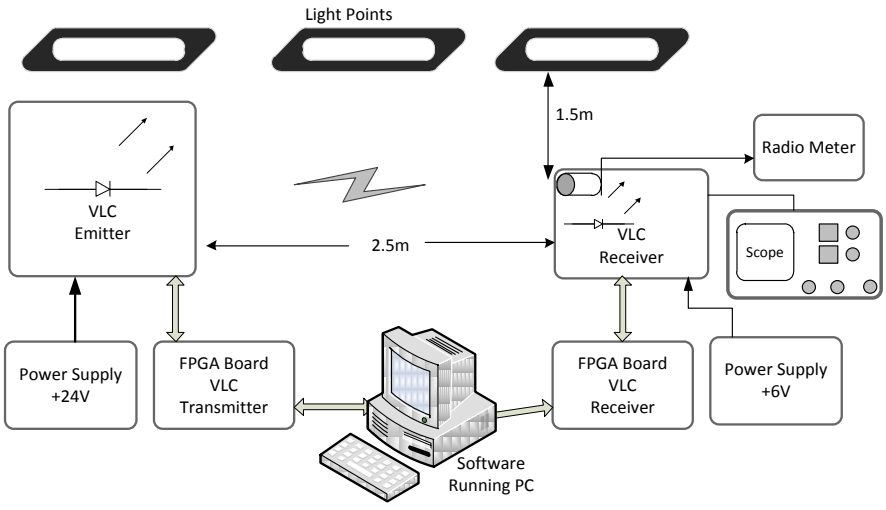

Fig. 6.4: Experiment Set-up for Measurement of PER in Laboratory setting with the Effect of Office lights

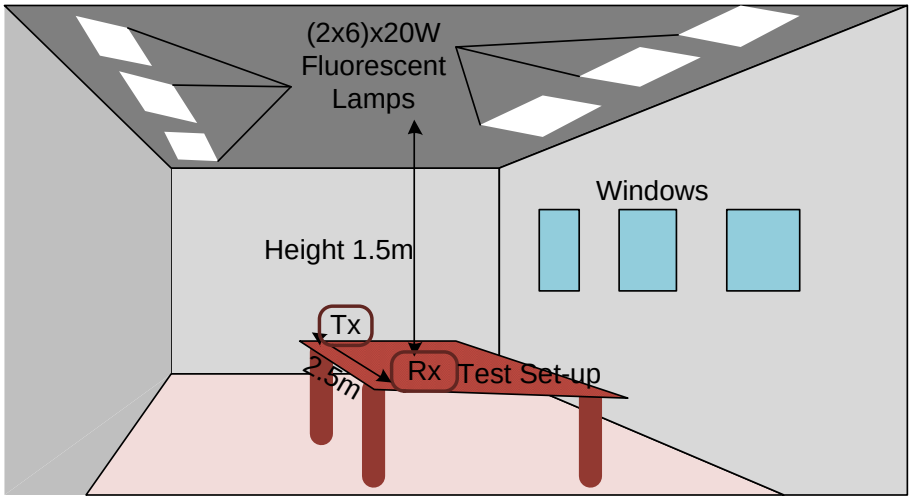

Fig. 6.5: Experiment Room showing Light points

lights (lights ON), a normal laboratory operation. 12x20W fluorescent light bulbs were located at a height of 1.5m from the receiver. The room light arrangement for this experiment is displayed in Fig. 6.5, while a snap shot is shown in Fig. IV of appendix-I. More than 250 Lux of flux were measured at all corners of the room while over 450 Lux were measured in the line between transmitter and receiver. Measurement values of average received power and background noise are shown in the Table 6-1.

In the laboratory set-up, two configurations were made in the receiver to study the effect of channel noise. In the first configuration, real channel condition is set by disabling the noise

Table 6-1 - Average Received and Background Noise Power

Parameters		Value	Parameters		Value
Room Lights OFF	Daytime (09.00Hrs - 17.30Hrs)	Average power (W/cm^2) $0.2867x10^{-5}$	**Room Lights ON**	Day Time	Average power (W/cm^2)$2.365x10^{-6}$
		Background Noise (W/cm^2) $6.835x10^{-8}$			Background Noise (W/cm^2) $6.630x10^{-7}$
	Night time (18.45Hrs	Average power (W/cm^2) $6.835x10^{-6}$		Night Time	Average power (W/cm^2) $2.61x10^{-5}$
Flux Room Lights ON		>430 Lux. (all along the Txr and Rxr)			
		>250 Lux. (rest of the room location)			

generating block (AWGN block) inside the FPGA. In this case, we were able to receive all the *messages* correctly. System was then configured to enable noise generation inside the FPGA so that, additional noise can be added to the real channel noise.

This experiment was performed to enable the comparison with the results obtained with the direct connection configuration. The results for different SNRs are presented in Fig. 6.6. There is a drop in the successfully detected messages (*message hit*) as compared to the wired connected result, which is expected. The *message hit* is the ratio between the number of successfully collected *messages* and the number of sent *messages*. However, because of the small distance between emitter and receiver the difference between presence and absence of light in *message hit* is very small. That is, the system performance in the presence of office light is satisfactory.

We also measured the *packet error rate* (*PER*) given as the ratio of *lost packet* and the number of total received *packets*. A *packet* consists of a 10 bits PN sequence, *lost packets* are incorrectly received *packets*. If a single bit in 10 bits is wrong, a *packet* is said to be in error. The PER for different SNR values is illustrated in Fig. 6.7. A similar performance is recorded in the three different cases. Here too, it is seen that the performance of VLC system with lights ON/OFF in the indoor environment not only remains similar but also robust against interfering

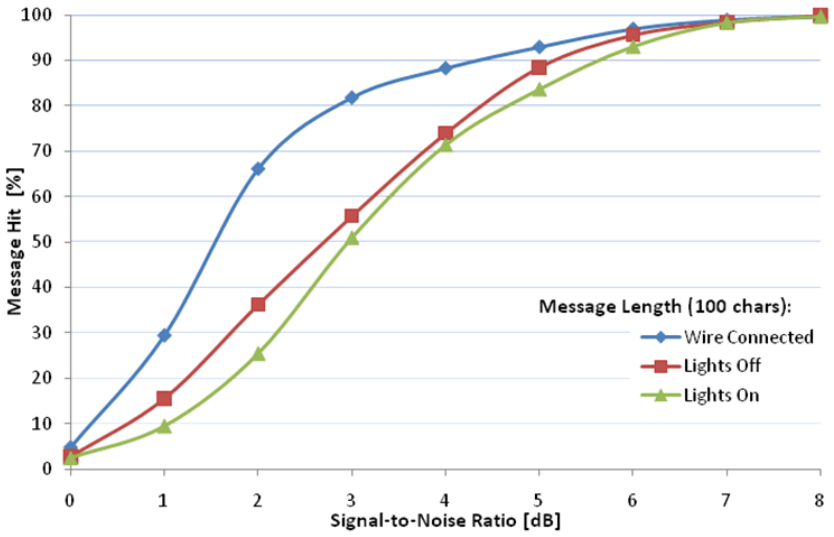

Fig. 6.6: Percentage of Message hit for Different Environments over SNR

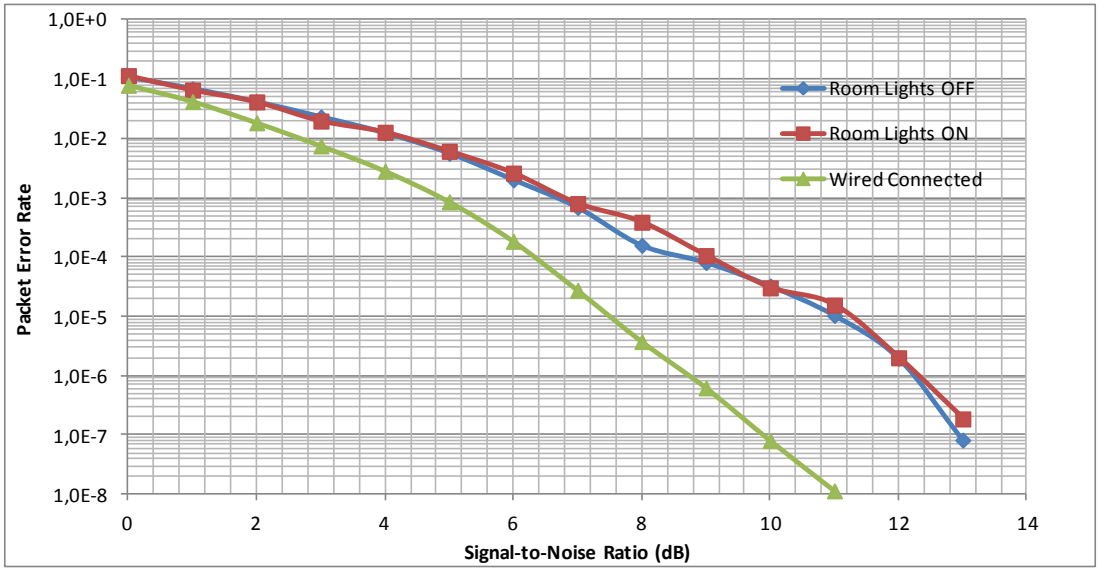

Fig. 6.7: Packet Error Rate for Different Environments over SNR

lights. The effect of channel noise is observed on the difference between the two tests, wired connected and laboratory set-up.

The results from laboratory and indoor experiments were encouraging, however, the situation may not be as favorable in outdoor. As we have discussed before, there are many factors due to which performance of the VLC systems may deteriorate in outdoor. The following section discusses the set-up and results from outdoor experiments.

6.3 Outdoor Environment Experimental Set-up

A series of experiments were performed in outdoor scenarios. Three of the main scenarios are presented and discussed here. All the tests were performed according to the transceiver parameters specified in Table 6-2. The emitter was configured to send 26000 messages containing 25 bytes of random data. On the other hand, the receiver was prepared to store statistics on the number of messages received and the number of packets with and without errors. After collecting a total of 5 million packets, the number of wrong packets received was measured.

The three scenarios were:

(i) Controlled Environment,

(ii) Night time on Road with Street/Road Lights, and

(iii) Day time under Bright Sun Light.

6.3.1 Controlled Environment

An experiment was performed in a closed pavilion of 60 x 40m. This experiment was carried out at night without any environment light. The emitter and receiver were set at a height of 2.5m and 0.85m above ground respectively. An IR filter with wavelength of 750-1200nm was

Table 6-2: Experimental Parameters for Transceiver

Emitter		Receiver	Message	
Data Rate	No. of Sent messages	Sampling Frequency	Type	Length
200 kpbs	26000	1 MHz	Random	25 bytes

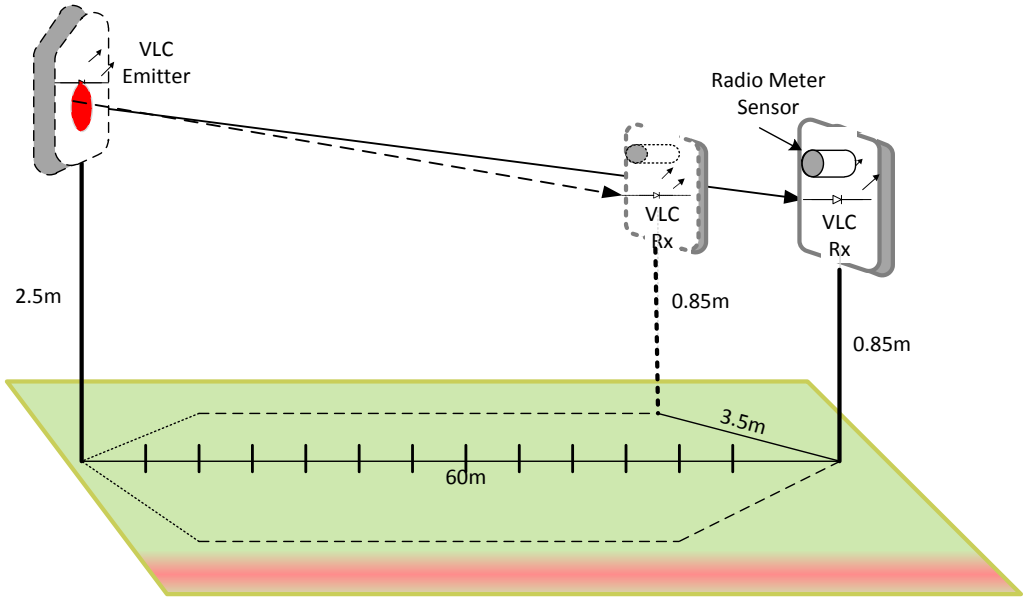

Fig. 6.8: Experiment Scenario in Pavilion of 60x40m, Controlled Environment

used after the photo detector. The experiment scenario (as shown in Fig. 6.8) was set-up so that the effect of light reflection is minimized. Images of the pavilion during measurements are also shown in appendix-I Fig. V. Message received and packet error rate were recorded on axial distance as well as at an offset of 3.5m (considering the width of a road lane) from axis. This was performed in order to verify if data reception was possible in both lanes. Results are summarized towards the end in section 6.3.4.

6.3.2 Night time on Road with Street Light

This is other situation in which the performance of the VLC system was evaluated. In this case, the experiment procedure was carried out during night time, under street lights. The set-up scenario is shown in Fig. 6.9 a snap shot image is presented in Fig. VI of appendix-I. The receiver and the emitter were aligned at a height of 1.10m from ground. Height of lamp posts and distance between them was 4m and 30m respectively. (Note-This set-up exists in our university campus and not the main road/highway)

The drop in the received packet was recorded when measurements were taken just under the lamp posts. Results are summarized in section 6.3.4.

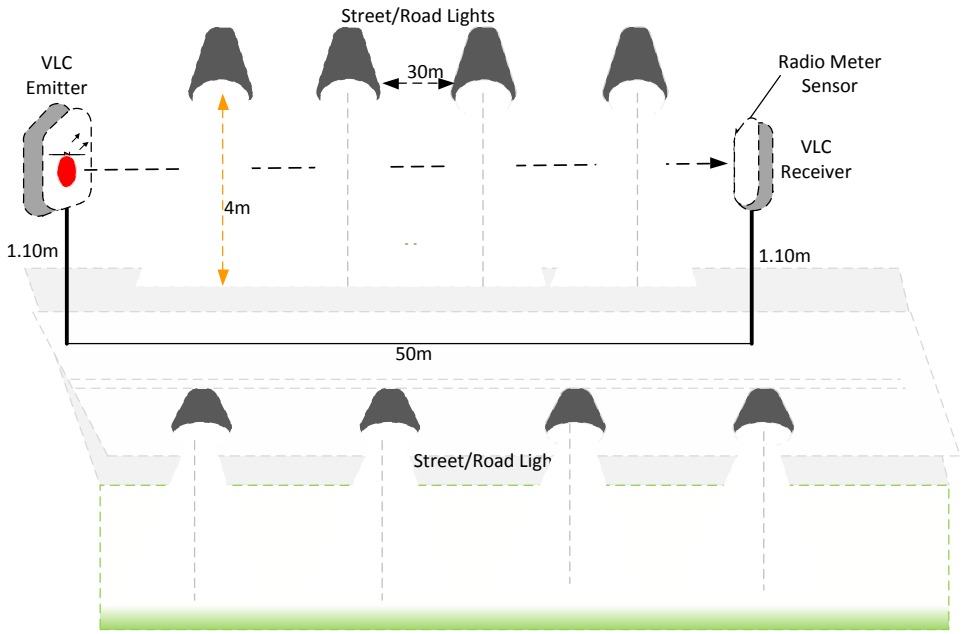

Fig. 6.9: Experiment Scenario under Road lights

6.3.3 Day time under Bright Sun Light

Although dark environments exist in real scenario, the biggest challenge for VLC systems remain during day time under bright sky. It is considered that sky and ambient background result in large DC currents and should be blocked when receiver uses DC blocking capacitor at the input. However, challenges remain, since bright sky light will obfuscate the emitted intensity from the emitter as distance between emitter and receiver increases. Therefore, VLC systems performance under bright sky sun light is expected to be drastically deteriorated. However, this is one of the most challenging scenarios in real applications, where VLC performance needs to be evaluated.

Towards this end, we carried out experiments at noon during bright sun light. The system set-up is shown in Fig. 6.10 while snap shot is given in Fig. VII in appendix-I. In this case, the receiver and the emitter were aligned at a height of 1.10m and measurements were taken on axial distances. A small (1 inch) artificial cap made of paper was put around the photo detector to protect from direct sun light falling on the photo detector and thus avoiding saturating receiver. The IR filter with photo detector was also retained. The arrangement is shown in Fig. 6.11. With this setting, receiver was able to receive over 70% of messages up to a distance of 40m, and around 50% of messages we sent up to a distance of 50m. Results are summarized in the following section.

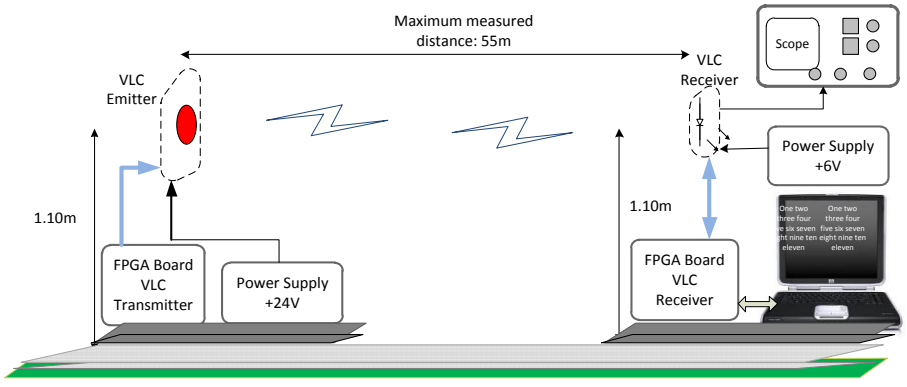

Fig. 6.10: Experiment Set-up under Bright Sun Light

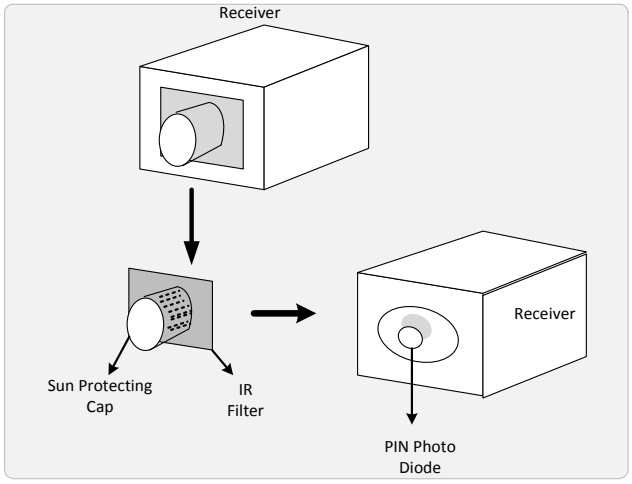

Fig. 6.11: Arrangement for Photo Detector with Sun Protecting Cap and IR Filter

6.3.4 Results Summary from Outdoor Experiments

This section summarizes the results for the previously presented scenarios. Based on these settings, we measured the *message hit* percentage (received messages) over distance, the *packet error rate* for different distances, the *synchronization losses* and *packet losses*. Average received power over distance is also measured and presented.

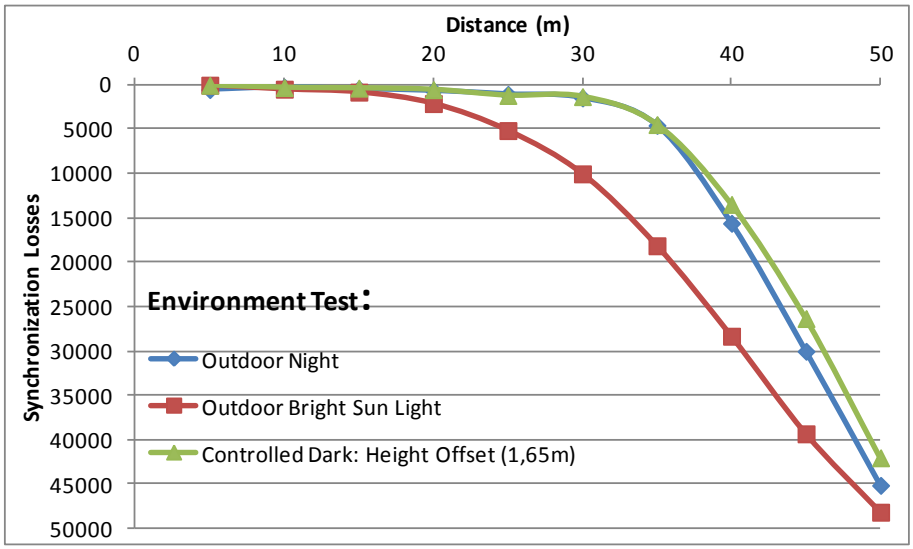

Fig. 6.12: Synchronization Losses in Different Conditions

Fig. 6.12 shows the loss in synchronization, i.e. when DSSS receiver is not able to synchronize with the emitter. The synchronization loss occurs if more than one bit in a *packet* is in error. As can be seen, this parameter is dependent on distance and of course interference. In addition, it was also observed that larger length of *message* results in more synchronization losses. Confirming the results on section 6.2.1 Fig. 6.12 shows that the receiver remains synchronized for distance up to 35m. However as distance increases, loss in synchronization also increases. Synchronization loss causes drop in the received message and thereby *packet loss* resulting in large packet errors. A *packet* is said to be lost if more than one bit is in error. Fig. 6.12 also shows that outdoor scenarios with direct sun light exposure are more prone to synchronization losses. This is due to degradation of the SNR in these situations.

Therefore, increase in packet loss leads to more synchronization time for the receiver to get synchronized. Loss in received message is also caused because of the increase in distance between the emitter and the receiver. This is illustrated in Fig. 6.13. The figure shows loss in received message for all 3 scenarios presented above. It is observed that performance of the system in these cases remains stable and nearly equal. For a distance of around 40m the system receives over 65% of sent messages. However, when tests are undertaken right below

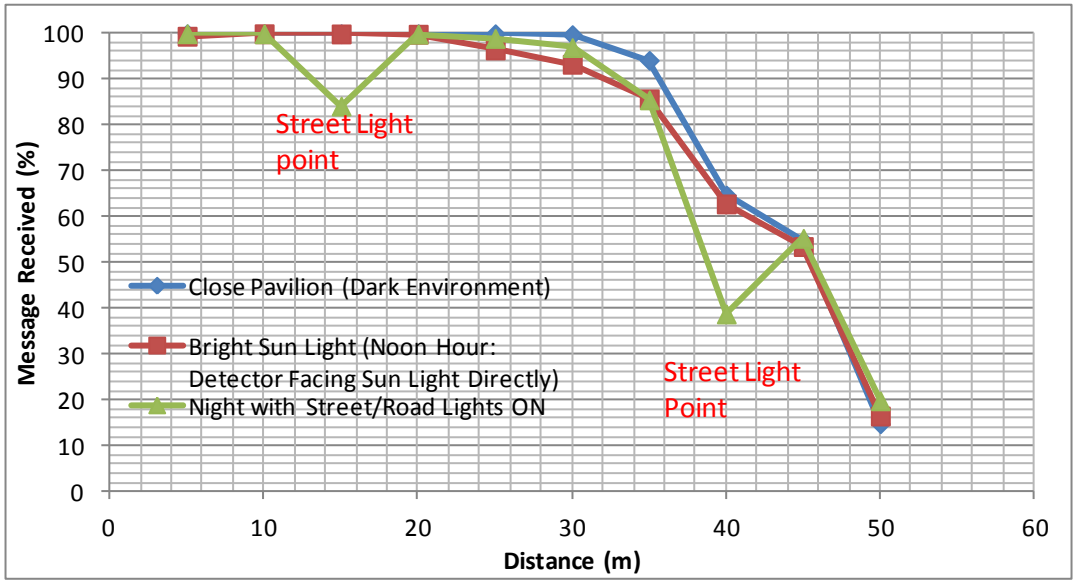

Fig. 6.13: Received Message for Different Distances

the lamp posts percentage of the received messages is reduced. For smaller distances, the drop in received messages is small however, at larger distance the drop also increases.

Synchronization loss increases both *packet loss* (more than 1 bit is in error in a packet) and *packet error rate.* Fig. 6.14 shows the percentage of *packet loss* over distance. It is observed that the performance of VLC system remains better in night than during day time.

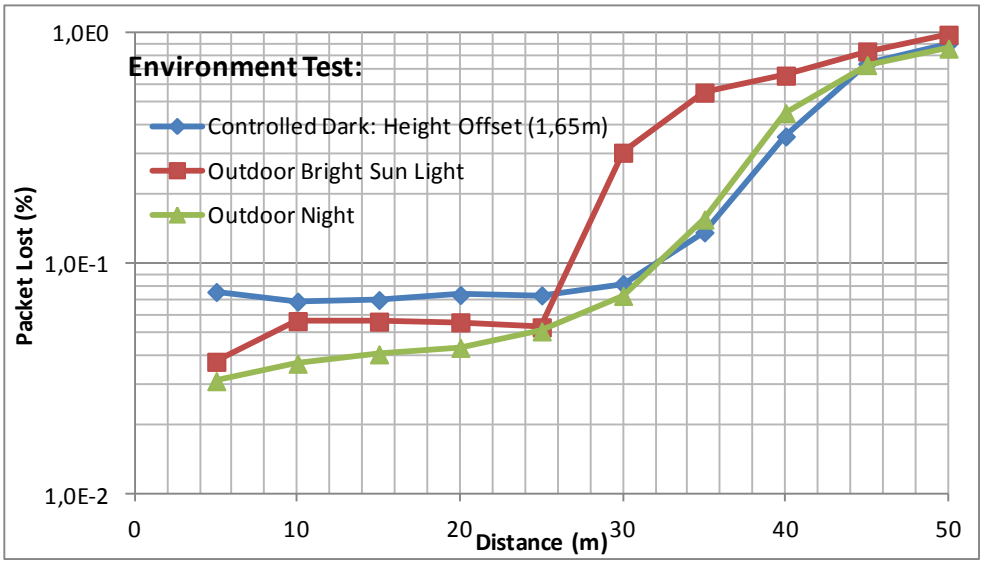

Fig. 6.14: Packet Loss in Different Environment

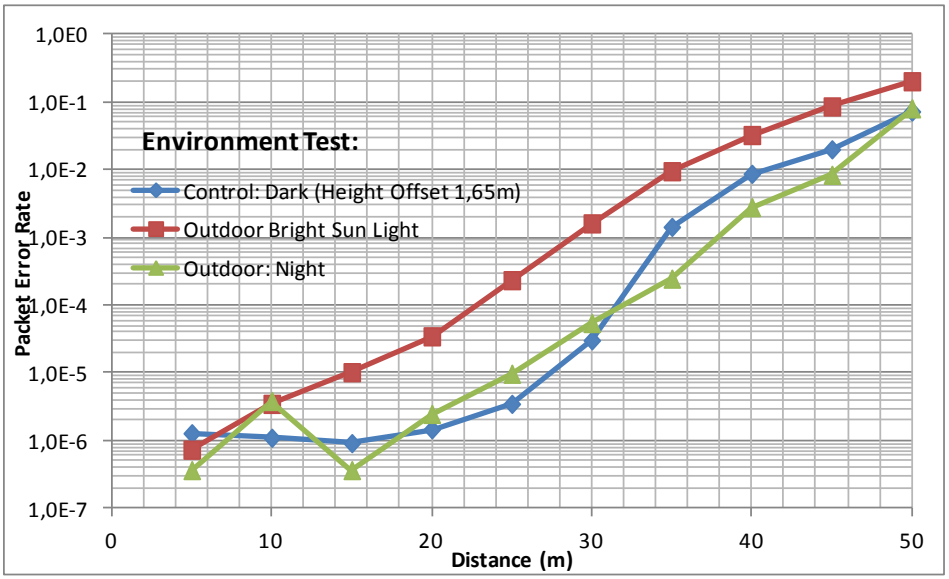

Fig. 6.15: Packet Error Rate over Distance

However, up to 30m of distance system performs well, packet loss remains below 0.1%. As distance increases system starts losing packets, this is most evident during daytime, where the packet loss increases faster.

Fig. 6.15 and Fig. 6.16 present packet error rate for different scenarios over distance. It is observed that during day time under sun light the performance degradation is almost uniform, while during night times, packet error rate variations are found, due to the local nature of the artificial lights. It can also be seen from Fig. 6.16 that tests undertaken directly underneath the lamp posts resulted in higher packet error rates. This is due to the direct influence of local noise spots.

In Fig. 6.17, packet error rate performance is presented on emitter axis and also at 3.5m offset. This measurement enables to examine the coverage area of the VLC emitter for multilane road, considering the width of road to be 3.5m. Although packet error rate is high in the second lane, this result provides important inputs for further improvements in light design issues as the half power angle (hpa) for the LEDs to be used, or, the use of traffic lights at smaller height on traffic posts to serve nearer distances. It is seen for the second lane that from around 15m of distance from the emitter, nearly one packet is found to be in error from every

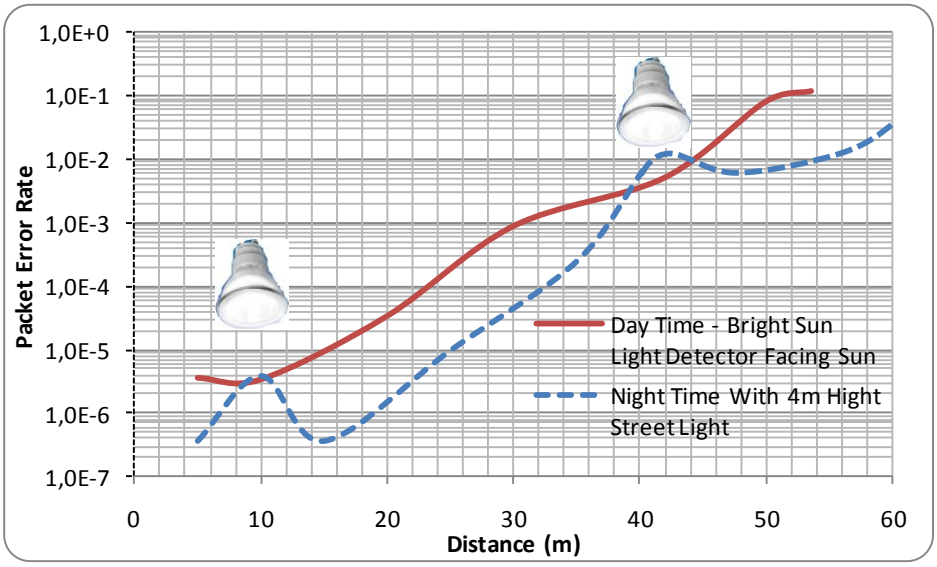

Fig. 6.16: Effect of Lamp posts on Packet Error Rate.

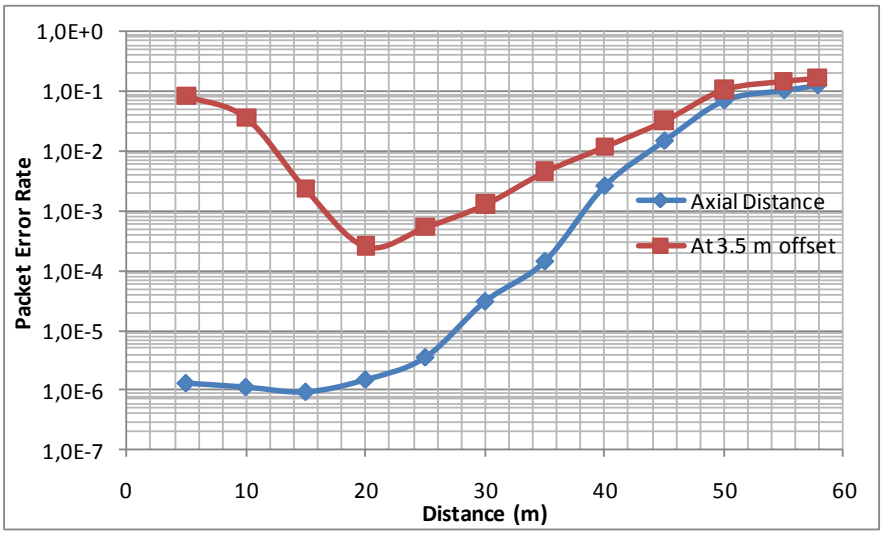

Fig. 6.17: PER Performance on axis and offset of 3.5m

1000 sent packets, that is, PER is 10^{-3}. For shorter distances error rate is even higher.

The performance of the system is highly dependent on received power. The received power is inversely proportional to the square of the distance. Hence, as receiver moves away further, the drop in received power. Fig. 6.18 shows the average received power over the measuring distance for both on-axis and off-axis of 3.5m. It is observed that when received

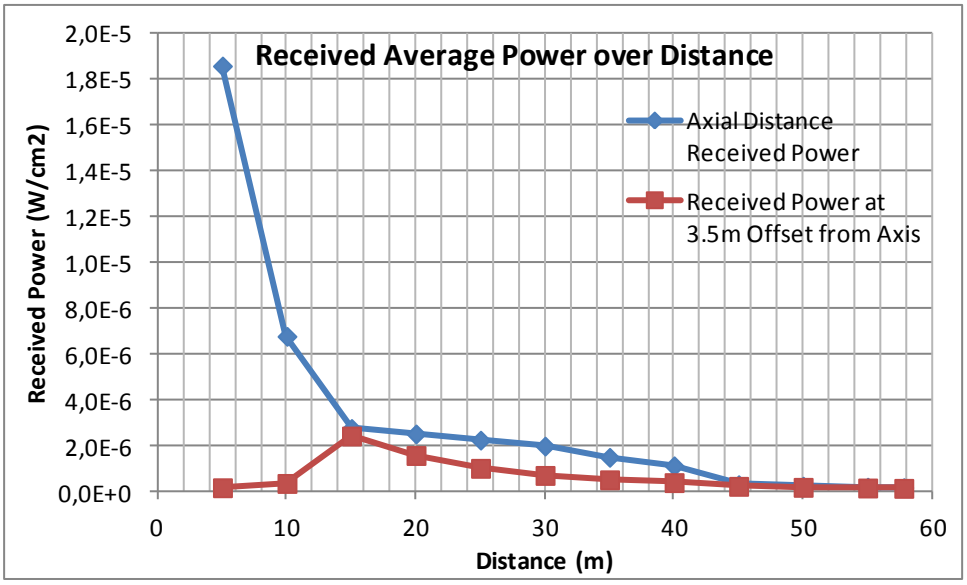

Fig. 6.18: Average Received Power (w/cm^2)

power remains above 2μW/cm^2, almost all messages are received; however, when the average received power drops below 1μW/cm^2, the receiver starts losing packets. The same results were obtained using emitter illumination measurements. Of course, the receiver noise levels play a role here.

The implementation and experiments offer many inputs and guidelines that must be considered in the design of robust VLC systems. There are considerable areas for improvements. The next chapter presents the concluding remarks and guidelines for future works in this area.

6.4 Concluding Remarks

This chapter presented the experimental validation of the VLC prototype system. Several experiments were performed in different environments and atmospheric conditions. Measurements of performance parameters such as missed messages, loss of packets and packet error rate were examined and presented. The achieved results show that VLC systems can be used for the specific application. The achieved results are encouraging however, they also highlighted the possibilities to improve system's performance.

CHAPTER 7: CONCLUSIONS

Summary

This chapter summarizes the most relevant conclusions of this work. Important findings from the prototype design and experimental results are highlighted. VLC technology involves many challenges and some of them are illustrated. Finally, some guidelines for future works that can be followed are also summarized.

7.1 Summary of the works and Contributions

VLC systems leveraging benefits from LED advancements have been recognized an important technology. This can offer ubiquitous communication for the reason that light can be made available at all places. In intelligent transportation systems, VLC has a novel and important application on human and material safety. In this thesis, VLC technology in ITS has been investigated in detail. A low cost VLC prototype was developed and designed under a number of limiting factors that will be explained in discussion below. Several experiments were performed in different environments to validate the design and implementation. A number of associated original contributions are also summarized here.

A first important contribution can be described as the proposed OSI based VLC layer architecture in ITS, and its integration with current ITS trends. Usage of VLC technology will allow the removal of many IR and short range communication systems, thereby minimizing the cost without loss of functionality. Since the development of ITS architectures is ongoing, it is highly desirable to consider roles that can be played by VLC technology in these frameworks.

Development and design of an emitter model has been another important contribution. An emitter model was developed based on a co-centric array of LEDs, with optimized placement to offer high illumination in a service area of interest. Algorithms were developed, able to optimize a number of important parameters involved in the emitter design, as well as, road traffic system set-up. The algorithm provides many important design parameter information from a number of available options. A comparative study was conducted through experiment with a designed traffic emitter and one of the commercially available traffic light models. It was observed that the performance of the designed model is better than the commercially available. Though, commercially available designs have differences and variations from one developer to other. It is assumed that the commercial design was developed to comply with standard traffic signal specifications. However, its add on utilization as traffic information broadcast system will offer improvement in traffic lights design. This study will certainly provide significant inputs for designers in future, as this design ensures

optimum illumination in the desired service area thereby offering added potential usage as communication device, maintaining the standard traffic specifications. In the designed traffic light, a larger number of HB-LEDs can be integrated to cover more service area. With experimental and measurement results it is assessed that the present design can use full capacity of around 370 LEDs (in place of 240 used now) and even with high intensity (> 12000 mcd, which are available), and also wide half power angle (> 15º).

Development, implementation and use of DSSS SIK based modulation technique can be considered to be another major contribution in this work. This is the first time that DSSS based VLC systems have been developed and results are encouraging. A number of implementation methods were validated before making use of a FPGA implementation for the final prototype. Results from simulation and experiments are almost similar, which support the work performed. An important finding from the experiment motivates the implementation of DSSS based modulation for indoor applications in multiuser scenarios, for which the technique is popular in RF technology.

Another important contribution which can be discussed is channel characterization. VLC channel is highly dependent on atmospheric conditions and environment. Some of the important situations and environments were considered and characterized. Experimental validation could not be done for all these situations because of the dependency on atmospheric conditions and also because of proper logistics in those situations.

Furthermore, there have been many minor contributions, such as hardware implementation and prototype design. Optoelectronic parts of receiver and emitter were designed using discrete components evaluating the final performance. Similarly, a number of algorithms were implemented in FPGA based VLC architecture. Some of the important observations that can be registered here are the improvement of receiver architecture in respect of high dynamic range and automatic gain control mechanism. It is also observed that a receiver concentrator can offer a large gain especially in the presence of sun light. For small data range, such as in the range of few tens of kbps, use of multiple photo detectors and combiner can potentially enhance the performance. Similarly, increasing the speed of the ADC

in FPGA development board will allow higher data rates which has been a limitation in our design.

However, with the available results important conclusions can be derived. To say, consider the designed traffic light is in place at traffic post and a vehicle with the VLC receiver approaching this point at a speed of 60kmph. If we consider a service area of around 30-35m from traffic post for which our prototype guarantees successful delivery of message, the vehicle will have approximately two seconds to cross this distance. In the meantime, traffic light VLC emitter sending traffic safety information at a rate of 200kbps will transmit 400kbits of information. If a message comprising of 10kbits of data is broadcasted, the emitter will repeat around 40 times of information data during the passage of the vehicle in this service area which can be read, or viewed by the driver driving the vehicle. Therefore, the designed VLC system can be effectively deployed and used in ITS to assist driver for safe driving on the road. Furthermore, with enhanced design as discussed before, the service area can be increased. Therefore, VLC systems are not only suitable for the novel applications of road traffic safety but also identify itself to be an integral part of ITS. However, there are important challenges ahead.

7.2 Main Challenges and Future Works

Though VLC systems have multiple benefits, there are some challenges. We discuss here two main broad challenges. They are:

(i) Deployment of VLC, and
(ii) Technological challenges.

7.2.1 VLC Deployment

This is one of the major challenges we anticipate. It involves city municipal administration, regulatory bodies, traffic lights and vehicle manufacturers, and of course users. Though, there are standard guidelines to be followed on the installation of traffic lights, they are sometimes overlooked. In order to deploy VLC systems for their effective operation the standard

guidelines must be followed and it will also be necessary to make some adjustment in the installation of LED-based traffic lights. For example, 200mm diameter traffic lights can be placed at a recommended height of around 2.5m to 3m on road side traffic post while 300mm diameter traffic lights need to be placed above the road at a height of approximately 5m. Similarly, for traffic light manufacturers, they are supposed to follow the recommended design which seems to be a very difficult problem until a standard is in place. In addition to this, vehicle manufacturers should start promoting this technology by integrating low cost VLC receivers in the vehicles. Therefore, co-ordination among regulatory bodies and frameworks becomes promising.

Although, above perspectives look really challenging, they are not too complex, because, LED-based traffic lights are already replacing existing ones. VLC receiver is also cost effective and do not need much modifications on vehicles to install. Therefore, VLC systems can be deployed effectively for the quality of the intended applications.

7.2.2 Technological challenges

This is another important area to be addressed by scientific and research community for effective and wide spread deployments of VLC systems in ITS. In particular, there are few technical issues to be addressed. We briefly summarized them as:

- ***Long Range Limitation***: Because of LoS path requirement, the technology is considered to be suitable for short and medium range communication. Long range communication is possible using multihop technique in vehicular environments however; minimizing the effect of ambient and other noise sources to achieve this still remains an issue.
- ***Uplink Design***: Using illumination sources is naturally suited to broadcast applications. But designing a VLC system for bidirectional transmission and reception would be really difficult. However, this design will offer many value added applications and services, most importantly Internet access while on move. Such integrated services may enhance the deployment.

- ***Increasing Data Rate***: In order to enable Internet access or dedicated services which demand high data rate, different modulation techniques must be adopted. Equalization techniques show improvement in data rate especially in the indoor applications. Could this technique be valid in outdoor, when system implementation requires low cost and simplicity? Furthermore, limited bandwidth of the LEDs is another major challenge for high-speed communication. Therefore, the study must address on these issues for enhanced performance and advanced deployments.

7.2.3 Future Works

This work encountered many challenges. Some of them are tackled and solved, some of them partially addressed and some of them are left for further investigation. The most important among them to be addressed in the future are:

- Designing an automatic gain control high sensitive receiver: This is very challenging. Our design can offer very high sensitivity and gain but the system is not instantly-stable. If automatic gain control mechanisms are introduced, the receiver will not saturate. Therefore, more complex optoelectronic receiver architectures can be investigated and designed for the use in VLC systems.
- Exploring DSSS further: It is observed that DSSS based VLC system works. However, because of limitations such as, ADC speed a PN sequence of length 10 has been used. Performance is expected to be improved by using longer sequences.
- Designing Adaptive Modulation Scheme: There are many modulation techniques which can be used in the system in different conditions. For example, in the I-LPPM, the use of equalizer and even DSSS are likely to perform better over L-PPM or OOK. Therefore, a particular modulation technique could be used depending on applications and environments. Furthermore, Optical MIMO is another interesting and challenging area which can be explored for data rate improvement.
- Full Duplex VLC Systems in Vehicular Environment: It is interesting to investigate and design full duplex mode of VLC systems to take full advantage of intelligent transportation and road safety applications. It will be challenging to implement a VLC

system where the vehicle in front receives a message and relay it using vehicle's brake lights to the vehicle running behind. Similarly, ad-hoc modes in vehicular environment would be interesting.

In fact, VLC is a new emerging technology and has huge applications in the outdoor as well as indoor. The area needs to be explored to take full advantage of its unprecedented bandwidth and ubiquitous availability. It should take full advantage of advancement of LED technology. From above challenges, many interesting topics can be researched.

REFERENCES

This section presents the list of the most relevant references related to this work. In order to allow an efficient way to consult the references, these lists were organized into different categories firstly according to the contents of the chapters, and secondly, order of appearance in the chapter. The categories are arranged in alphabetical order.

Basic and Optical Communications Books

[1] S. Chandrasekhar, "Radiative Transfer", Clarendon, 1950.

[2] A. Ishimaru, "Wave Propagation and Scattering in Random Media", IEEE Press Series in Electromagnetic Theory, 1997.

[3] R M Gagliardi and S Karp, "Optical Communications", John Wiley & Sons, NY 1976,

[4] S B Alexander, "Optical Communication Receiver Design", SPIE Optical Engineering Press, 1997.

[5] R. E Ziemer and W. H. Tranter, "Principles of Communications Systems, Modulation, and Noise", 4th Ed. NY, John Wiley & Sons, 1995

[6] Rosen. Joe and Gothard. Lisa Quinn, "Encyclopedia of Physical Science," Infobase Publishing, 2009.

[7] Marvin K. Simon, Jim K. Omura, and Robert A. Scholtz, "Spread Spectrum Communications Handbook," 1st Ed. 2001

[8] J Proakis, "Digital Communication," 4th Ed. Mc. Graw Hill, 2003

[9] S. Karp, R. M. Gagliardi, S. E. Moran, and L. B. Stotts, "Optical Channels: Fibers, Clouds, Water, and the Atmosphere (Applications of Communications Theory) Plenum, 1988.

[10] I. Bar-David and R. Krishnamoorthy, "Barker code position modulation for high rate communication in the ISM bands," in *Spread Spectrum Techniques and Applications Proceedings, IEEE 4th International Symposium on*, 1996, vol.3, pp. 1198-1202.

Government and Scientific Organization Reports

[11] World Health Organization, “Ten Causes of Death”, WHO, 2008.

[12] IEEE 802.11p,”Wireless Access in Vehicular Environment (WAVE)”, IEEE, 2010.

[13] International Agency for Research on Cancer, World Health Organization, “IARC Classifies Radio Frequency Electromagnetic Fields as Possible Carcinogenic to Humans”, Press Release No. 208, 31 May 2011.

[14] Joint Industry and Traffic Engineering Council Committee, "Vehicle Traffic Control Signal Heads- Light Emitting Diode (LED) Circular Signal Supplement," JITECC, 2005.

[15] The Colour Science Association of Japan,” Handbook of Colour Science, 2nd Ed. University of Tokyo Press, 1998.

Infrared Communication

[16] K. K. Wong, T. O'Farrell, and M. Kiatweerasakul, "Infrared wireless communication using spread spectrum techniques," *Optoelectronics, IEE Proceedings*, vol. 147, pp. 308-314, 2000.

[17] Hyuncheol Park and Barry, J.R, "Modulation analysis for wireless infrared communications," *1995. ICC '95 Seattle, 'Gateway to Globalization', IEEE International Conference on Communications*, vol. 2, pp. 1182 - 1186, 1995.

[18] R. L. Aguiar, A. Tavares, J. L. Cura, E. De Vaaconcelos, L. N. Alves, R. Valadas, and D. M. Santos, "Considerations on the design of transceivers for wireless optical LANs," in *Optical Wireless Communications (Ref. No. 1999/128), IEE Colloquium*, pp. 2/1-231, 1999.

[19] J. R. Barry, J. M. Kahn, E. A. Lee, and D. G. Messerschmitt, "High-speed nondirective optical communication for wireless networks," *Network, IEEE*, vol. 5, pp. 44-54, 1991.

[20] J. M. Kahn, and. J. R. Barry, "Wireless infrared communications," *Proceedings of the IEEE*, pp. 265-298, 1997.

[21] M. Gebhart, E. Leitgeb, and J. Bregenzer, "Atmospheric effects on optical wireless links," in *Telecommunications, ConTEL'2003. Proceedings of the 7th International Conference*, vol.2, pp. 395-401, 2003

[22] D. Kedar and S. Arnon, "Optical wireless communication through fog in the presence of pointing errors," *Applied Optics*, vol. 42, pp. 4946–4954, 2003.

[23] K.W. Fischer, M.R. Witiw, and E. Eisenberg, "Optical attenuation in fog at a wavelength of 1.55 micrometers," *Elsevier, Atmospheric Research*, vol. 87, pp. 252–258, 2008.

[24] R. M. Pierce, J. Ramaprasad, and E. C. Eisenberg, "Optical attenuation in fog and clouds," *Proc. SPIE 4530*, pp. 58–71, 2001.

[25] S. J. Urachada K., Yasuo K., Akira I., and James A. R., "Channel modeling for optical wireless communication through dense fog," *Journal of Optical Networking*, vol. 4, pp. 291-299, 2005.

[26] Adriano J. C. Moreira, Rui T. Valadas, A.M de Oliveria Duarte., "Optical interference produced by artificial light," *Wireless Networks*, vol. 3, pp. 131-140, May 2, 1997.

[27] J. M. Kahn, W. J. Krause, and J. B. Carruthers, "Experimental characterization of non-directed indoor infrared channels," *IEEE Transactions on Communications*, vol. 43, pp. 1613-1623, 1995.

[28] Adriano J. C. Moreira, António M. R. Tavares, Rui T. Valadas, A. M. de Oliveira Duarte, "Modulation methods for wireless infrared transmission systems - Performance under ambient light noise and interference," in *Wireless Data Transmission Conference - SPIE's Photonics East Symposium* Philadephia, USA, vol. 2601, pp. 226-237, 1995.

[29] M. D. Audeh and J. M. Kahn, "Performance evaluation of baseband OOK for wireless indoor infrared LAN's operating at 100 Mb/s," *IEEE Transactions on Communications*, vol. 43, pp. 2085-2094, 1995.

[30] Kwang-Cheng Chen, Tai-Yuen Cheng, "Signaling Methods of IR PHY," Submitted to IEEE 802.11 Standardization Project, Sep. 1993.

[31] F. R. Gfeller, P. Bernasconi, W. Hirt, C. Elisii, and B. Weiss, "Dynamic Cell Planning for Wireless Infrared In-House Data Transmission," SpringerLink, Mobile Communications Advanced Systems and Components, Lecture Notes in Computer Science, vol. 783, pp.261-271, 1994.

[32] T. O'Farrell and M. Kiatweerasakul, "Performance of a spread spectrum infrared transmission system under ambient light interference," in *Personal, Indoor and Mobile Radio Communications, The Ninth IEEE International Symposium*, pp. 703-707 vol.2, 1998.

[33] A. J. C. Moreira, R. T. Valadas, and A. M. de Oliveira Duarte, "Characterization and modeling of artificial light interference in optical wireless communication systems," in *Personal, Indoor and Mobile Radio Communications, 'Wireless: Merging onto the Information Superhighway', Sixth IEEE International Symposium*, pp. 326-331, 1995.

Intelligent Transportation and Vehicular Communication Systems

[34] S. Eichler, "Performance Evaluation of the IEEE 802.11p WAVE Communication Standard," in *Vehicular Technology Conference, VTC-2007 Fall, IEEE 66th*, pp. 2199-2203. 2007.

[35] S. Yousefi, E. Altman, R. El-Azouzi, and M. Fathy, "Analytical Model for Connectivity in Vehicular Ad Hoc Networks," *IEEE Transactions on Vehicular Technology*, vol. 57, pp. 3341-3356, 2008.

[36] P. Cencioni and R. Di Pietro, "VIPER: A vehicle-to-infrastructure communication privacy enforcement protocol," in *Mobile Adhoc and Sensor Systems, MASS'2007. IEEE International Conference*, pp. 1-6, 2007.

[37] M. Raya and J.P. Hubaux, "Securing Vehicular Ad Hoc Networks," *Journal of Computer Security*, vol. 15, pp. 39-68, 2007.

[38] K. Evensen, "Intelligent Transport Systems, European Standardization for ITS: WG2 Architecture," in *ETSI TC ITS Workshop*, Sophia Antipolis, 5 Feb. 2009.

[39] M. Wada, T. Yendo, T. Fujii, and M. Tanimoto, "Road-to-vehicle communication using LED traffic light," in *Proceedings of the IEEE Intelligent Vehicles Symposium,*, pp. 601-606, 2005.

[40] R. K. Takayuki Tsuzuki, "Inter-Vehicle Communication Protocol using Common Spreading Code," in *Proceedings of the IEEE Intelligent Vehicles Symposium*, pp. 376-381, 2000.

[41] Navin Kumar, Luis Nero Alves, and Rui L. Aguiar, "VLC Layer Architecture for ITS," Submitted to *IEEE ITS Magazine*, Feb 2011.

[42] Navin K**.,** Luis Nero Alves and Rui L. Aguiar, "Traffic Light as Road Side Unit for Road Safety Information Broadcast using Visible Light Communication", for the book *Roadside Networks for Vehicular Communications: Architectures, Applications and Test Fields, Publisher. IGI Global,* Apr. 2011.

Light Emitting Diodes and Traffic Lights

[43] M. S. Shur and R. Zukauskas, "Solid-State Lighting: Toward Superior Illumination," *Proceedings of the IEEE,* vol. 93, pp. 1691-1703, 2005.

[44] S. Kitano, S. Haruyama, and M. Nakagawa, "LED road illumination communications system," in *IEEE 58th Vehicular Technology Conference*, pp. 3346-3350, 2003.

[45] A. Zukauskas, M. S. Shur, and R. Gaska, "Introduction to Solid-State Lighting*"*. Wiley's General Components and Devices, New York: Wiley, Apr. 2002.

[46] M. R. Krames, O. B. Shchekin, R. Mueller-Mach, G. O. Mueller, Z. Ling, G. Harbers, and M. G. Craford, "Status and Future of High-Power Light-Emitting Diodes for Solid-State Lighting," *Journal of Display Technology*, vol. 3, pp. 160-175, 2007.

[47] J. O'Connell, "The Philadelphia story," Traffic Technology International, New York 1997.

[48] Intelligent Transportation Systems, "Stop-Go in Singapore," ITS International, New York, 2000.

[49] F. Kimura, T. Takahashi, Y. Mekada, I. Ide, H. Murase, T. Miyahara, and Y. Tamatsu, "Measurement of Visibility Conditions toward Smart Driver Assistance for Traffic Signals," in *Intelligent Vehicles Symposium IEEE*, pp. 636-641, 2007.

[50] B. L. Cole, and Brown, B., "Optimum intensity of red road-traffic signal lights for normal and protanopic observers," *J. Opt. Soc. Amer,* vol. 56, pp. 516-522, 1966.

[51] Fisher A. J., "A photometric specification for vehicular traffic signal lanterns: Part, 1 luminous intensity necessary for the detection of signals on the line of sight," Institute of Highway and Traffic Research University of New South Wales, 1969.

[52] Wyszecki G and Stiles WS, "Colour Science", *New York: Wiley*, 2nd Ed., 1982.

[53] A. Carl K, "New ITE Standards for Traffic Signal Lights," Intelligent Transportation Systems, 2005.

[54] I. Moreno, C.C. Sun, and R. Ivanov, "Far field condition for light emitting diode arrays," *Applied Optics,* vol. 48, no.6, pp. 1190-1197, 2009.

[55] Ivan Moreno and Ching-Cherng Sun, "Modeling the radiation pattern of LEDs," *Optical Society of America, Optics xpress,* vol. 16, pp. 1808-1819, 2008.

Simulation and Implementation Tools

[56] Xilinx, "Spartan-3E FPGA Starter Kit Board User Guide," Xilinx, 2008.

[57] Xilinx, "Additive White Gaussian Noise (AWGN) Core v1.0 - Product Specification," Xilinx, 2002.

[58] A. Ghazel, E. Boutillon, J. L. Danger, G. Gulak, and H. Laamari, "Design and performance analysis of a high speed AWGN communication channel emulator," in *Communications, Computers and signal Processing, PACRIM' 2001 IEEE Pacific Rim Conference*, vol.2, pp. 374-377 2001.

[59] Xilinx, "Using Digital Clock Managers (DCMs) in Spartan-3 FPGAs." vol. XAPP462 (v1.1) Xilinx, 2006.

Visible Light Communication Concepts

[60] Navin Kumar, Nuno Lourenço, Michal Spiez and Rui L. Aguiar, "Visible Light Communication Systems Conception and VIDAS," IETE Technical Review, vol. 25, no. 6, pp. 359-367, Nov-Dec 2008.

[61] Navin Kumar, Luis Nero Alves, and Rui L. Aguiar, "Visible Light Communication for Advanced Driver Assistant Systems,"7th International Conference on Telecommunication (ConfTele'09), Feb. 2009.

[62] Y. Tanaka, Haruyama, S.and Nakagawa, M, "Wireless optical transmissions with white coloured LED for wireless home links," in *PIMRC, The 11th IEEE International Symposium on Personal, Indoor and Mobile Radio Communications,* , pp. 1325 – 1329, 2000.

[63] M. Akanegawa, Y. Tanaka and M. Nakagawa, "Basic study on traffic information system using LED traffic lights," *IEEE Trans. On Intelligent Transportation System,* vol. 2, pp. 197-203, 2001.

[64] S. Iwasaki, M. Wada, T. Endo, T. Fujii, and M. Tanimoto, "Basic Experiments on Parallel Wireless Optical Communication for ITS," in *Intelligent Vehicles Symposium IEEE*, pp. 321-326, 2007.

[65] T. Hara, S. Iwasaki, T. Yendo, T. Fujii, and M. Tanimoto, "A New Receiving System of Visible Light Communication for ITS," in *Intelligent Vehicles Symposium IEEE*, pp. 474-479, 2007.

[66] N. Kumar, L. Nero. Alves, and R. L. Aguiar, "Design and analysis of the basic parameters for traffic information transmission using VLC," in Proceedings of IEEE *Wireless Communication, Vehicular Technology, Information Theory and Aerospace & Electronic Systems Technology, Wireless VITAE'2009,* pp. 798-802, 2009.

[67] Navin Kumar, Nuno L, Luis Nero Alves, and R. L. Aguiar, "LED-based Traffic Light Emitter Model for Road Safety Applications," Submitted to *Journal of Transportation Research: Part C,* Mar 03, 2011.

[68] Y. Tanaka, T. Komine, S. Haruyama, and M. Nakagawa, "Indoor visible light data transmission system utilizing white LED lights," *IEICE Transactions on Communications*, vol. E86b, pp. 2440-2454, Aug 2003.

[69] Haswani B. W, Toshihiko K., Shinichiro H., and Masao N., "Visible Light Communication with LED Traffic Lights Using 2-Dimensional Image Sensor," *IEICE Trans. Fundamentals*, vol. E89-A, pp. 654-659, 2006.

[70] Hidemitsu S, Shinichiro H and Nakagawa M, "Experimental Investigation of Modulation Method for Visible-Light Communication," *IEICE Trans. Commun.*, vol. E89-B, pp. 3393-3400, 2006.

[71] M. Hoa Le, D. O'Brien, G. Faulkner, Z. Lubin, L. Kyungwoo, J. Daekwang, and O. YunJe, "High-Speed Visible Light Communications Using Multiple-Resonant Equalization," *Photonics Technology Letters, IEEE*, vol. 20, pp. 1243-1245, 2008.

[72] Z. Lubin, D. O'Brien, H. Le-Minh, L. Kyungwoo, J. Daekwang, and O. Yunje, "Improvement of Data Rate by using Equalization in an Indoor Visible Light Communication System," in *Circuits and Systems for Communications, 4th IEEE International Conference*, pp. 678-682, 2008.

[73] Dmingos Terra, Navin Kumar, Nuno Lourenço, Luis Nero Alves, and Rui L. Aguiar "Design, Development and Performance Analysis of DSSS-based Transceiver for VLC", *in Proceedings IEEE, EUROCON'2011*, Lisbon, pp. 1-4, Apr. 2011.

[74] Navin Kumar, Domingos Terra; Nuno Lourenço; Luis Nero Alves, and Rui L. Aguiar," Visible Light Communication for Intelligent Transportation in Road Safety Application", *in Proceedings of IEEE IWCMC'2011, Vehicular Communications Symposium*, Istanbul, pp. 1513-1518, Jul 2011.

Web Pages and Links

[75] ITS, "Intelligent Transportation Systems," http://www.its.dot.gov/research.htm, 2010.

[76] PREVENT, "Project PREVent," http://www.prevent-ip.org/, 2010.

[77] CALM, "Communication Access for Land Mobile,"

http://www.isotc204wg16.org/concept, 2010.

[78] C2C, "Car 2 Car Communication Consortium."

http://www.car2car.org, Car2X Communication System, 2008.

[79] SAFESPOT, "SAFESPOT Integrated Project, Cooperative vehicles and road infrastructure for road safety." http://www.safespot-eu.org/., 2010.

[80] IETF, "Mobile AdHoc Networks (MANET)."

http://datatracker.ietf.org/wg/manet/., 2011.

[81] GEONET, "Geographic addressing and routing for vehicular communications," http://www.geonet-project.eu/., 2010.

[82] SEVECOM, "Secure Vehicle Communication," http://www.sevecom.org/, 2010.

[83] COMeSafety, "Communication for eSafety," http://www.comesafety.org/, 2010.

[84] PREDRIVE, "Preparation for Driving Implementation and Evaluation of Car 2 X Communication Technology,"

http://www.pre-drive-c2x.eu/index.dhtml/444d919dde59571535mo/-/deDE/-/CS/-/., 2010.

[85] ITS. Safety, "Vehicle Safety Communication," http://www.resourceguide.its.dot.gov/., 2009.

[86] IEEE TG7, "VLC Working Group," in *IEEE 802.15.7,*

http://www.ieee802.org/15/pub/TG7.html., 2010.

[87] New York State Department of Transportation, "Evaluation of NYSDOT LED Traffic Installation," http://www.nyserda.org/New, 2010.

[88] Institute of Transport Research, "Comparison of LED Traffic Signal Specifications," http://www.lrc.rpi.edu/programs/lighting/Transformation/led/LEDTrafficSignalComparision.asp., 2009.

[89] National Institute for Resources and Environment, "Measurement of size distribution of aerosol by bistatic system," in *NIRE*.
http://www.aist.go.jp/NIRE/annual/1999/21.htm., 2000.

[90] Qualcomm, "CDMA,"
http://www.qualcomm.com/ProdTech/cdma/training/cdma25/m5/m5p01.html., 2009.

[91] Hamamatsu, "Photodiode Technical Information,"
http://sales.hamamatsu.com/assets/applications/SSD/photodiode_technical_information.pdf., 2003.

[92] Xilinx, "Third Party Embedded Solutions Providers,"
http://www.xilinx.com/ise/embedded/epartners/listing.htm., 2011.

[93] Xilinx, "Embeded Product Board Kits,"
http://www.xilinx.com/products/boards_kits/embedded.htm., 2009.

APPENDIX-I

In this appendix some of snapshots of the experiments are illustrated.

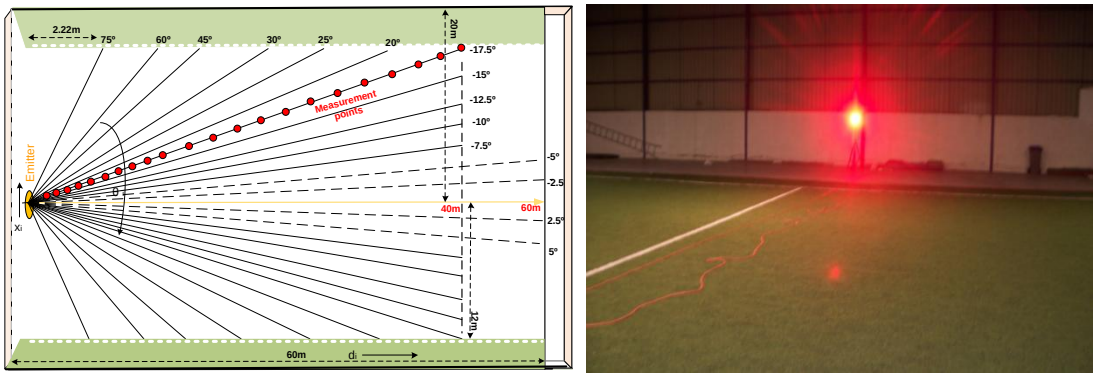

(a) (b)

Fig. I: (a) Measurment Irradiance Distribution; (b) A Pavilion of Size 60x40m

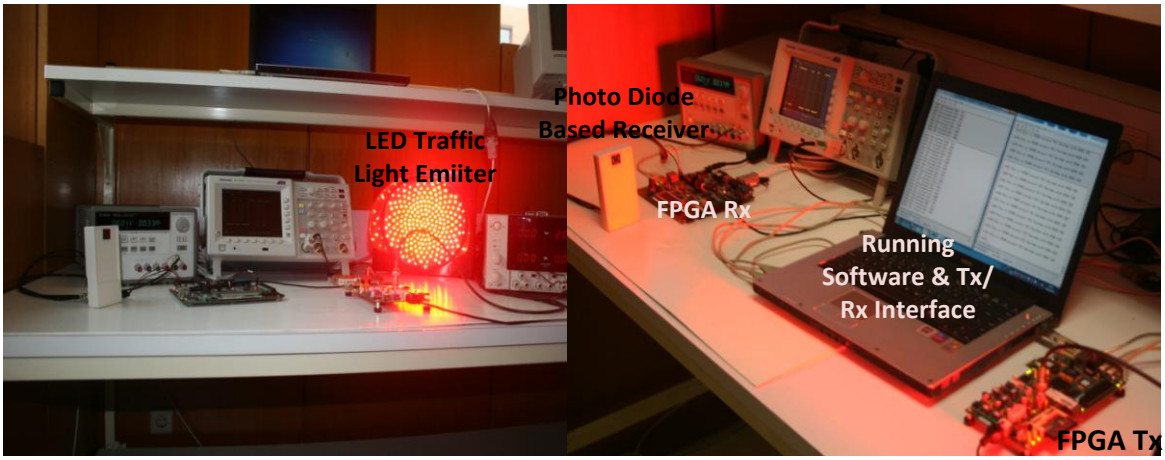

Fig. II: Prototype under test in Lab Setting (work bench)

Fig. III: Experiment Room Showing Light points

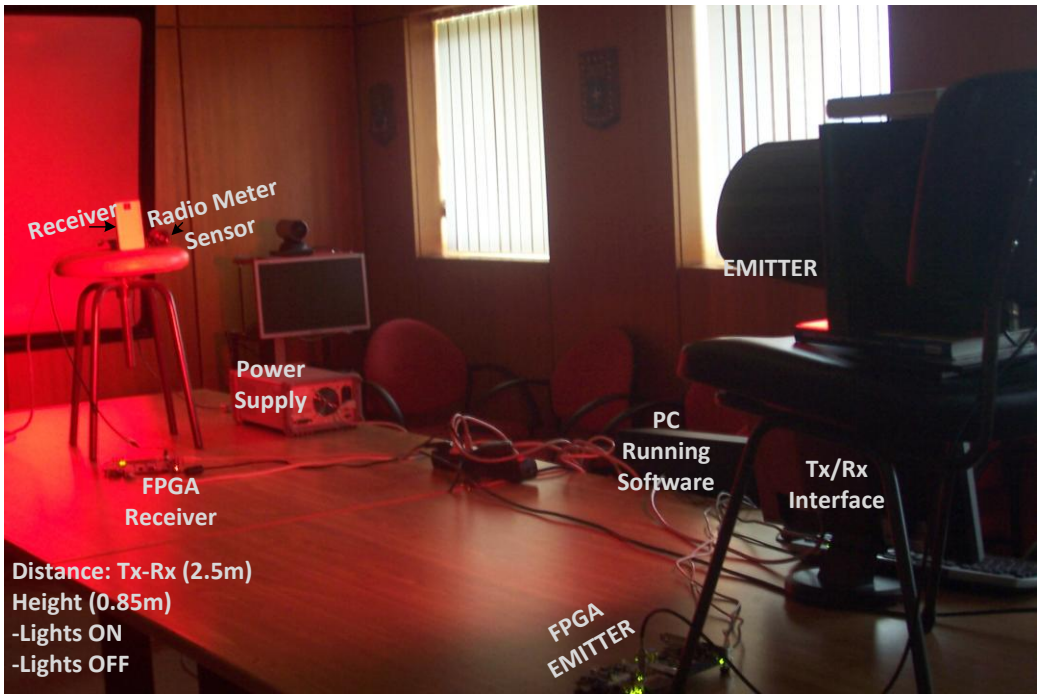

Fig. IV: Measurement of BER in Lab Setting with the Effect of Office lights

Fig. V: Pavilion of 60x40m for Controlled Environment Data Measurement

Fig. VI: Experimental set-up under road lights

Fig. VII: Snap shots from System Set-up under Bright Sun Light

Table. I: Light Metrology Equipment Specifications

Items Name	Parameters	Description and Value
ILT1700 (International Light Technology)		Radiometry, Photometry, low light measurements
	Accuracy	0.2PicoAmps to 2MilliAmps
Light Sensor SED033	Si Photo detector Measurement range	$2.41e^{-10}$ to $2.41e^{-1}$ W/cm^2
	Wavelength	400-700 nm
	Area of detector	33 mm^2
Data Logging Light Meter HD450 (EXTECH Instruments)		Measures Illuminance in Lux with Cosine corrected response
	Range	Up to 400,000 Lux
	Resolution	0.1 Lux
Light Sensor	Si photo diode with spectral response filter	Approximated photopic response
Power Meter (Institute of Telecommunication)	Range of Measurement	1µW – 2W
Sensor Si FD S1010	Rise Time	45 ns
	Area	94.1 mm^2 (9.7 x 9.7 mm)
	Spectral Range	400 – 1100 nm

Table. II: Experimental Measured values From Three Detectors

Dist (m)	Power meter (µW)			ILT 1700 (Irradiance) (µW/cm^2)			HD 450 (Illuminance)	
Angle (º)	5º	2.5º	0º	0º	2.5º	5º	2.5º	0º
1	690.0	450.0	550.0	1610.0	1270.0	1820.0	2710.0	3670.0
2	410.0	320.0	380.0	870.0	750.0	987.0	1729.0	2205.0
3	260.0	200.0	240.0	540.0	453.0	571.0	1029.0	1296.0
4	75.0	70.0	64.0	145.0	141.0	135.0	337.0	310.0
5	48.0	46.0	42.0	94.0	92.8	87.3	217.0	207.0
7.5	22.0	21.0	20.0	43.4	42.2	40.1	91.0	96.1
10	13.0	12.0	9.0	24.5	24.2	23.0	45.0	55.5
12.5	8.0	8.0	7.3	15.7	15.7	14.5	38.0	35.0
15	5.6	5.6	5.1	11.0	11.0	16.2	26.0	24.6
17.5	4.1	4.1	3.8	8.1	8.2	7.5	19.7	18.0
20	3.2	3.2	2.9	6.2	6.3	5.7	15.2	13.7
22.5	2.6	2.5	2.5	5.0	5.0	4.6	11.9	11.0
25	2.2	2.1	2.0	4.0	4.1	3.8	9.7	8.9
27.5	2.0	1.9	1.9	3.3	3.4	3.7	8.0	7.3
30	1.8	1.6	1.7	2.8	2.9	2.6	6.7	6.2
32.5	1.6	1.5	1.6	2.3	2.4	2.2	5.7	5.2
35	1.5	1.4	1.5	2.1	2.1	1.9	4.9	4.5
37.5	1.4	1.3	1.4	1.8	1.8	1.7	4.2	3.8
40	1.3	1.2	1.4	1.6	1.6	1.5	3.6	3.3
42.5	1.2	1.1	1.3	1.4	1.4	1.3	3.2	2.9
45	1.1	1.1	1.3	1.3	1.3	1.2	2.8	2.6
47.5	1.1	1.1	1.2	1.1	1.2	1.0	2.5	2.3
50	1.1	1.1	1.2	1.0	1.0	1.0	2.2	2.0
52.5	1.1	1.1	1.2	0.9	0.9	0.9	2.0	1.8
55	1.1	1.1	1.2	0.8	0.9	0.8	1.7	1.6
57.5	1.1	1.1	1.2	0.8	0.8	0.7	1.5	1.4